NUREG/CR-6655, Vol. 1
ORNL/TM-13692/V1

Sensitivity and Uncertainty Analyses Applied to Criticality Safety Validation

Methods Development

Prepared by
B. L. Broadhead, C. M. Hopper, R. L. Childs, C. V. Parks

Oak Ridge National Laboratory

U.S. Nuclear Regulatory Commission
Office of Nuclear Regulatory Research
Washington, DC 20555-0001

AVAILABILITY NOTICE

Availability of Reference Materials Cited in NRC Publications

NRC publications in the NUREG series, NRC regulations, and *Title 10, Energy,* of the *Code of Federal Regulations,* may be purchased from one of the following sources:

1. The Superintendent of Documents
   U.S. Government Printing Office
   P.O. Box 37082
   Washington, DC 20402–9328
   <http://www.access.gpo.gov/su_docs>
   202–512–1800

2. The National Technical Information Service
   Springfield, VA 22161–0002
   <http://www.ntis.gov/ordernow>
   703–487–4650

The NUREG series comprises (1) brochures (NUREG/BR-XXXX), (2) proceedings of conferences (NUREG/CP-XXXX), (3) reports resulting from international agreements (NUREG/IA-XXXX), (4) technical and administrative reports and books [(NUREG-XXXX) or (NUREG/CR-XXXX)], and (5) compilations of legal decisions and orders of the Commission and Atomic and Safety Licensing Boards and of Office Directors' decisions under Section 2.206 of NRC's regulations (NUREG-XXXX).

A single copy of each NRC draft report is available free, to the extent of supply, upon written request as follows:

Address: Office of the Chief Information Officer
Reproduction and Distribution
Services Section
U.S. Nuclear Regulatory Commission
Washington, DC 20555–0001
E–mail: <DISTRIBUTION@nrc.gov>
Facsimile: 301–415–2289

A portion of NRC regulatory and technical information is available at NRC's World Wide Web site:

<http://www.nrc.gov>

All NRC documents released to the public are available for inspection or copying for a fee, in paper, microfiche, or, in some cases, diskette, from the Public Document Room (PDR):

NRC Public Document Room
2120 L Street, N.W., Lower Level
Washington, DC 20555–0001
<http://www.nrc.gov/NRC/PDR/pdr1.htm>
1–800–397–4209 or locally 202–634–3273

Microfiche of most NRC documents made publicly available since January 1981 may be found in the Local Public Document Rooms (LPDRs) located in the vicinity of nuclear power plants. The locations of the LPDRs may be obtained from the PDR (see previous paragraph) or through:

<http://www.nrc.gov/NRC/NUREGS/SR1350/V9/lpdr/html>

Publicly released documents include, to name a few, NUREG-series reports; *Federal Register* notices; applicant, licensee, and vendor documents and correspondence; NRC correspondence and internal memoranda; bulletins and information notices; inspection and investigation reports; licensee event reports; and Commission papers and their attachments.

Documents available from public and special technical libraries include all open literature items, such as books, journal articles, and transactions, *Federal Register* notices, Federal and State legislation, and congressional reports. Such documents as theses, dissertations, foreign reports and translations, and non-NRC conference proceedings may be purchased from their sponsoring organization.

Copies of industry codes and standards used in a substantive manner in the NRC regulatory process are maintained at the NRC Library, Two White Flint North, 11545 Rockville Pike, Rockville, MD 20852–2738. These standards are available in the library for reference use by the public. Codes and standards are usually copyrighted and may be purchased from the originating organization or, if they are American National Standards, from—

American National Standards Institute
11 West 42nd Street
New York, NY 10036–8002
<http://www.ansi.org>
212–642–4900

DISCLAIMER

This report was prepared as an account of work sponsored by an agency of the United States Government. Neither the United States Government nor any agency thereof, nor any of their employees, makes any warranty, expressed or implied, or assumes any legal liability or responsibility for any third party's use, or the results of such use, of any information, apparatus, product, or process disclosed in this report, or represents that its use by such third party would not infringe privately owned rights.

NUREG/CR-6655, Vol. 1
ORNL/TM-13692/V1

Sensitivity and Uncertainty Analyses Applied to Criticality Safety Validation

Methods Development

Manuscript Completed: October 1999
Date Published: November 1999

Prepared by
B. L. Broadhead, C. M. Hopper, R. L. Childs, C. V. Parks

Oak Ridge National Laboratory
Managed by Lockheed Martin Energy Research Corporation
Oak Ridge, TN 37831-6370

C. W. Nilsen, NRC Project Manager

Prepared for
Division of Systems Analysis and Regulatory Effectiveness
Office of Nuclear Regulatory Research
U.S. Nuclear Regulatory Commission
Washington, DC 20555-0001
NRC Job Code W6479

ABSTRACT

This report presents the application of sensitivity and uncertainty (S/U) analysis methodologies to the code/data validation tasks of a criticality safety computational study. Sensitivity and uncertainty analysis methods were first developed for application to fast reactor studies in the 1970s. This work has revitalized and updated the available S/U computational capabilities such that they can be used as prototypic modules of the SCALE code system, which contains criticality analysis tools currently used by criticality safety practitioners. After complete development, simplified tools are expected to be released for general use.

The S/U methods that are presented in this volume are designed to provide a formal means of establishing the range (or area) of applicability for criticality safety data validation studies. The development of parameters that are analogous to the standard trending parameters forms the key to the technique. These parameters are the D parameters, which represent the differences by group of sensitivity profiles, and the c_k parameters, which are the correlation coefficients for the calculational uncertainties between systems; each set of parameters gives information relative to the similarity between pairs of selected systems, e.g., a critical experiment and a specific real-world system (the application).

The use of a generalized linear-least-squares methodology (GLLSM) tool is also described in this report. The application of the GLLSM tool in this work is largely to provide a preliminary understanding of the magnitude of the D and c_k parameters and the number of experiments needed to rigorously define applicability and properly estimate the bias and uncertainty due to data. This work has determined that c_k values of 0.80 and higher or D values of 0.40 and lower constitute systems that are similar to the extent that they are useful in the determination of bias and associated uncertainty for interpolation and extrapolation scenarios. Initial analyses have also shown that in order for the bias and associated uncertainty estimates to be meaningful, it is anticipated that about five or more very highly correlated systems (c_k of 0.90 or higher) or more than about 10 moderately correlated systems (c_k of 0.80 or higher) should be included in the validation exercises.

These methods and guidelines will be applied to a sample validation for uranium systems with enrichments greater than 5 wt % in Volume 2 of this document. This sample validation will compare these newly proposed methods with more traditional procedures. A side-by-side comparison of the results and procedures, along with guidance on their use, is also presented.

CONTENTS

ABSTRACT . . . iii

LIST OF FIGURES . . . vii

LIST OF TABLES . . . xi

EXECUTIVE SUMMARY . . . xiii

ACKNOWLEDGMENTS . . . xvii

1 INTRODUCTION . . . 1
- 1.1 Purpose . . . 1
- 1.2 Background . . . 1
- 1.3 Overview of Approach . . . 1

2 SENSITIVITY THEORY . . . 5
- 2.1 Sensitivity Sequence Development . . . 6
- 2.2 Demonstration of Application . . . 7
  - 2.2.1 ^{235}U-Fission Cross Section . . . 7
  - 2.2.2 ^{238}U-Capture Cross Section . . . 14
  - 2.2.3 Hydrogen Total Cross Section . . . 23
  - 2.2.4 Summary . . . 23

3 UNCERTAINTY ANALYSIS THEORY . . . 31

4 GENERALIZED LINEAR-LEAST-SQUARES METHODOLOGY . . . 35
- 4.1 Application of GLLSM to Validation . . . 37
- 4.2 Testing of GLLSM with Low-Enriched U Systems . . . 37
  - 4.2.1 Tests with Experimental Data . . . 38
  - 4.2.2 Lessons Learned for Use of Correlation Coefficients . . . 49

5 INTEGRAL PARAMETER APPLICATIONS . . . 51

6 SUMMARY . . . 65

7 REFERENCES . . . 67

APPENDIX A — Covariance Concepts . . . 69

APPENDIX B — Derivation of the Generalized Linear-Least-Squares Equations . . . 75

LIST OF FIGURES

Figure **Page**

1. Total sensitivity trends with H/X for $U(2)F_4$ and $U(5)_3O_8$ systems 8

2. Total sensitivity trends with H/X for $U(2)F_4$ and $U(11)O_2$ systems 9

3. Comparison of ^{235}U-fission sensitivity profiles for $U(2)F_4$ systems with H/X values of 195, 614, and 972 10

4. Comparison of ^{235}U-fission sensitivity profiles for $U(2)F_4$ H/X = 195, and $U(5)_3O_8$ H/X = 147 and 757 11

5 Comparison of ^{235}U-fission sensitivity profiles for $U(11)O_2$ systems with H/X values of 0, 3, and 5 12

6. Comparison of ^{235}U-fission sensitivity profiles for $U(11)O_2$ systems with H/X values of 10, 20, and 40 13

7. Comparison of ^{235}U-fission sensitivity profiles for $U(11)O_2$ systems with H/X values of 80, 200, and 300 15

8. Comparison of ^{235}U-fission sensitivity profiles for $U(11)O_2$ systems with H/X values of 400, 600, and 1000 16

9. Comparison of ^{238}U-capture sensitivity profiles for $U(2)F_4$ systems with H/X values of 195, 614, and 972 17

10. Comparison of ^{238}U-capture sensitivity profiles for $U(2)F_4$ H/X = 195, and $U(5)_3O_8$ H/X = 147 and 757 18

11. Comparison of ^{238}U-capture sensitivity profiles for $U(11)O_2$ systems with H/X values of 0, 3, and 5 19

12. Comparison of ^{238}U-capture sensitivity profiles for $U(11)O_2$ systems with H/X values of 10, 20, and 40 20

13. Comparison of ^{238}U-capture sensitivity profiles for $U(11)O_2$ systems with H/X values of 80, 200, and 300 21

14. Comparison of ^{238}U-capture sensitivity profiles for $U(11)O_2$ systems with H/X values of 400, 600, and 1000 22

15. Comparison of H total cross-section sensitivity profiles for $U(2)F_4$ systems with H/X values of 195, 614, and 972 24

16. Comparison of H total cross-section sensitivity profiles for $U(2)F_4$ H/X = 195, and $U(5)_3O_8$ H/X = 147 and 757 25

LIST OF FIGURES (continued)

Figure **Page**

17. Comparison of H total cross-section sensitivity profiles for $U(11)O_2$ systems with H/X values of 0, 3, and 5 26

18. Comparison of H total cross-section sensitivity profiles for $U(11)O_2$ systems with H/X values of 10, 20, and 40 27

19. Comparison of H total cross-section sensitivity profiles for $U(11)O_2$ systems with H/X values of 80, 200, and 300 28

20. Comparison of H total cross-section sensitivity profiles for $U(11)O_2$ systems with H/X values of 400, 600, and 1000 29

21. Predicted values of (e-a)/c as a function of the number of experiments included for 2-wt % UF_4 systems (0.4% experimental uncertainty) 40

22. Predicted values of (e-a)/c as a function of the number of experiments included for 2-wt % UF_4 systems (0.1% experimental uncertainty) 41

23. Predicted values of (e-a)/c as a function of the number of experiments included for 2-wt % UF_4 systems (H/X = 294 system omitted from analysis) 42

24. Predicted values of (e-a)/c as a function of the number of experiments included for 2-wt % UF_4 systems. The 2% experiments were added in the following H/X sequence: 195, 406, 496, 614, 294, 972. 44

25. Predicted values of (e-a)/c as a function of the number of experiments included for 5-wt % U_3O_8 systems (0.4% experimental uncertainty) 45

26. Predicted values of (e-a)/c as a function of the number of experiments included for 5-wt % U_3O_8 systems (0.1% experimental uncertainty) 46

27. Predicted values of (e-a)/c as a function of the number of experiments included for 5-wt % U_3O_8 systems (0.1% experimental uncertainty, H/X = 245 system omitted) 47

28. Predicted values of (e-a)/c as a function of the number of experiments included for 5-wt % U_3O_8 systems (0.4% experimental uncertainty) 48

29. Dependence of the predicted (e-a)/c values on the inclusion of experiments in various ranges of correlation coefficients 50

30. D_n profile for $U(2)F_4$ H/X = 195 and $U(11)O_2$ H/X = 0 systems; Total D_n = 1.7986 53

31. D_n profile for $U(2)F_4$ H/X = 195 and $U(11)O_2$ H/X = 200 systems; Total D_n = 0.1261 54

32. D_n profile for $U(2)F_4$ H/X = 195 and $U(11)O_2$ H/X = 1000 systems; Total D_n = 0.4271 55

LIST OF FIGURES (continued)

Figure **Page**

33. D_c profile for $U(2)F_4$ H/X = 195 and $U(11)O_2$ H/X = 0 systems; Total D_c = 0.7938 56

34. D_c profile for $U(2)F_4$ H/X = 195 and $U(11)O_2$ H/X = 200 systems; Total D_c = 0.3086 57

35. D_c profile for $U(2)F_4$ H/X = 195 and $U(11)O_2$ H/X = 1000 systems; Total D_c = 0.6201 58

36. D_s profile for $U(2)F_4$ H/X = 195 and $U(11)O_2$ H/X = 0 systems; Total D_s = 0.7381 59

37. D_s profile for $U(2)F_4$ H/X = 195 and $U(11)O_2$ H/X = 200 systems; Total D_s = 0.6085 60

38. D_s profile for $U(2)F_4$ H/X = 195 and $U(11)O_2$ H/X = 1000 systems; Total D_s = 0.5198 61

39. Comparison of D_n, D_s, D_c values with c_k values for benchmark database with respect to $U(11)O_2$ H/X = 500 system 63

40. Comparison of D_{sum} values with c_k values for benchmark database with respect to $U(11)O_2$ H/X = 500 system 64

LIST OF TABLES

Table **Page**

1 Cross-correlation coefficients (due to cross sections) for k_{eff} of 2% and 5% systems 32

2 Cross-correlation coefficients (due to cross sections) for k_{eff} of 11% systems 33

3 Comparison of correlation coefficients (due to cross sections) for k_{eff} of 2%, 3%, 5%, and 11% systems . . 34

4 Properties of 2-wt % UF_4 experiments 39

5 Properties of 5-wt % U_3O_8 experiments 39

6 D parameters for H/X = 195 $U(2)F_4 + CH_2$ as compared with $U(11)O_2 + H_2O$ 52

EXECUTIVE SUMMARY

This report develops the formalisms necessary for the application of sensitivity and uncertainty (S/U) analysis methodologies to the code/data validation tasks of a criticality safety study. The specific investigation tasks involved the formal determination of the range (or area) of applicability for a set of critical benchmarks and the means of using that benchmark set for applications requiring interpolation and extrapolation of that range.

The validation requirements in ANSI/ANS-8.1-1998 define the area(s) of applicability as follows: *the limiting ranges of material compositions, geometric arrangements, neutron energy spectra, and other relevant parameters (such as heterogeneity, leakage, interaction, absorption, etc.) within which the bias of a calculational method is established.*

The standard also notes that *the area(s) of applicability of a calculational method may be extended beyond the range of experimental conditions over which the bias is established by making use of trends in the bias. Where the extension is large, the method should be supplemented by other calculational methods to provide a better estimate of the bias, and especially of its uncertainty in the extended area (or areas), and to demonstrate consistency of computed results.*

The standard is vague on how to establish areas of applicability. No guidance is given with respect to determining what constitutes a valid range or under what conditions the range is breached. The second statement does little to clarify the situation because the methods used to extend the areas of applicability are not stated.

A great deal of judgement is often needed in the current validation techniques in order to establish the area of applicability. A number of parameters are currently used in establishing bounds for the application of the supporting critical benchmarks. These parameters include hydrogen-to-fissile nuclide ratio (H/X), average energy group causing fission (AEG), energy of average lethargy causing fission (EALF) and others. Each of these parameters can be useful in establishing *possible* areas of applicability; however, most systems have multiple variables and their simultaneous variation can make a *definite* determination of applicability difficult. The combined variations in H/X, soluble poison concentrations, reflected/unreflected geometry, enrichment, and impurity concentrations may be treated poorly by using single- or even multiple-parameter trend curves. Similarly, no method is available to determine if there is sufficient *coverage* for the entire range of the parameter in ill-defined trend curves. For example, given systems with H/X values of 200, 500, and 1500: is there coverage of the entire range from 200–1500? If experiments with H/X of 0 and 50 are added, is there adequate coverage from 0–1500? If two of these systems have soluble poison levels of 200 and 500 ppm, is there sufficient coverage for 0–500 ppm levels of poison over the full range of H/X? These are difficult questions, with answers typically derived from expert judgement.

A useful tool in establishing similarities between systems is the use of sensitivity coefficients. Physically sensitivity coefficients are defined such that they represent the percentage effect on some response due to a 1% change in an input parameter. For fissionable material systems, an appropriate response is the effective neutron multiplication of the system (k_{eff}), with the current input parameters of interest being the nuclear reaction probabilities or cross sections. These sensitivities can be presented either as "total" sensitivities, where the relative cross-section change is uniform over all energies, or as a "profile," where the change in k_{eff} due to cross sections is given as a function of the energy of the cross section. The total sensitivity, while interesting, is not unique and therefore is unable to completely characterize similarities between systems. For example, two very different systems *could* have the same total sensitivities because they represent the integral over all energies of the sensitivity profiles. However, it was shown in this work that the plot of total sensitivities as a function of a key parameter, like H/X, does give insight into the possible ranges of these parameters that could be considered as defining similar systems. For regions of the

parameter where the total sensitivities are constant or have a linear slope with respect to the key parameter, the full-sensitivity profiles clearly indicate that the systems are very similar to each other, since the shape and magnitude of the sensitivity profiles are very nearly the same.

The full-sensitivity profiles can be generated in the selected problem neutron-energy-group structure for each material and may include reaction types (e.g., fission, capture, scatter) or other parameters such as χ (fission spectrum) or $\bar{\nu}$ (neutrons per fission). For a typical critical system (comprising a few materials, i.e., ^{235}U, ^{238}U, H, O, etc.), some 20 such profiles are usually generated. Sensitivity profiles were generated for six critical systems with $U(2)F_4$ fuel and H/X values of 195, 294, 406, 496, 614, and 972; two critical systems of $U(5)_3O_8$ stereotex blocks with H/X values of 147 and 757; and 14 hypothetically critical systems of $U(11)O_2$ with H/X values of 0, 3, 5, 10, 20, 40, 80, 200, 300, 400, 500, 600, 800, and 1000. These profiles give considerable information about the particular systems; however, the amount of information is too large to be of general use (20 profiles with about 40 values each, i.e., one for each energy group). Therefore, a method of obtaining the differences between the sensitivity profiles for pairs of systems was devised to reduce the amount of needed information to only a few parameters, while maintaining the uniqueness of the information present in the full sensitivity profiles.

Tests of different potential integral parameters derived from the sensitivity profiles were carried out in order to determine a norm that would best satisfy the needed similarity determination. The most promising set of parameters is a family of "D" value norms as defined below:

$$D_n = \sum_{i=1}^{g} \left| S_{nai} - S_{nei} \right|$$

$$D_c = \sum_{i=1}^{g} \left| S_{cai} - S_{cei} \right|$$

$$D_s = \sum_{i=1}^{g} \left| S_{sai} - S_{sei} \right| ,$$

where S is the relative sensitivity of k_{eff} for the safety application, a, or experimental configuration, e, to $\bar{\nu}$(n) for energy group i, or to the capture (c) or to scattering (s) cross sections.

These coefficients are useful in making a quick determination of the similarity between pairs of systems. Since the range of D values is from 0–2, values of D that are greater than 1 are clearly indicative of dissimilar systems. Based on a comparison of the respective sensitivity profiles and expert judgement, it appears that values of D that are about 0.40 or less indicate similar systems. Additionally, a D_{sum} parameter, which consists of a sum of the D_n, D_c, and D_s values, was shown to be a good indicator of similarity if its value is less than 1.2. These D values are quite useful because they give an indication of similarity with respect to individual materials and reaction processes. Besides determination of D_n, D_c, and D_s as an integral system quantity, these values can also be tabulated for each material in the problem, (i.e., D_n values are tabulated for both ^{235}U and ^{238}U for low-enriched systems). As a result, the D parameters can be used to imply that certain systems are similar with respect to a given isotope and possibly not similar with respect to another isotope. This information can be extremely useful in determining which systems should be included in a criticality safety validation, and the range over which those systems can be used for validation.

An alternative approach to exploring the similarity of systems is using uncertainty analyses. This procedure involves the propagation of estimated cross-section uncertainty information to the calculated k_{eff} value of a given

system via the sensitivity coefficients. Mathematically, this is accomplished by a quadratic product of the sensitivity profile vectors by material and reaction type with the cross-section uncertainty matrices by material and reaction type. The result of this procedure is not only an estimate of the uncertainty in the system k_{eff} for a given system, but also an estimate of the correlated uncertainty *between* systems. These correlated uncertainties can be represented by correlation coefficients, which effectively represent the degree of correlation (0 = no correlation, 1 = full correlation, −1 = full anticorrelation) in the uncertainties between the two systems. This parameter, denoted as c_k, has not only the desirability of a single quantity relating the two systems, but the similarity of the systems is measured in terms of uncertainty, not just sensitivity. As a result of this work, it appears that a c_k value of about 0.8 or higher is indicative of similar systems. These correlation coefficients are felt to be particularly useful when used in traditional trending analyses for criticality safety validation. When used as a trending parameter in these analyses, the correlation coefficient should relate to the degree in which the uncertainties in the critical benchmarks are coupled with the uncertainties in the application of interest. This coupling with the common uncertainties in the various systems is expected to closely mimic the coupling in predicted biases and associated uncertainties between the various systems, since they should both be related to the cross-section uncertainties. The underlying assumption in this approach is that the cross-section processing biases and modeling approximations are either small or they are identified and included in the analysis.

The uncertainties in the calculated values of k_{eff} for each of the 2–11 wt % systems described above were generated, along with their D values and correlation coefficients, the c_k values. The standard deviation values for the uncertainty in the calculated system k_{eff} value range from 0.87 to 1.91%. The highest uncertainties correspond to the lowest H/X values due to the fact that a harder spectrum enhances the sensitivity to the higher-energy cross sections, which are usually less well known than the thermal values. The correlation coefficients among the 2–5 wt % systems are all 0.80 or higher (with the exception of two systems with H/X values over 700), indicating that most of these systems are similar to each other. Another way of looking at the 0.80 correlation coefficient is that 80% of the variance is common to all these systems. Thus, these systems are expected to behave in a very similar manner with respect to bias determinations for the SCALE 44-group cross-section library on which these results are based.

By comparing c_k values among the 14 systems with 11 wt % UO_2, (using a criterion of 0.8 or greater to indicate similar systems) conclusions regarding similar systems are nearly identical to those based on a comparison of detailed sensitivity profiles. Comparison of the detailed sensitivity profiles allow visual confirmation of the degree of similarity between two systems. The c_k results indicate that the H/X of 0 system is only similar to the H/X of 3 system and then only marginally so (c_k is 0.8328). For H/X values between 5 and 1000, similar systems are indicated if the H/X values are within a factor of about 5.

The final issue addressed in this work is an interpretation of the D and c_k parameters with respect to how they relate to interpolation and extrapolation conditions of a criticality safety validation. The key issues are the magnitudes of the c_k and D parameters and the number of systems needed for a meaningful estimate of bias and associated uncertainty. Once these quantities are determined, a number of options are available for determination of bias and associated uncertainty. A standard trending approach can be performed with only those experiments deemed to be similar. As mentioned previously, these D and c_k parameters can be used in a traditional trending analysis for the determination of the predicted bias and associated uncertainty. An alternative approach to the traditional trending analysis for the determination of biases and associated uncertainty is the use of the generalized linear-least-squares methodology (GLLSM).

Physically the GLLSM is designed to predict a revised set of data such that differences between the measured and calculated values of k_{eff} are minimized for the entire set of criticals used in the data validation process. The inputs

needed for such an analysis are almost identical to the concepts presented thus far — the sensitivity coefficients, the cross-section uncertainties, the actual calculated and measured k_{eff} values — but with the addition of an estimate of the uncertainty in the measured k_{eff} value for each critical experiment. Mathematically, the GLLSM represents a combination of measurements. These measurements include the experimental values of k_{eff} for each critical benchmark as well as the calculated value of k_{eff} obtained by utilizing evaluated nuclear data from differential cross-section measurements. This calculation is simply the transport analysis determination of the system multiplication factor, k_{eff}. The identification of a calculated value for k_{eff} as an integral "measurement" with uncertainties consisting of the evaluated cross-section uncertainty contribution and method uncertainty contributions (uncertainties in the transport method determination of k_{eff} and data processing methods) is the key to understanding the GLLSM approach. The "data changes" that result from the application of the GLLSM can then be used to predict (via interpolation or extrapolation) the bias and associated uncertainty for *any* application determined to be relevant to the benchmark area of applicability.

One of the benefits of the GLLSM approach is that not only can the bias and associated uncertainty for a given application be estimated, the cumulative "combination" of critical benchmarks can be used to determine the convergence of the procedure. Questions that can be addressed include: *how many* experiments are needed to verify an application, and *how much* correlation to the application is necessary in order to validate the application area?

This work applied a GLLSM tool to the set of $U(2)F_4$ and $U(5)_3O_8$ systems. From an analysis of the results, it appears that for correlation coefficients equal to 0.9 or higher, about 5–10 experiments are needed. For correlation coefficients between 0.80 and 0.89 approximately 10–20 experiments are needed (although these rules of thumb were not sufficient for some systems). The primary factor in whether systems with correlation coefficients between 0.80 and 0.89 produce convergence is believed to be the "completeness" of the experiments (i.e., do the other experiments with lower c_k values provide validation of the application system for all important cross sections and energy ranges?). Further development of the concept of completeness is currently in progress.

ACKNOWLEDGMENTS

This work was supported by the U.S. Nuclear Regulatory Commission under Project JCN W6479, "Development and Applicability of Criticality Safety Software for Licensing Review." The direction of C. W. Nilsen, the NRC project manager, along with D. R. Damon, S. A. Parra and K. J. Hardin, the NRC technical monitors, is acknowledged.

The technical work described in the report has been presented to several audiences and the reports have been reviewed by individuals with a wide spectrum of interests and experience. This process has been valuable to the authors and appreciation to those willing to provide opinions and feedback is gratefully appreciated. In particular the authors would like to recognize the efforts of D. R. Damon and S. A. Parra who provided review comments for the NRC. Useful discussions and technical reviews were also received from R. M. Westfall, W. C. Jordan, and J. F. Mincey of ORNL. The initial suggestions from J. J. Wagschal of the Hebrew University, Jerusalem, relative to presenting the methodology as well as his careful review of the final report were of great benefit to the authors. Similarly the comments and suggestions provided by R. L. Murray of N. C. State University, M. L. Williams of Louisiana State University, R. E. Wilson of Safe Sites of Colorado, Keyes Niemer of Duke Engineering and Services, and F. Trumble of Westinghouse Safety Management Systems helped the authors identify areas where improved clarity and explanation were needed.

1 INTRODUCTION

1.1 Purpose

The purpose of this report is to present research performed to demonstrate that sensitivity and uncertainty (S/U) analysis methodologies can be used to help establish areas of applicability related to the validation of computational codes and data for nuclear criticality safety. In addition, rigorous, quantitative methods that can estimate the bias and associated uncertainty due to nuclear cross-section data are explored. This estimated bias and uncertainty can be utilized in defining adequate margins of subcriticality.

1.2 Background

The validation requirements in ANSI/ANS-8.1-1998[1] define the area(s) of applicability as follows: *the limiting ranges of material compositions, geometric arrangements, neutron energy spectra, and other relevant parameters (such as heterogeneity, leakage, interaction, absorption, etc.,) within which the bias of a calculational method is established.*

The standard also notes that *the area(s) of applicability of a calculational method may be extended beyond the range of experimental conditions over which the bias is established by making use of trends in the bias. Where the extension is large, the method should be supplemented by other calculational methods to provide a better estimate of the bias, and especially of its uncertainty in the extended area (or areas), and to demonstrate consistency of computed results.*

The standard is vague on how to establish areas of applicability. No guidance is given with respect to determining what constitutes a valid range or under what conditions the range is breached. The second statement does little to clarify the situation in that the methods used to extend the areas of applicability are not stated.

A more formal procedure for defining the area(s) of applicability is needed, so that systems that appear to be similar can indeed be shown to be (or not to be) in the same area of applicability. Systems can indeed appear to be similar, but in actuality be very different. That is, systems with small-versus-medium concentrations of poison material behave very differently, even though they may "look" the same. Another problem can be an "interpolation" within ranges that are very broad. It is difficult to determine if the entire range is covered by its endpoint conditions without some formal process to verify similarity.

1.3 Overview of Approach

The concept of similarity is somewhat vague itself. How similar is similar? It is proposed that a useful gauge of system similarity would be sensitivity coefficients. Sensitivity coefficients are defined physically such that they represent the percentage effect on some response due to a fractional (e.g., typically a 1%) change in an input parameter. For fissionable material systems, one of the appropriate responses is the effective neutron multiplication of the system (k_{eff}) relative to input parameters of interest (e.g., the nuclear reaction probabilities or cross sections). These sensitivities can be presented either as "total" sensitivities, where the cross-section change is uniform over all energies, or as a "profile," where the change in k_{eff} due to cross sections is given as a function of the energy of the cross section. The total sensitivity, while interesting, is not unique and, therefore, is lacking in its ability to characterize the similarities between systems. For example, two very different systems *could* have the same total sensitivities since they represent the integral over all energies of the sensitivity profiles. These sensitivity profiles can be generated for each material and may include various reaction rates (e.g., scatter, absorption, fission) as well as χ (fission spectrum) and $\bar{\nu}$ (neutrons per fission). For a typical system (comprising a few materials, i.e., ^{235}U,

^{238}U, H, O, etc), some 20 such profiles are usually generated. These profiles give a great deal of information about the particular system, because they provide the effect on k_{eff} for differential changes in the cross-section information or other system parameters. However, the amount of information is too large to be of general use (20 profiles with about 40 values each, i.e., one for each energy group). Some type of norm for measuring these differences in sensitivities would be useful to reduce the amount of information to a few parameters. The sensitivity theory utilized in this work will be given in Section 2. The results of various norms to represent sensitivity differences will be discussed in Section 5.

Another method for exploring the similarity of systems is to use uncertainty analyses. This method involves the propagation of estimated cross-section uncertainty information to the calculated k_{eff} value of a given system using the sensitivity coefficients. Mathematically, this is accomplished by a quadratic product of the sensitivity profile vectors by nuclide and reaction type, with the cross-section uncertainty matrices determined by nuclide and reaction type. The result of this method is not only an estimate of the uncertainty in the system k_{eff} for a given system, but the procedure also provides estimates of the correlated uncertainty *between* systems. These correlated uncertainties can be represented by correlation coefficients, which effectively represent the degree of correlation (0 = no correlation, 1 = full correlation, −1 = full anticorrelation) in the uncertainties between the two systems. This parameter is desirable, not only because it provides a single quantity relating the two systems, but because the similarities of the systems are measured in terms of uncertainty, not just sensitivity. Therefore, two systems with identical sensitivities with respect to a well-known nuclide of medium importance could be determined to be dissimilar if they have differing sensitivities to a nuclide of high importance, and with large uncertainties. Similarly, two systems that may appear different, could be deemed similar if they have similar large sensitivities to a nuclide with large uncertainties, but very different sensitivities to a well-known nuclide. These correlation coefficients are felt to be particularly useful when used in traditional trending analyses for criticality safety data validation. When used as a parameter in the trending analyses, the correlation coefficient should relate to the degree in which the uncertainties in the critical benchmarks are coupled to the uncertainties in the application of interest. This coupling to the common uncertainties in the various systems is expected to very closely mimic the coupling in predicted bias and associated uncertainty between the various systems, since they should both be related to the cross-section uncertainties. Details of the uncertainty analysis theory are presented in Section 3.

The use of the previously described sensitivity and uncertainty analysis techniques are intended to help provide a formal and rigorous approach to the determination of area(s) of applicability for criticality safety validation per ANSI/ANS-8.1. As mentioned earlier, the correlation coefficient can be used as the parameter in a traditional trending analysis for the determination of expected bias and associated uncertainty for specific applications in criticality safety. An alternative approach to the traditional trending analysis for the determination of bias and uncertainty is the use of the so-called generalized linear-least-squares methodology (GLLSM). Physically the GLLSM is designed to predict adjustments in the underlying data such that differences among the measured and calculated values of k_{eff} are minimized for the entire set of criticals used in the data validation process. The inputs needed for such an analysis are almost identical to the concepts presented thus far — the sensitivity coefficients, the cross-section uncertainties, the actual calculated and measured k_{eff} values — but with the addition of an estimate of the uncertainty in the measured k_{eff} values. Mathematically, the GLLSM represents a combination of measurements. These measurements include the experimental values of k_{eff} for each critical benchmark and the calculated value of k_{eff} obtained by utilizing evaluated nuclear data determined from differential cross-sections measurements. This calculation is simply the transport analysis determination of k_{eff}. The identification of a calculated value of k_{eff} as an integral "measurement" with uncertainties consisting of the evaluated cross-section uncertainty contribution and method uncertainty contributions (uncertainties in the transport method determination of k_{eff} and data processing methods) is the key to understanding the GLLSM approach. The "data changes" that result from the application of the GLLSM can then be used to predict the bias and associated uncertainty for *any*

similar application where the area of application corresponds to an interpolation or extrapolation scenario. The GLLSM approach is described in detail in Section 4.

One of the benefits of the GLLSM approach is that not only can the bias and associated uncertainty for a given application be estimated, the cumulative "combination" of critical benchmarks can be used to determine the convergence of the procedure. For example, questions that need to be addressed include: *how many* experiments are needed to validate computations for a safety application, and *how much* correlation to the application is necessary in order to validate the area of applicability? A separate question is: *can* the validation be performed collectively with a set of benchmarks, none of which are considered explicitly to be in the area of applicability for the application? The last subject is especially provocative in that experiments that are not even critical experiments could be used to validate a criticality safety application. The first two topics will be discussed in this report, while the last is the topic of ongoing research.

Currently, these techniques are felt to be valuable in many areas where the set of available, "relevant" experiments seems to be limited with respect to current applications of interest. These areas include, but are not limited to, the extension of criticality data validation for UO_2 fuel enrichments greater than 5 wt %, low-moderation applications where H/X values approach zero, mixed-oxide systems with the introduction of weapons-grade plutonium, incorporation of burnup credit (use of spent fuel nuclides), and fissile material waste applications where the matrix includes nuclides not available in the type and quantity found in critical experiments.

2 SENSITIVITY THEORY

The techniques used in this work to generate sensitivity information for the various critical benchmarks are based on the familiar perturbation theory of reactor analysis. Textbooks provide a progression from a one-group neutron diffusion model[2] to a two-group model[3] to a multigroup transport version.[4] Research papers[5–8] examine the higher-order perturbation effects and show relationships between various formulations. From those generalized approaches, we extract the specific theory for the generation of k_{eff} sensitivities. For a full derivation of the general sensitivity equations, the reader is referred to Refs. 9 and 10.

Considering the Boltzmann transport equation written in the form:

$$[A - \lambda B]\phi = 0 \tag{1}$$

where $\lambda = 1/k_{eff}$; and a perturbed system

$$[A' - \lambda' B']\phi' = 0 \ , \tag{2}$$

the adjoint equation to Eq. (1) is

$$[A^* - \lambda B^*]\phi^* = 0 \ . \tag{3}$$

Multiplying Eq. (2) by ϕ^*, and integrating over all phase space (indicated by the bracket notation < >), yields

$$\langle \phi^*(A' - \lambda' B')\phi' \rangle = 0 \ . \tag{4}$$

Defining:

$$\begin{aligned} A' &= A + dA \\ B' &= B + dB \\ \lambda' &= \lambda + d\lambda \end{aligned} \tag{5}$$

and inserting in Eq. (4) leads to

$$\langle \phi^*(dA - \lambda dB - Bd\lambda - d\lambda dB)\phi' \rangle = 0 \ . \tag{6}$$

Ignoring second-order terms ($d\lambda dB$), assuming use of the unperturbed flux, and solving for the reactivity perturbation yields

$$d\lambda/\lambda = \langle \phi^*(dA - \lambda dB)\phi \rangle / \langle \phi^*(\lambda B)\phi \rangle \ . \tag{7}$$

Hence, the sensitivity of λ, with respect to the multigroup reaction x cross section, Σ_x, becomes

$$\frac{d\lambda/\lambda}{d\Sigma_x/\Sigma_x} = \frac{\Sigma_x}{\lambda} \frac{\langle \phi^*(dA/d\Sigma_x - \lambda dB/d\Sigma_x)\phi \rangle}{\langle \phi^* B \phi \rangle} \ . \tag{8}$$

Note that since $\lambda = 1/k_{eff}$, then $d\lambda/\lambda = -dk_{eff}/k_{eff}$ such that the above equation is essentially the defining equation for the k_{eff} relative sensitivity, S_x, where

$$S_x = \frac{dk_{eff}/k_{eff}}{d\Sigma_x/\Sigma_x} = \frac{-d\lambda/\lambda}{d\Sigma_x/\Sigma_x} .$$

In practice, the dA and dB terms in Eq. (8) are simple functions of the scattering, capture, fission cross sections represented symbolically as Σ_x. The evaluation of Eq. (8) then becomes an integration of the forward and adjoint fluxes and the cross sections over the entire system.

Typically, the energy dependence of the cross sections is represented by averaging the Σ_x quantities over an energy group i, represented as Σ_{x_i}. Insertion of these group quantities into Eq. (8) yields the definition of a sensitivity "profile," $S_{x_i} = \frac{dk_{eff}/k_{eff}}{d\Sigma_{x_i}/\Sigma_{x_i}}$, where group index i is varied to obtain the sensitivity for all groups.

2.1 Sensitivity Sequence Development

The k_{eff} sensitivity calculation, as described above, has previously been implemented in the FORSS[10] (Fantastic Oak Ridge Sensitivity System) package. The FORSS system was developed in the late 1970s primarily for use in the development of fast reactor systems. The FORSS system makes use of the evaluated nuclear data files (ENDF/B), covariance information, and results of integral experiments. Sensitivity formulas for multigroup discrete ordinates were developed and applied successfully to Argonne ZPR critical assemblies.[9] Extensive tests were made to assure internal consistency and achieve precision in sensitivity profiles. A version of the system is available from the Radiation Shielding Information and Computational Center (RSICC) as CCC-334. The FORSS system package placed into RSICC, while operational, is not complete (e.g., thermal upscatter is not operational). More complete versions of FORSS, while internally available in the 1980s at ORNL, were not maintained and documented as fast reactor funding dwindled.

At the beginning of this project, it was decided that the most appropriate procedure was to start with the RSICC version of FORSS and reactivate and enhance the individual modules with the goal of putting portions of the original system into the SCALE[11] system. The "SCALE philosophy" is to include standard well-known computer codes into an application-specific computational sequence with a single integrated input file. Using this philosophy as a guide, a one-dimensional (1-D) sensitivity sequence, SEN1,[12] was produced for use in this project and for subsequent release in future versions of SCALE. This sequence performs standard resonance processing tasks (BONAMI and NITAWL modules), then determines, using 1-D transport theory, the forward and adjoint angular fluxes needed for sensitivity coefficient generation. The XSDRNPM radiation transport code within the SCALE system is used to calculate the forward and adjoint angular fluxes. The sequence then calls modules VIP1D, LAKE, and PLOT, which computes the sensitivity coefficients, estimates the uncertainty in the system k_{eff} value, and plots the sensitivity profiles, respectively. The user input to SEN1 is very similar to the user input of the SCALE shielding module, SAS1, except that since k_{eff} sensitivities do not require a source input, a fixed source is not required.

A prototypic sequence to generate two-dimensional (2-D) sensitivities has also been developed for use in the current work. This capability is not as fully integrated into the SCALE system as the 1-D sensitivity module. The 2-D sensitivity package is based on 2-D discrete-ordinates code DORT,[13] which is not contained in the SCALE system. The documentation of the 2-D sensitivity module is included in the SEN1 documentation.[12]

The feasibility of generating three-dimensional (3-D) sensitivity coefficients, using Monte Carlo methods, was investigated as a separate task under this project. The results of this work have been documented.[14] This development of 3-D sensitivity methods is continuing.

2.2 Demonstration of Application

2.2.1 ^{235}U-Fission Cross Section

Sensitivity analyses can be excellent tools for understanding the underlying characteristics of systems. As an example of the information that can be gleaned from sensitivity plots, eight systems were analyzed using the 1-D and 2-D sensitivity tools. These systems include six systems[15] with $U(2)F_4$ fuel and H/X values of 195, 294, 406, 496, 614, and 972; and two systems[16] of $U(5)_3O_8$ stereotex blocks with H/X values of 147 and 757. Total sensitivity trends of k_{eff} for each of these systems to the ^{235}U fission, ^{238}U capture, and H total cross sections are plotted versus H/X in Figure 1. This curve gives a visual representation of the similarities between the various systems. It is clear from these curves that all of these system are "similar" with respect to ^{235}U-fission cross sections because the magnitude and slope of the sensitivities remain nearly constant over a large range of H/X values. It is less apparent that the systems are similar with respect to ^{238}U capture and H total cross sections, because the respective curves are further apart. However, the slopes of the curves are very nearly the same and constant and, therefore, provide an additional indicator that the systems are similar. To illustrate this point, Figure 2 gives plots of total sensitivity trends for $U(2)F_4$ versus $U(11)O_2$ systems. The sensitivity trends for the 11-wt % UO_2 systems look very similar to those of the 2-wt % UF_4 systems above an H/X of 200. The UF_4 curves are given for actual systems that had H/X values in the range 200 to 1000. The $U(11)O_2$ systems are "artificial" systems, that is to say that no such measurements exist, and they were generated for calculational comparison purposes. Each of these systems is a critical bare sphere with H/X values corresponding to 0, 3, 5, 10, 20, 40, 80, 500, 600, 800, and 1000. The curves below an H/X of 200 exhibit large changes in slope along with maxima and minima. Clearly the curves indicate that the systems are changing rapidly at low values of H/X. Although the total sensitivity of k_{eff} to the ^{235}U fission cross section (e.g., for H/X = 1000 and for H/X = 3) can be almost equal it does not always mean that the systems are similar. These curves are useful for determining trends within a family of systems; however, by themselves they should not be used as a formal basis for establishing similar systems.

In order to understand the details behind the total sensitivity trends shown in the previous two plots, it is necessary to look at the individual sensitivity profiles. Note that Figures 3–20 contain plots of the relative sensitivity per unit lethargy. The relative sensitivities are the energy-dependent quantities, S_{x_i} defined in Section 2. To smooth out the effects of variable energy group widths, these quantities have been divided by the group lethargy width, defined as $\ell n\left(E_i/E_0\right) - \ell n\left(E_{i+1}/E_0\right)$, where $E_0 = 10^7$ eV. This renormalization is not expected to alter the conclusions of this section since the procedure only smooths the plots. Shown in Figure 3 are the sensitivity profiles of three selected systems (i.e., $U(2)F_4$ with H/X of 195, 614, and 972) to the ^{235}U fission cross section. Even though there are slight spectrum variations in the three systems, it is clear that all three are most sensitive to the ^{235}U thermal (i.e., 0.02 to 0.1 eV) fission cross section, only to differing magnitudes. Figure 4 gives a similar comparison for systems of different compositions and different enrichments, namely to $U(2)F_4$ with H/X of 195, and $U(5)_3O_8$ with H/X of 147 and 757. These plots are interesting in that they show the near equivalence with respect to ^{235}U fission between 2 and 5 wt % systems. For H/X values within 30 to 50% of each other, the sensitivity plots are nearly identical.

Looking further at the sensitivity information for the 11 wt % systems, the differences between the H/X values of 0, 3, and 5 are clearly seen in Figure 5. The ^{235}U fission cross section of importance is very different for the system with H/X = 0. However, the systems with H/X values of 3 and 5 appear quite similar. In Figure 6, the ^{235}U fission sensitivities are given for systems with H/X values of 10, 20, and 40. It appears from these plots that

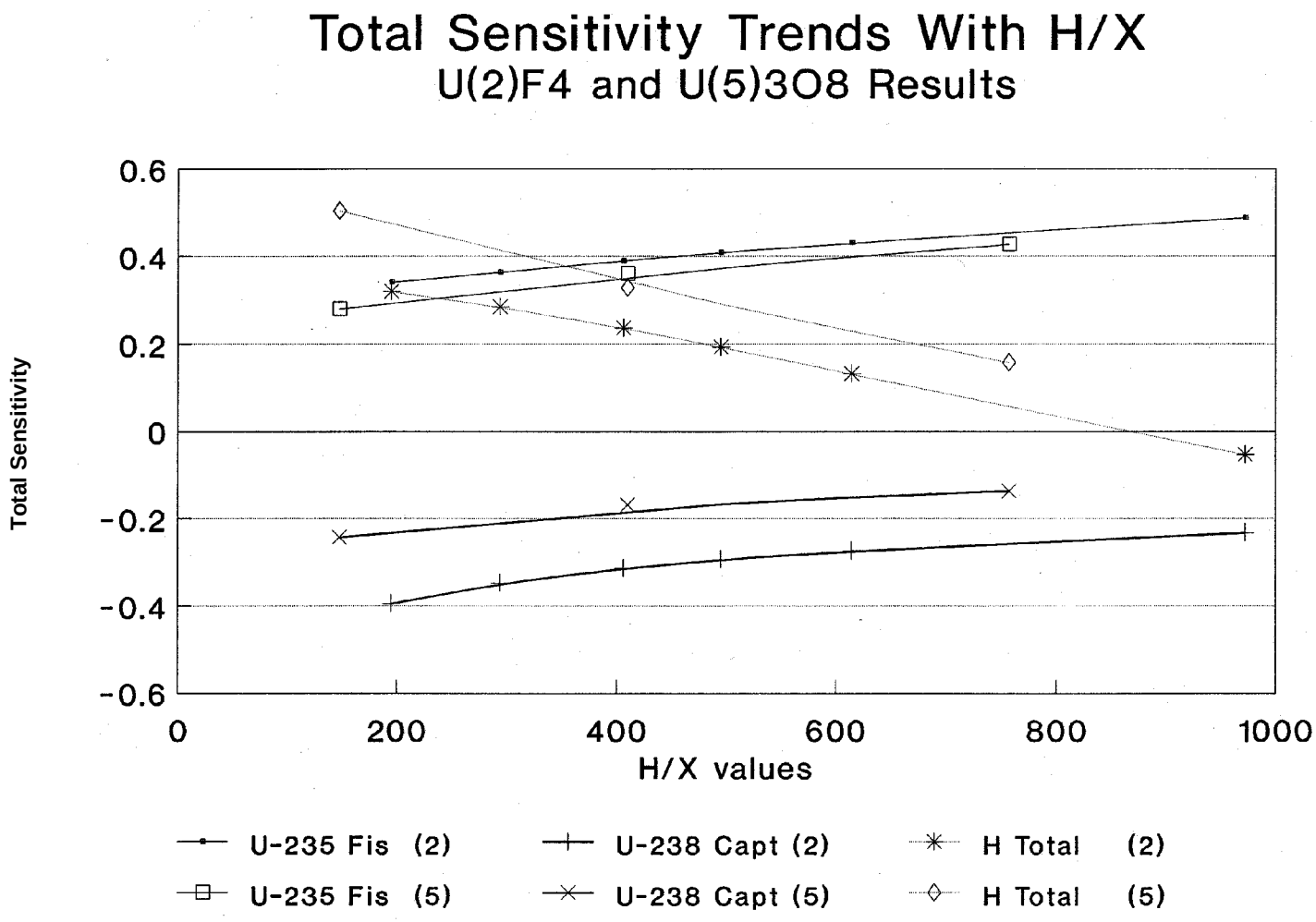

Figure 1 Total sensitivity trends with H/X for $U(2)F_4$ and $U(5)_3O_8$ systems

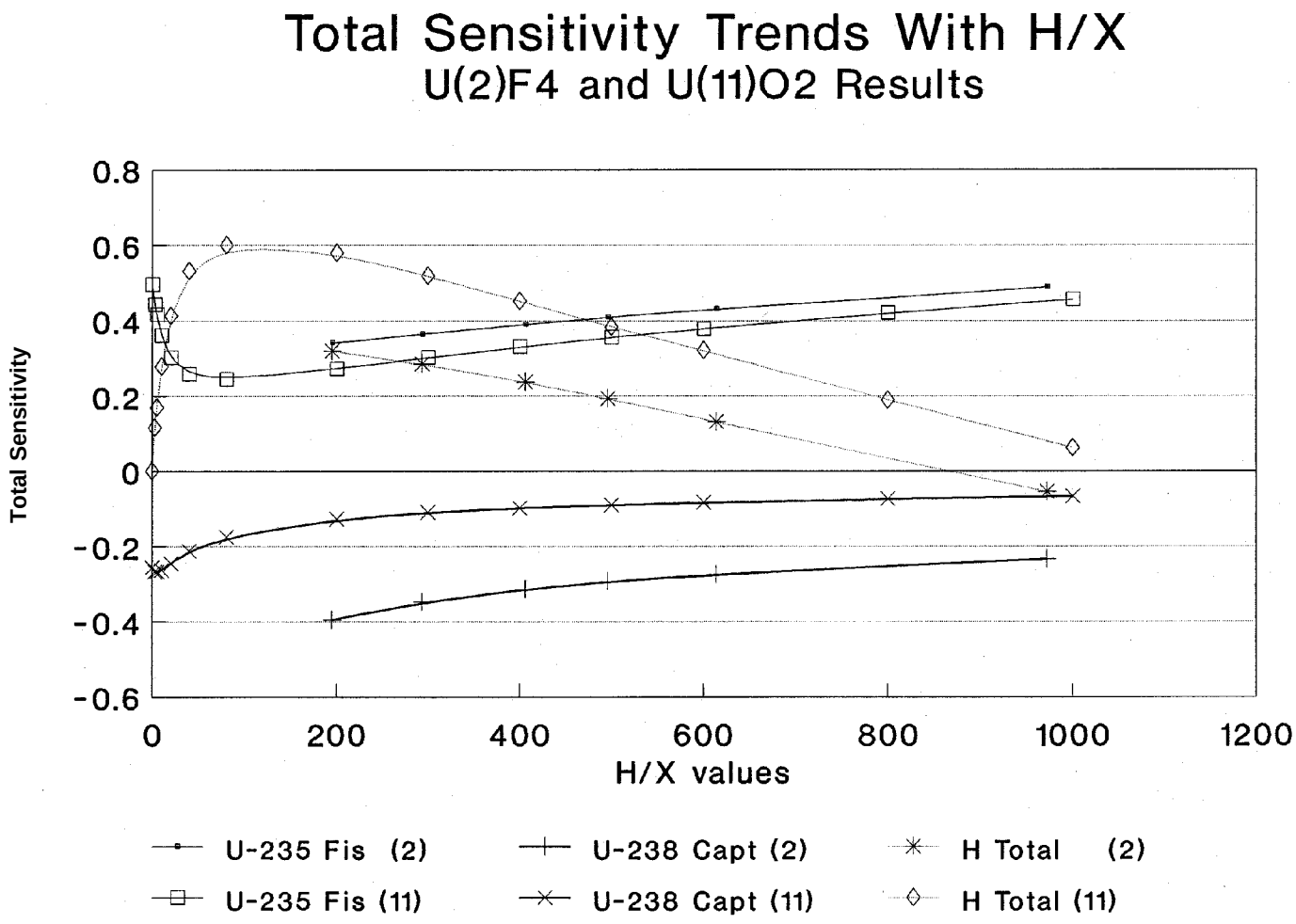

Figure 2 Total sensitivity trends with H/X for $U(2)F_4$ and $U(11)O_2$ systems

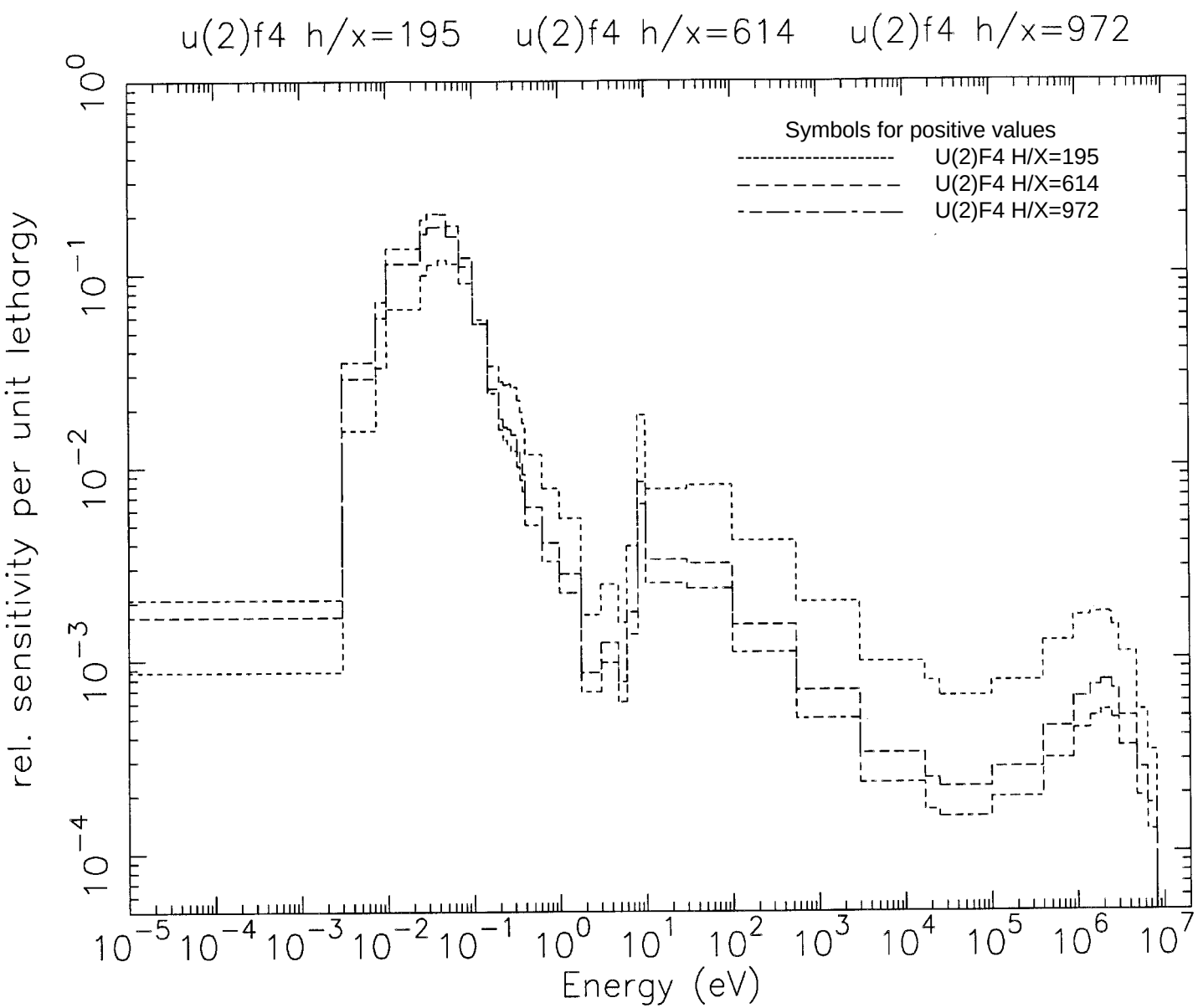

Figure 3 Comparison of ^{235}U-fission sensitivity profiles for $U(2)F_4$ systems with H/X values of 195, 614, and 972

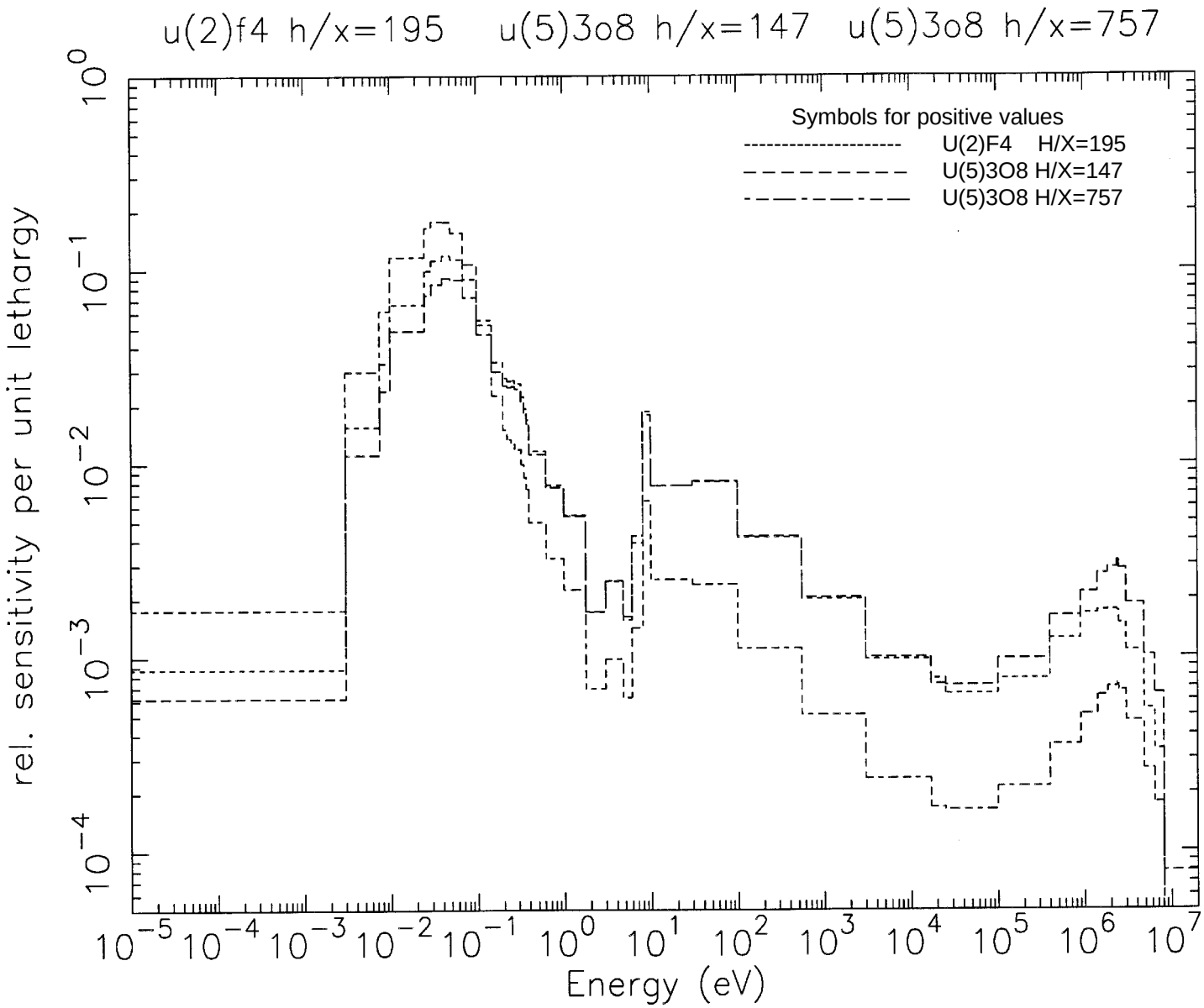

Figure 4 Comparison of ^{235}U-fission sensitivity profiles for $U(2)F_4$ H/X = 195, and $U(5)_3O_8$ H/X = 147 and 757

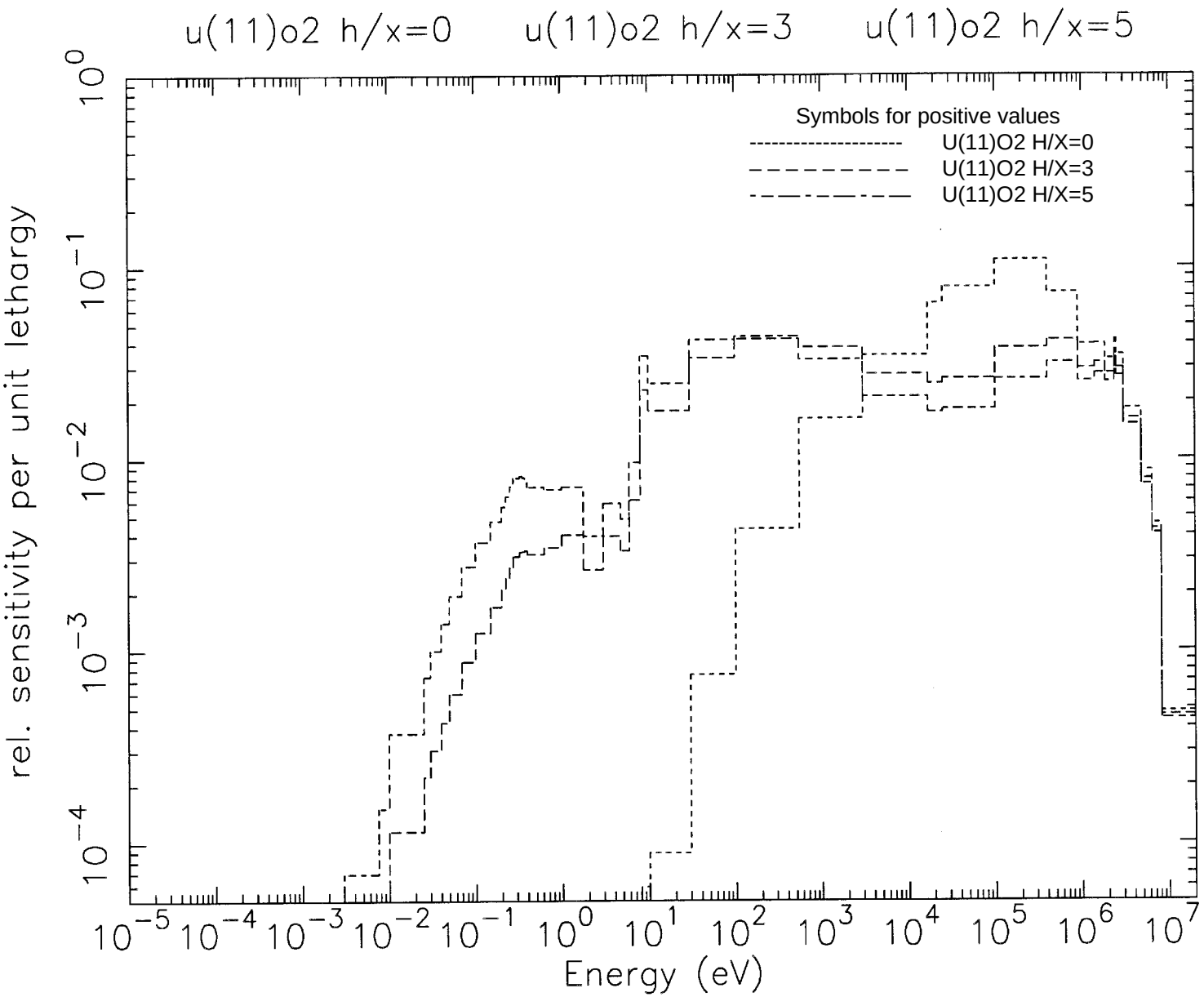

Figure 5 Comparison of ^{235}U-fission sensitivity profiles for U(11)O_2 systems with H/X values of 0, 3, and 5

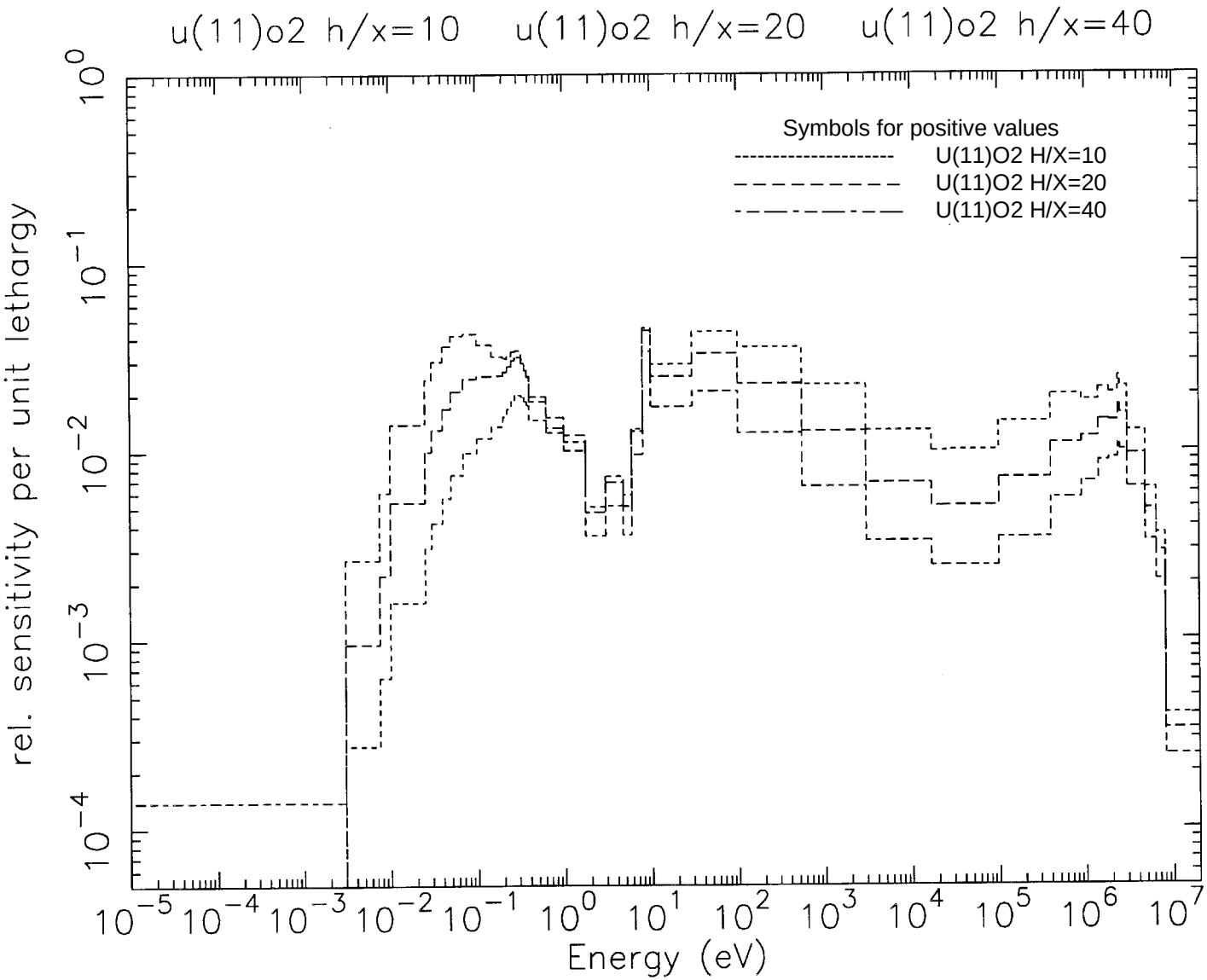

Figure 6 Comparison of ^{235}U-fission sensitivity profiles for U(11)O_2 systems with H/X values of 10, 20, and 40

none of these systems is similar to the other. Systems with an H/X of 80, 200, and 300, shown in Figure 7, and systems with H/X of 400, 600, and 1000, shown in Figure 8, have ^{235}U fission cross-section sensitivities that are very similar to each other. This region corresponds to the approximately linear region in the sensitivity trend plots shown in Figure 2. Thus, these results confirm that for linear portions of the trend plots, the systems are indeed very similar with respect to that material. The underlying physical phenomenon appears to be the similarity in the system spectra. Thus far, only the detailed sensitivity plots for ^{235}U-fission cross sections have been discussed. The behavior of the same systems with respect to the ^{238}U-capture cross-section sensitivities is discussed below.

2.2.2 ^{238}U-Capture Cross Section

A review of the detailed ^{238}U-capture total sensitivity trend plots for the $U(2)F_4$ systems shown in Figure 2 is useful for understanding the following discussion. The region from an H/X of 200 to 400 appears to be slightly non-linear with respect to the remaining portions of the trend plot. Observation of the full sensitivity profiles in Figure 9 for the $U(2)F_4$ systems with H/X values of 195, 614, and 972 indicates that in general the ^{238}U capture cross sections of most importance are the resonance region, especially at the lowest energy resonance of 6.67 eV and the thermal energy range of 0.02 to 0.1 eV. However, for the system with H/X = 195 the resonance cross sections just above the 6.67 eV resonance are also marginally important. This region, from 10 to 100 eV, is represented in the SCALE 44-group structure as two groups, when in actuality it consists of a number of resonances. The influence of these resonances appears to be the cause of the slight nonlinear response seen in the sensitivity trend curves for ^{238}U capture in systems with H/X values between 200 and 400. The decreased nonlinearity for the 11-wt % cases is discussed later.

In Figure 10, a comparison is made of the ^{238}U-capture sensitivity profiles for a $U(2)F_4$ system with H/X = 195 versus two $U(5)_3O_8$ systems with H/X values of 147 and 757. Here the ^{238}U-capture sensitivities are not as closely related as those for ^{235}U fission. However, it is still clear that all systems are still most sensitive to the ^{238}U-capture cross section in the same energy ranges, 0.02 to 0.1 eV and the 6.67 eV resonance.

The ^{238}U-capture sensitivity profiles are presented in Figure 11 for the $U(11)O_2$ systems with H/X values of 0, 3, and 5 for comparison purposes. The system with H/X of 0 is very "fast" with the highest sensitivity to the ^{238}U-capture cross section being in the 10 to 100 keV range. Interestingly, the sensitivity profiles for the two $U(11)O_2$ systems with H/X of 3 and 5 are "nearly identical." This situation is also true in Figure 12, where the sensitivities of k_{eff} to ^{238}U capture for $U(11)O_2$ systems with H/X values of 10, 20, and 40 are shown. Comparison of Figures 12 and 6 indicates that for ^{235}U fission, the region of H/X values between 10 and 40 is a transition region, while a lesser effect is seen for ^{238}U capture. This seeming contradiction is explained by noting that the ^{238}U thermal capture cross section is much smaller than the ^{235}U thermal fission cross section, negating the importance of ^{238}U thermal capture and making the transition much less severe. This observation is confirmed by noting the shape of the ^{238}U-capture total sensitivity trend curve in Figure 2, where the sensitivity changes very little through this transition region.

The comparison of the sensitivity profiles for ^{238}U capture for $U(11)O_2$ systems with H/X values of 80, 200 and 300 (Figure 13), and 400, 600, and 1000 (Figure 14) indicate again the similarities of these respective systems. Again noting the total sensitivity trends for ^{238}U capture seen in Figure 2, the nonlinear shape for the $U(2)F_4$ system is not as severe as that in the $U(11)O_2$ systems for H/X>200. Careful study of the detailed sensitivity profiles shows that for the low-enrichment (2-wt %) systems, the thermal (0.02–0.1 eV) ^{238}U-capture cross sections appear to be competing with those in the resonance range (10–100 eV). For the 11-wt % systems, the increased amount of ^{235}U combined with the corresponding decreased amounts of ^{238}U causes the ^{238}U capture to become less important in the thermal range.

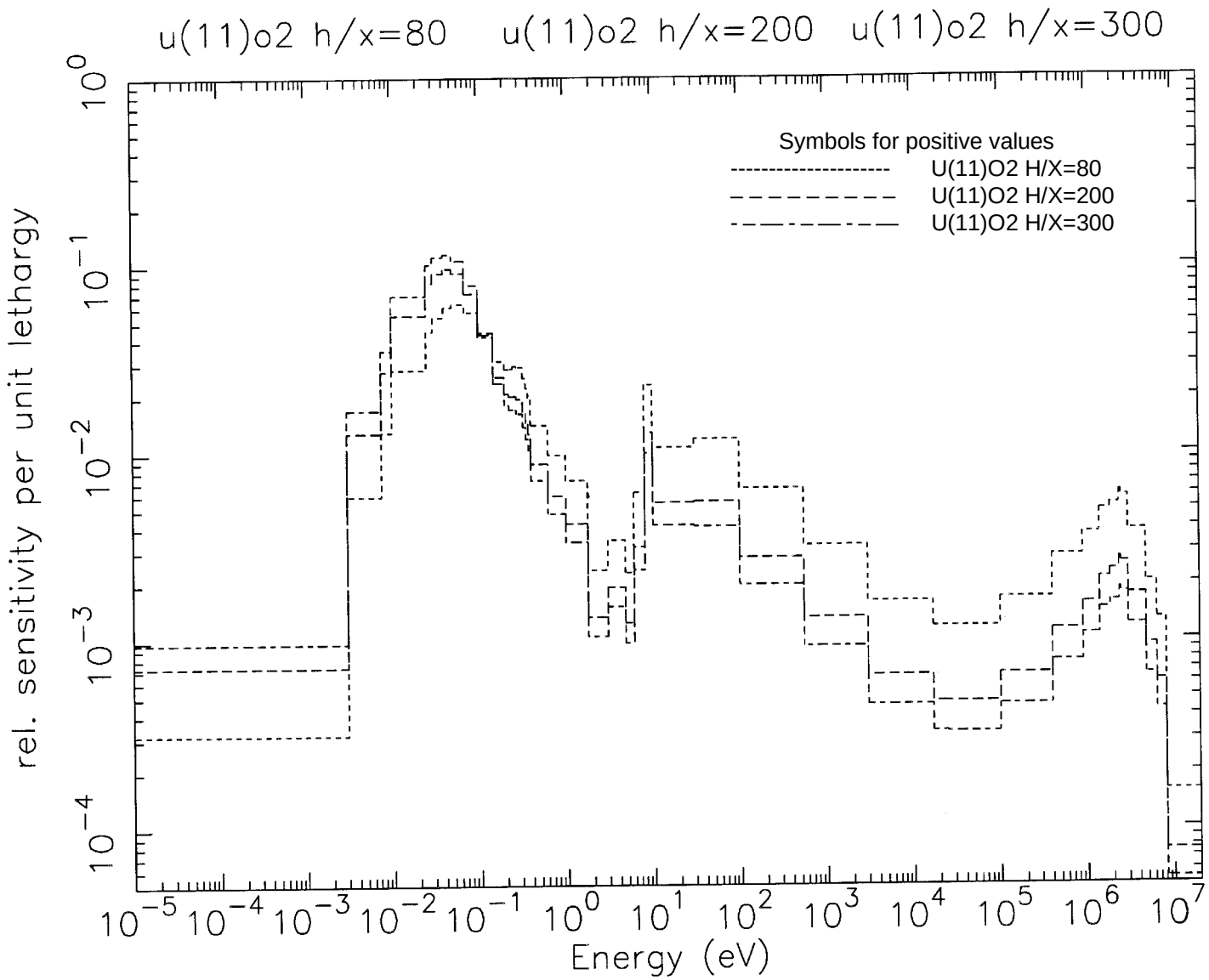

Figure 7 Comparison of ^{235}U-fission sensitivity profiles for $U(11)O_2$ systems with H/X values of 80, 200, and 300

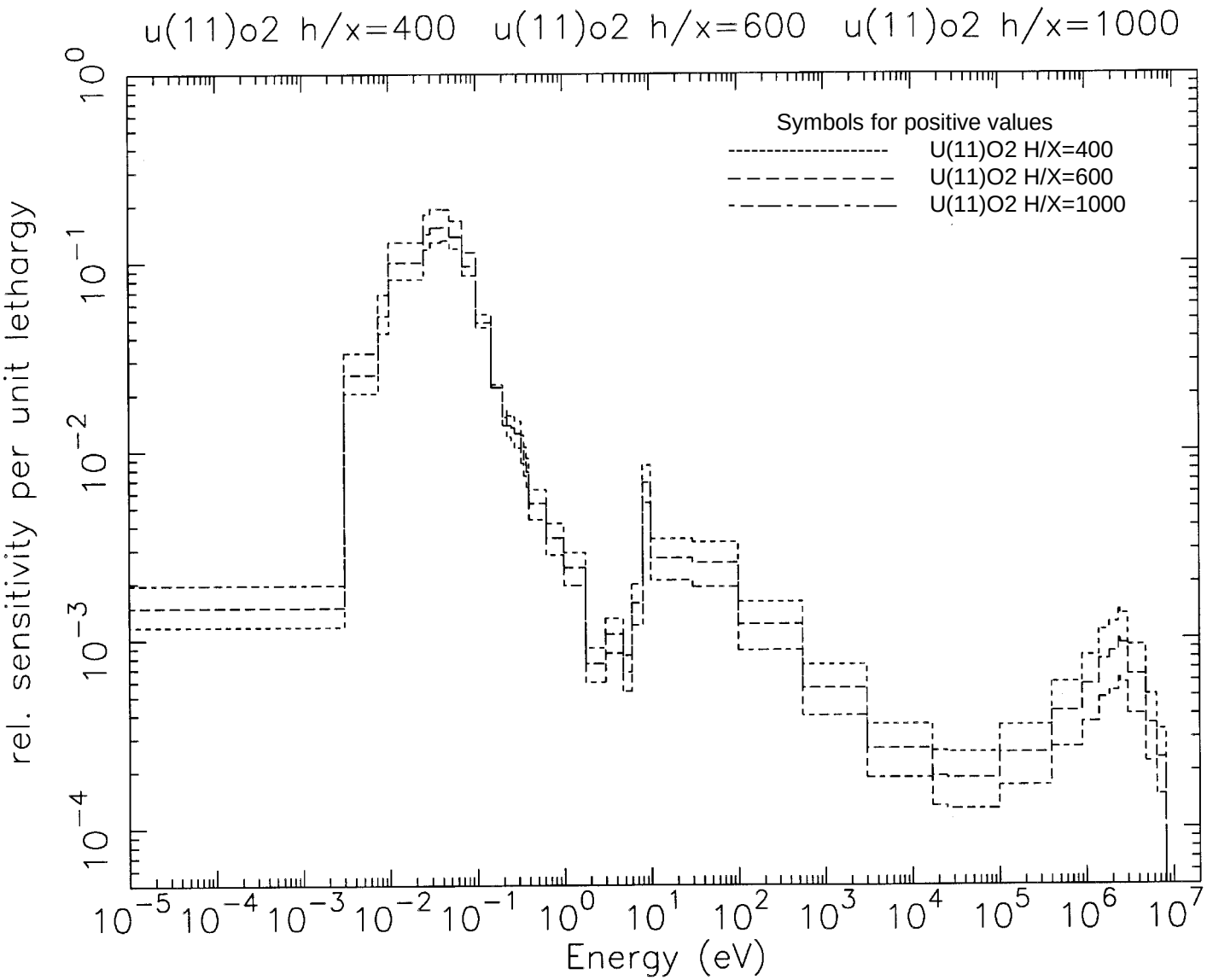

Figure 8 Comparison of ^{235}U-fission sensitivity profiles for U(11)O_2 systems with H/X values of 400, 600, and 1000

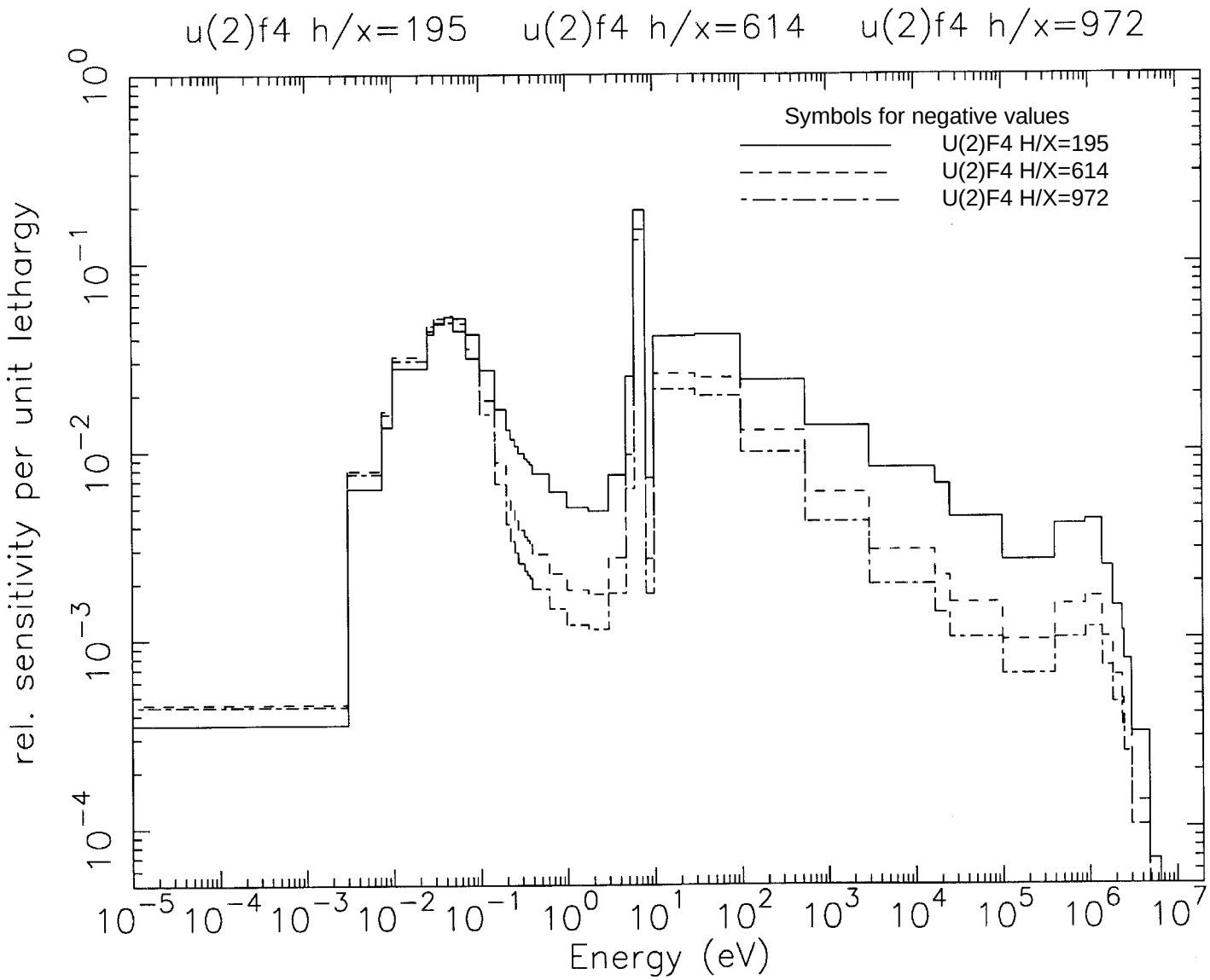

Figure 9 Comparison of ^{238}U-capture sensitivity profiles for $U(2)F_4$ systems with H/X values of 195, 614, and 972

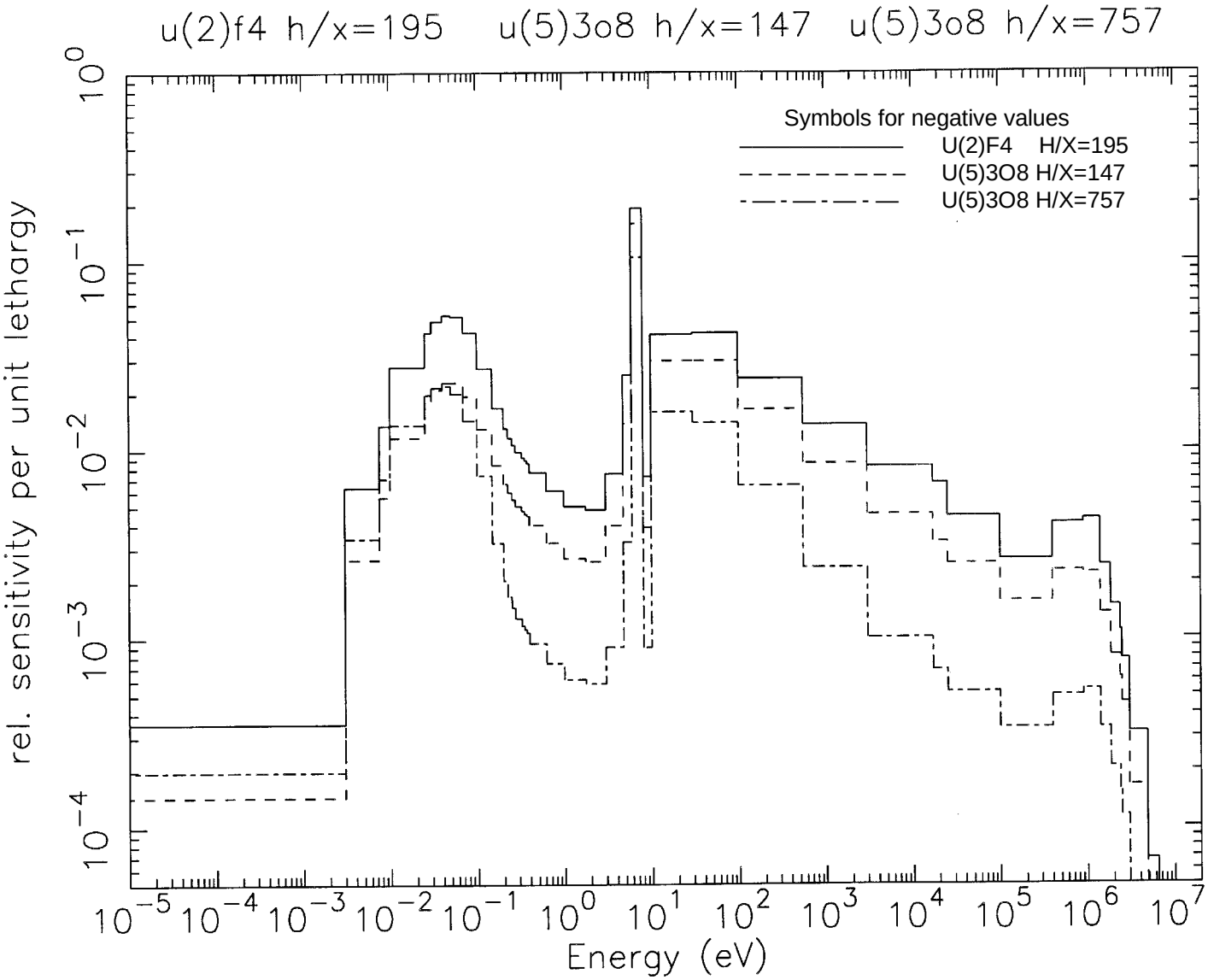

Figure 10 Comparison of ^{238}U-capture sensitivity profiles for $U(2)F_4$ H/X=195, and $U(5)_3O_8$ H/X=147 and 757

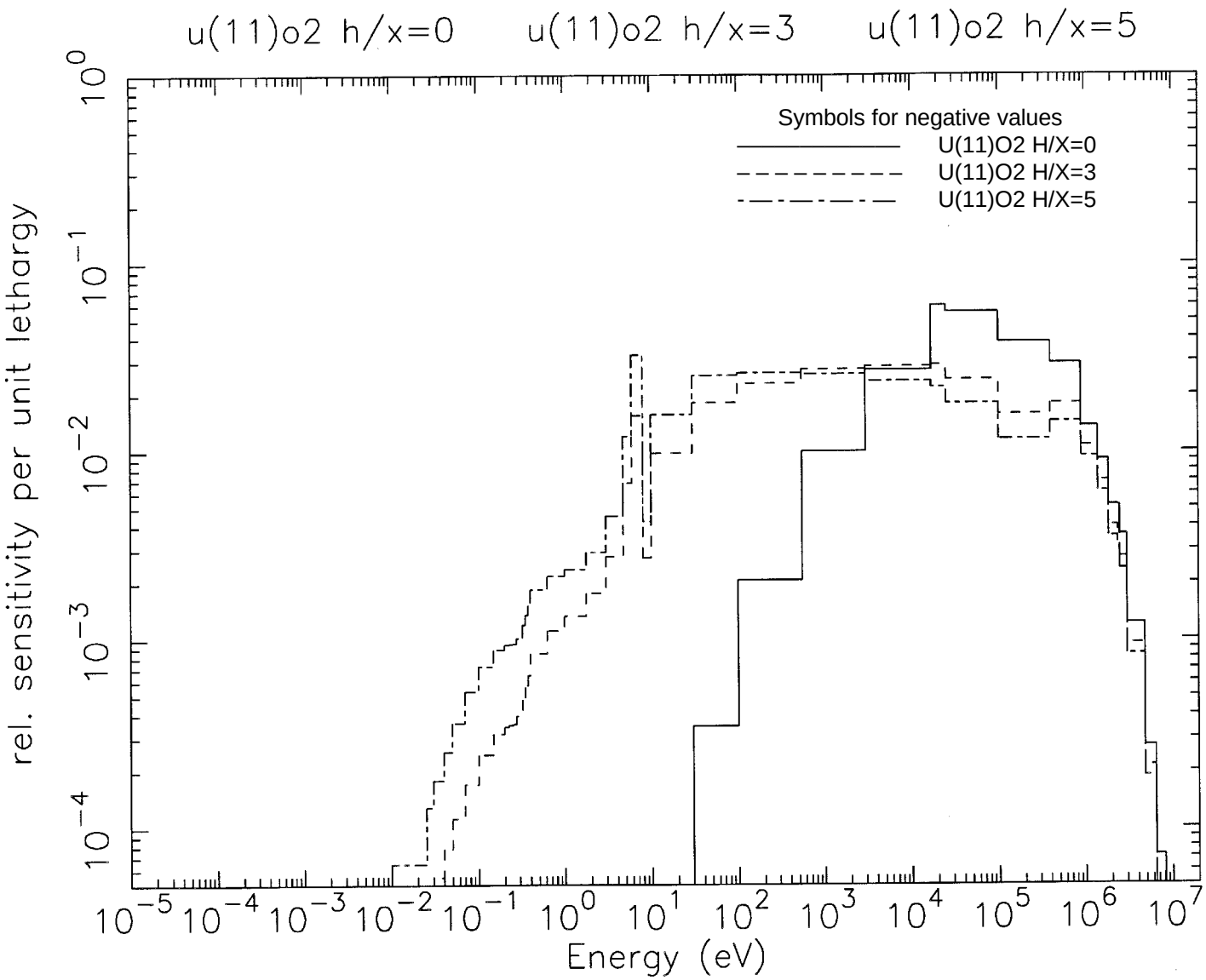

Figure 11 Comparison of ^{238}U-capture sensitivity profiles for U(11)O_2 systems with H/X values of 0, 3, and 5

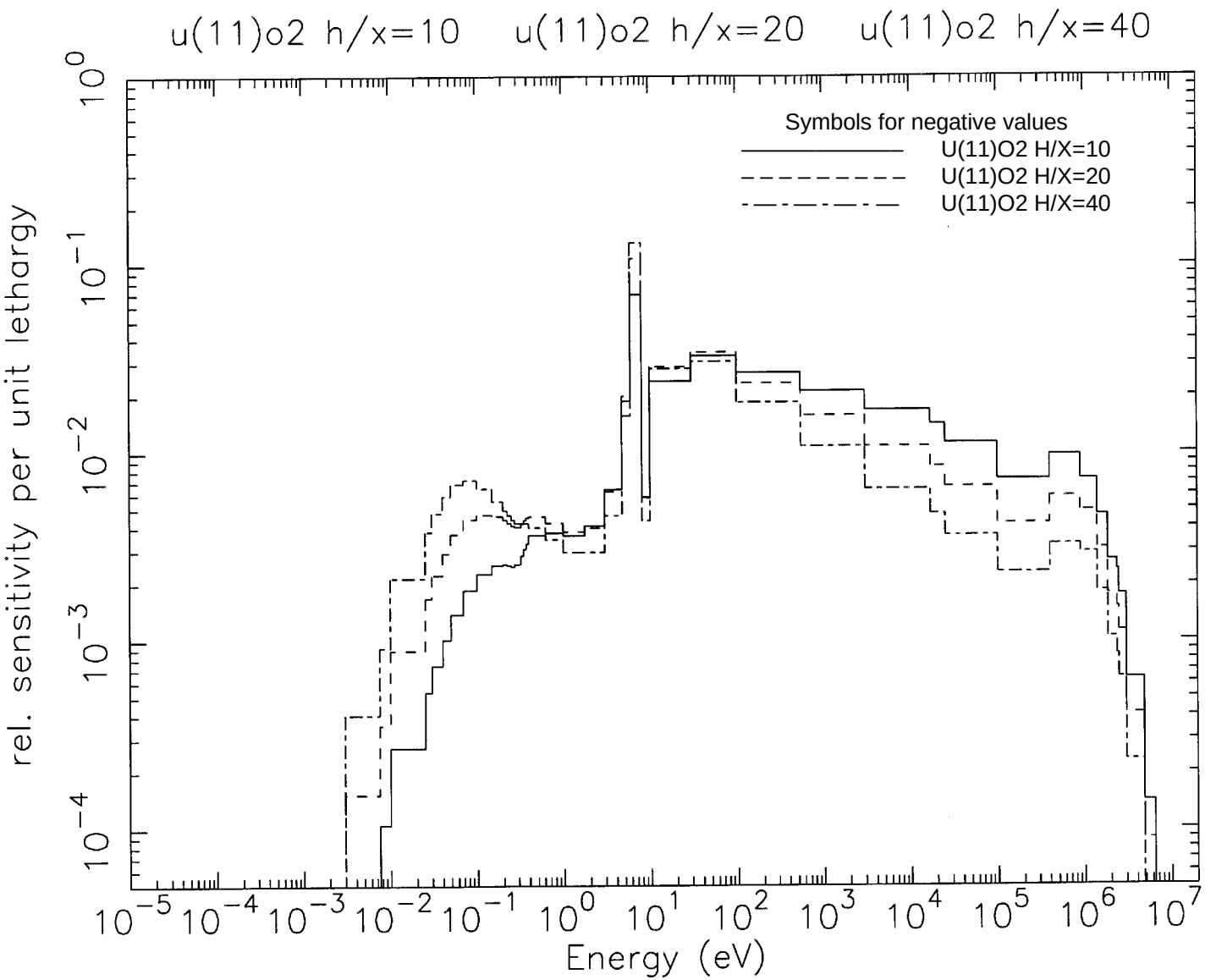

Figure 12 Comparison of ^{238}U-capture sensitivity profiles for $U(11)O_2$ systems with H/X values of 10, 20, and 40

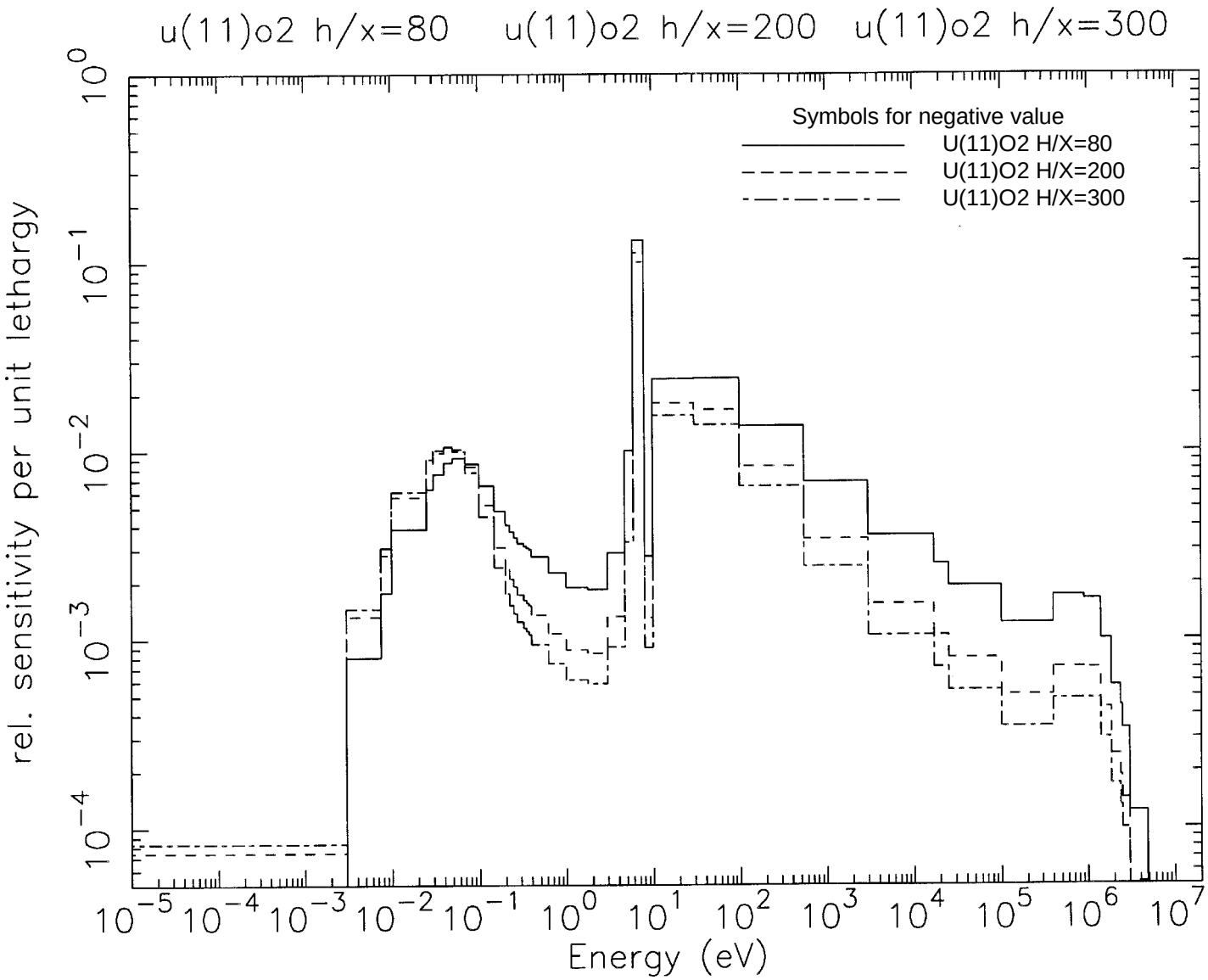

Figure 13 Comparison of ^{238}U-capture sensitivity profiles for U(11)O_2 systems with H/X values of 80, 200, and 300

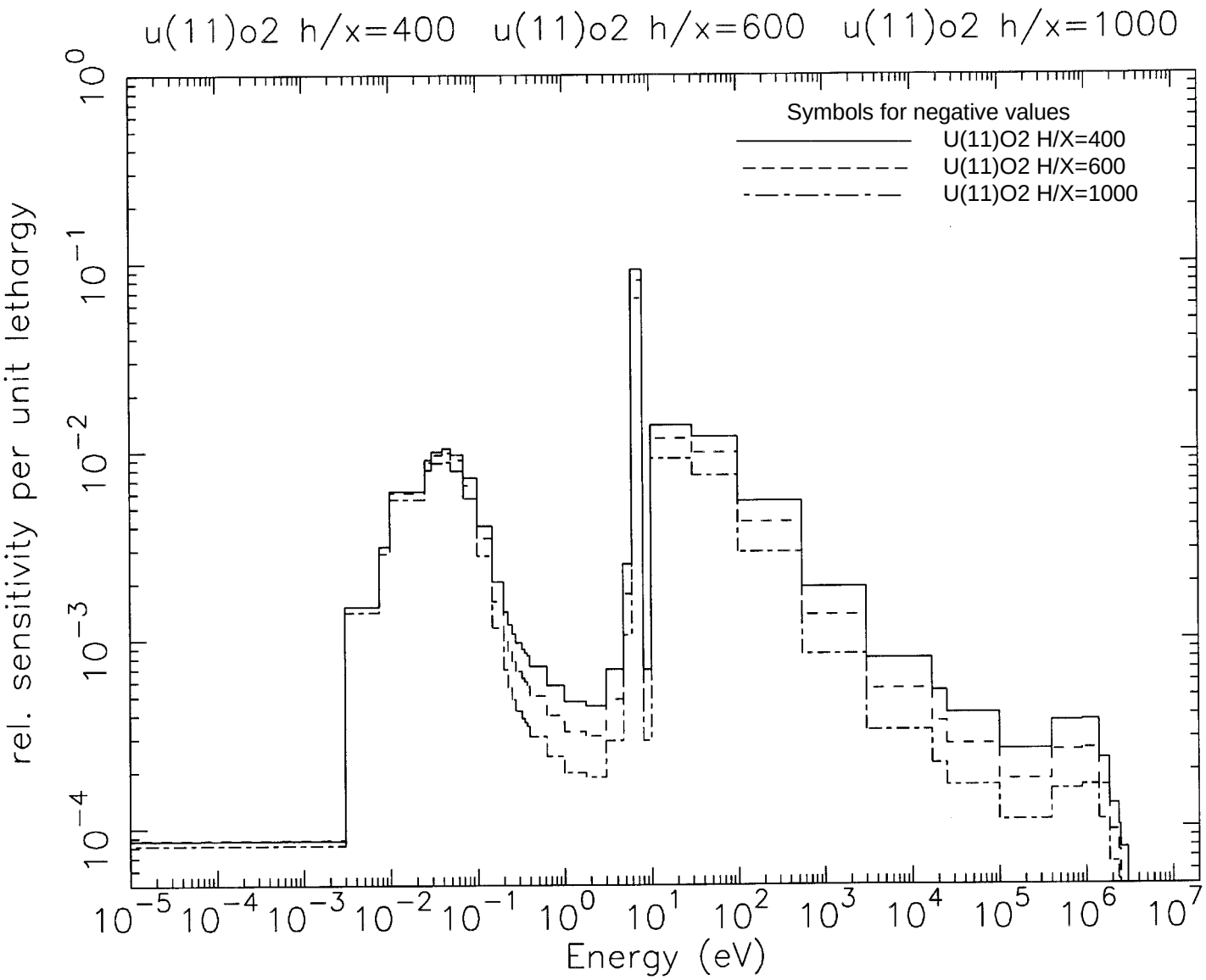

Figure 14 Comparison of ^{238}U-capture sensitivity profiles for U(11)O_2 systems with H/X values of 400, 600, and 1000

2.2.3 Hydrogen Total Cross Section

Lastly, the hydrogen sensitivity plots and their trends with respect to the systems H/X values were examined. If the previously mentioned "rules-of-thumb" hold, the prediction can be made that for H/X values of about 100 to 1000, the systems should largely be very similar with respect to hydrogen cross sections due to the linear behavior of the total sensitivity trends shown in Figures 1 and 2. In Figure 15, the hydrogen sensitivity profiles are given for H/X values of 195, 614, and 972 for the $U(2)F_4$ systems. At first glance these systems would appear to have large spectral changes. However, these plots are constructed differently from the previously reported plots and therefore require a slightly different interpretation. These plots give the sensitivity of the system k_{eff} to the hydrogen *total* cross section. In these cases the sensitivity to the total cross section is essentially the sum of the sensitivities of the scattering and capture cross sections. The scattering sensitivities are generally positive, whereas the capture sensitivities are always negative. Hence, the "spectral" changes are due to changes in the relative magnitudes of the scattering and capture components as the system goes from under-moderated to over-moderated. The "spectra" for individual scattering and capture components remain essentially unchanged as a function of H/X. The same conclusions can be reached for the comparison of hydrogen sensitivity profiles for the systems $U(2)F_4$ with H/X of 195 and $U(5)_3O_8$ with H/X values of 147 and 757 shown in Figure 16.

The hydrogen sensitivity comparisons for the $U(11)O_2$ systems are shown in the following figures: H/X values of 3 and 5 (Figure 17); H/X values of 10, 20, and 40 (Figure 18); H/X values of 80, 200, and 300 (Figure 19); and H/X values of 400, 600, and 1000 (Figure 20). For each figure, the individual scattering and capture sensitivity profiles appear to have relatively constant spectral shapes, giving rise to the conclusion of very similar systems with respect to the hydrogen cross sections. Indeed, for the individual scattering and capture portions, the spectral shapes of these sensitivity profiles are relatively constant over *most* of the H/X range from about 10 to 1000.

2.2.4 Summary

Analyses such as the preceding studies of Sections 2.2.1–2.2.3 are essential for understanding interaction mechanisms in the systems and are also valuable in determining the similarities between systems. However, for general validation studies, it is hoped that more concise methods could be developed to convey the same information in a more compact manner. These studies for more concise methods are described in Section 5.

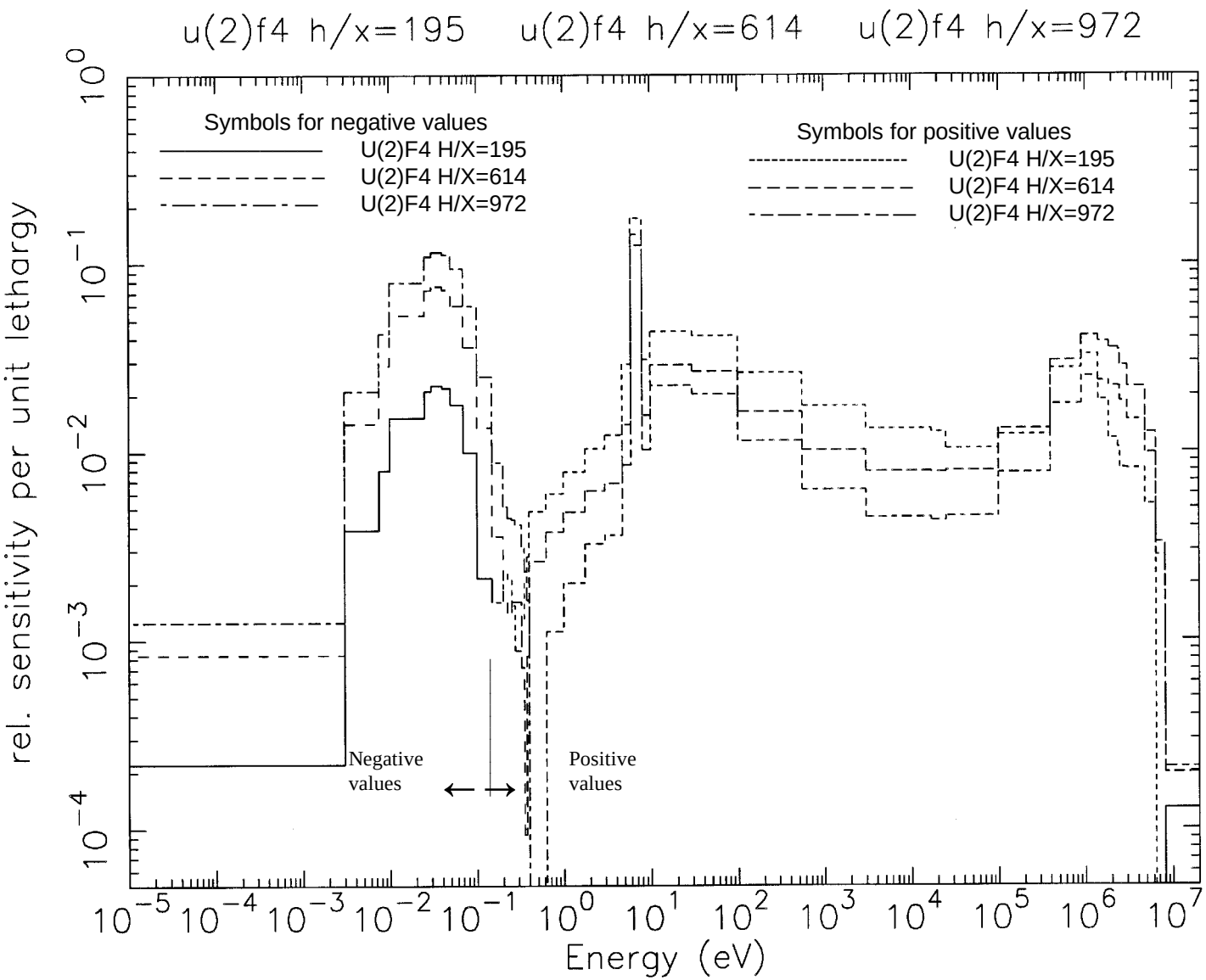

Figure 15 Comparison of H total cross-section sensitivity profiles for $U(2)F_4$ systems with H/X values of 195, 614, and 972

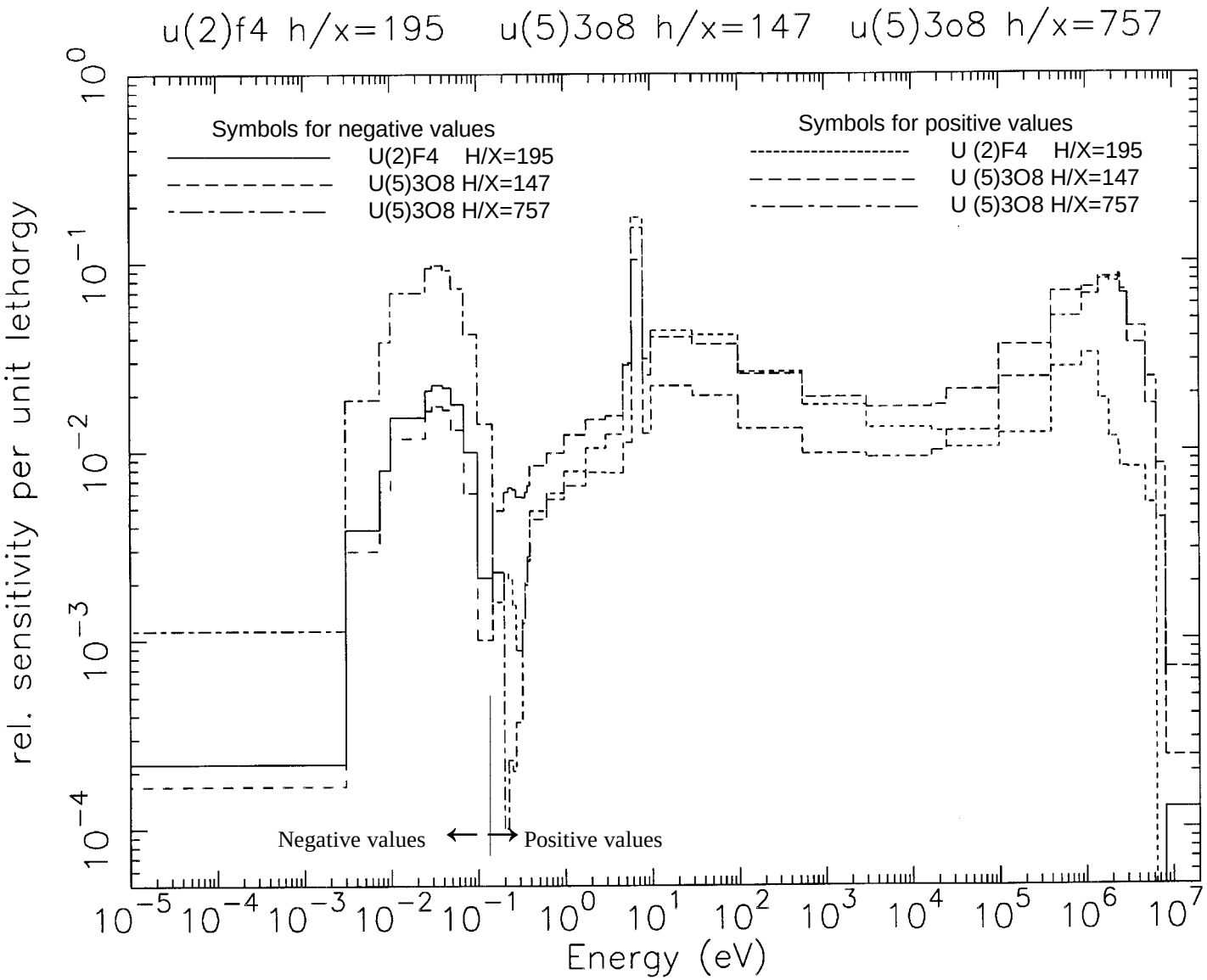

Figure 16 Comparison of H total cross-section sensitivity profiles for $U(2)F_4$ H/X = 195, and $U(5)_3O_8$ H/X = 147 and 757

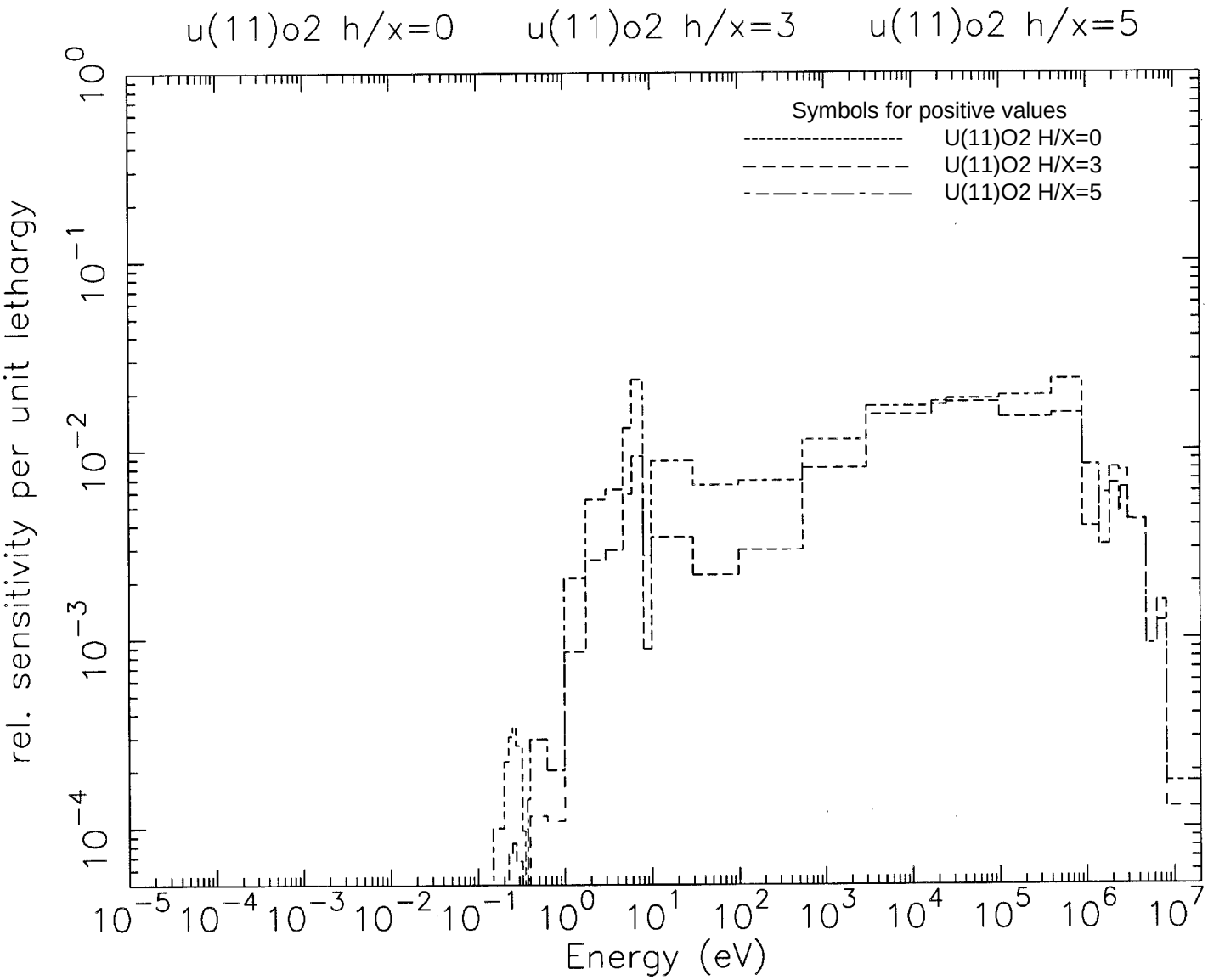

Figure 17 Comparison of H total cross-section sensitivity profiles for $U(11)O_2$ systems with H/X values of 0, 3, and 5

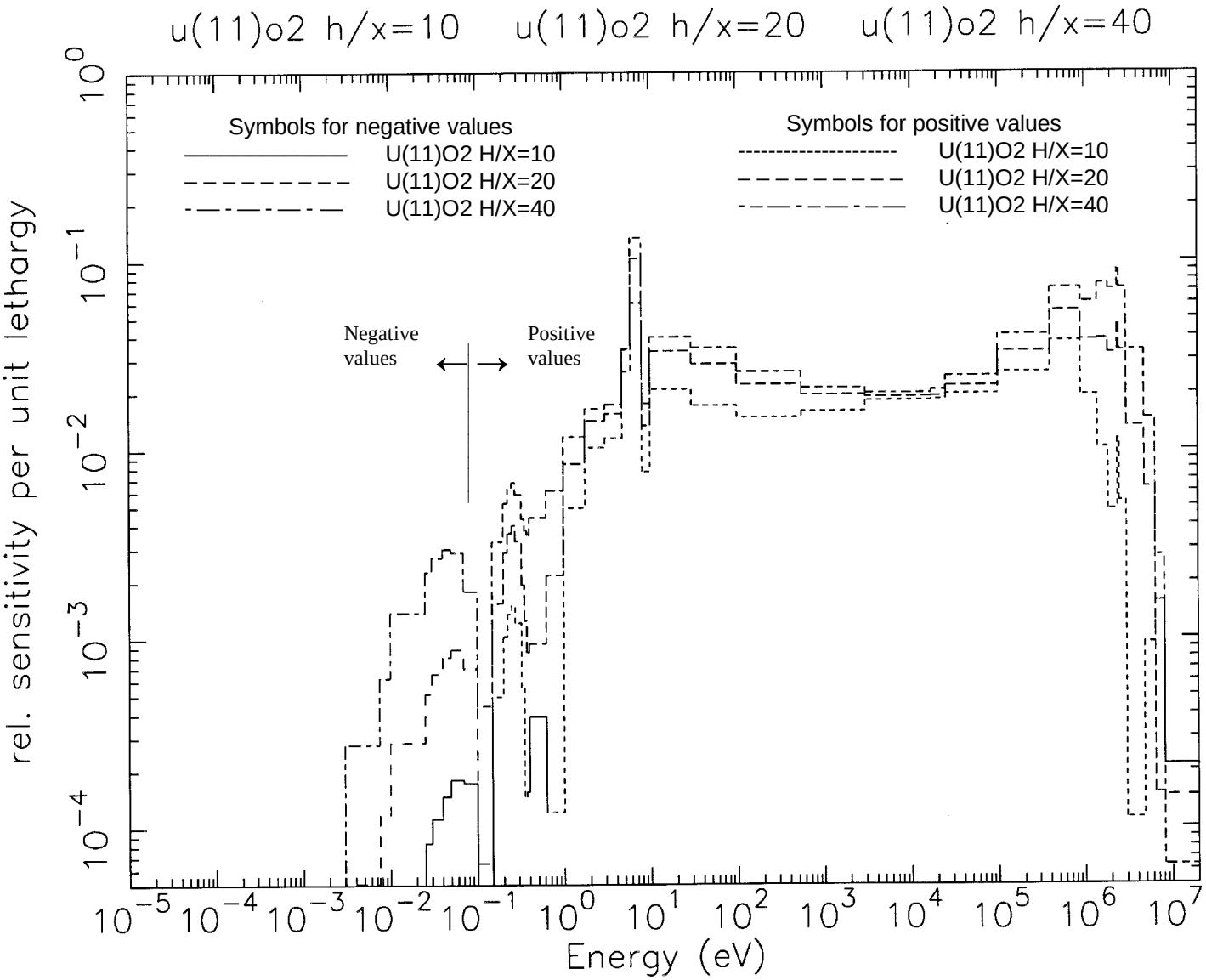

Figure 18 Comparison of H total cross-section sensitivity profiles for $U(11)O_2$ systems with H/X values of 10, 20, and 40

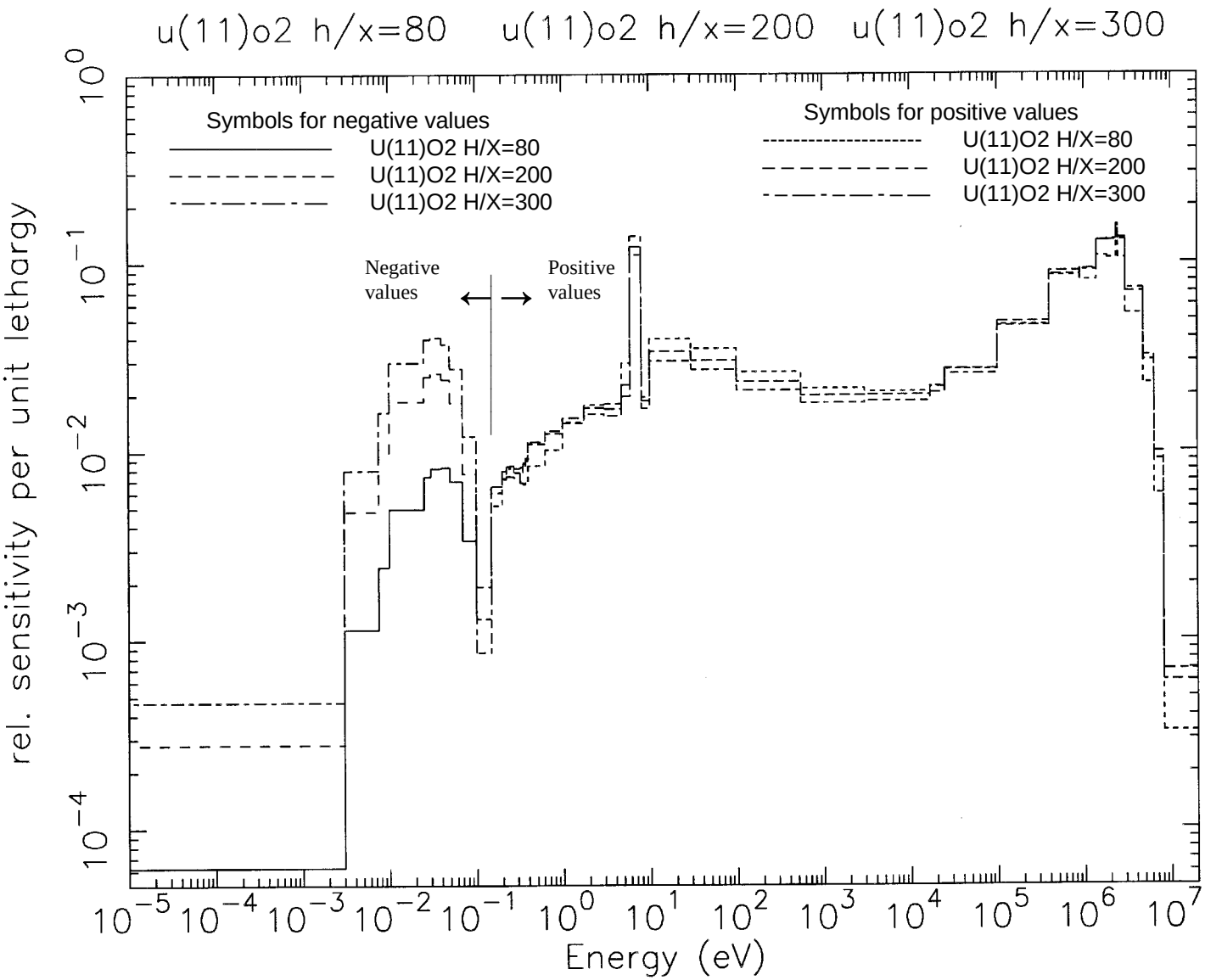

Figure 19 Comparison of H total cross-section sensitivity profiles for $U(11)O_2$ systems with H/X values of 80, 200, and 300

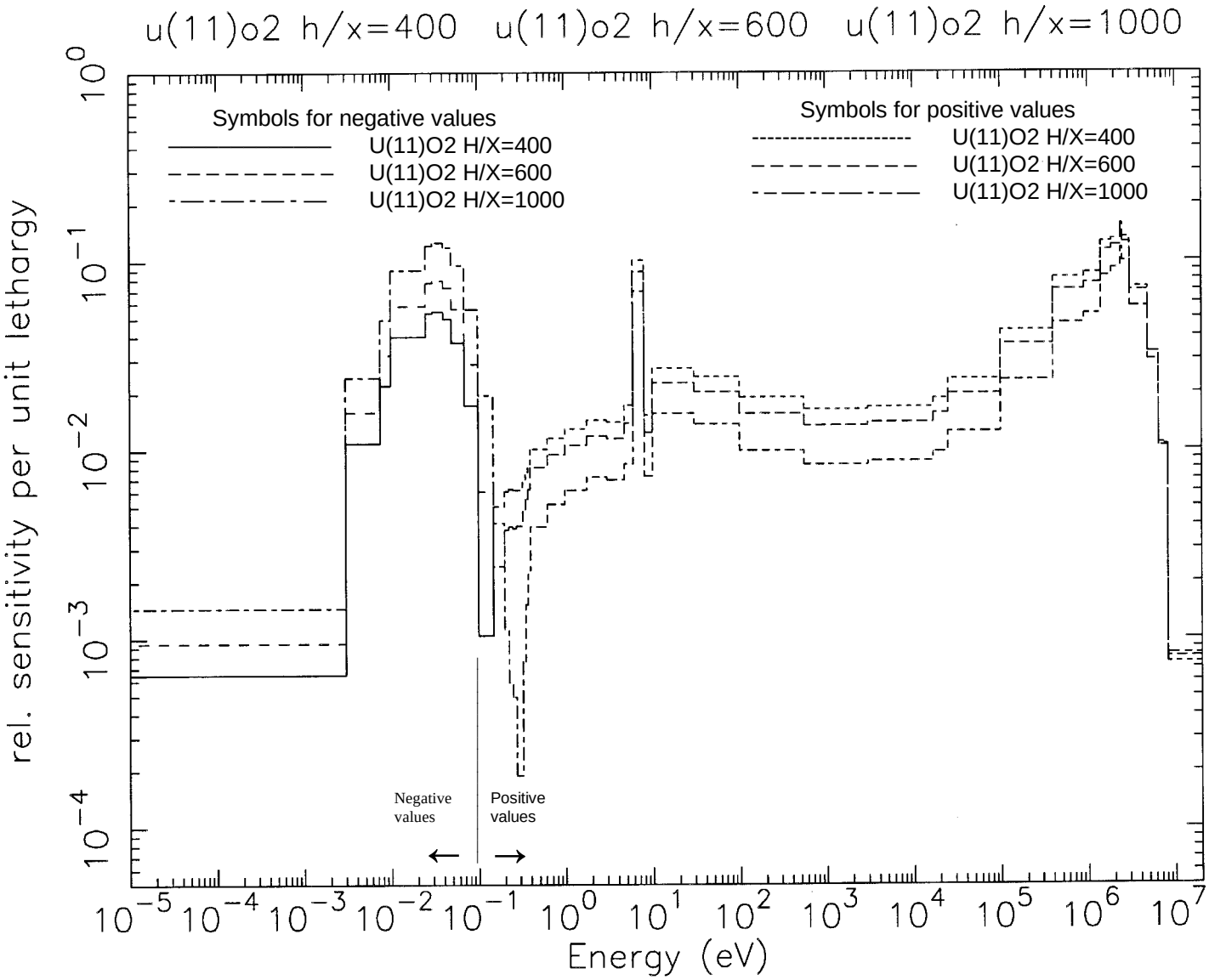

Figure 20 Comparison of H total cross-section sensitivity profiles for $U(11)O_2$ systems with H/X values of 400, 600, and 1000

3 UNCERTAINTY ANALYSIS THEORY

The determination of uncertainties in the calculated values of the system multiplication factor is accomplished by two steps: the estimation/processing of uncertainties in the underlying cross-section data and the propagation of those uncertainties to the system k_{eff} value. The techniques for processing cross-section uncertainty data are well-known[17, 18] and will be discussed here only briefly.

The two primary cross-section covariance processing codes, PUFF-2[17] and NJOY,[18] use very similar techniques. These codes are designed to read the covariance information from the ENDF/B files (typically files 31 and 33) and process it into a user-defined group structure. The codes generate an energy "supergrid," which is the combination of the energy group structures of the ENDF/B data, the processed cross-section data, and the user-defined energy grid. The covariance information contained in the ENDF/B data is then *expanded* onto the energy supergrid by assuming the *relative* uncertainty is constant over each ENDF/B group. This allows the relative variances to be generated onto the supergrid. The final step is to *collapse* the supergrid to the user-defined grid via the same weight functions that are used in the cross-section collapse. These techniques are appropriate for the so-called smooth cross sections in files 1 and 3. However, for the resonance region an alternative approach is used.

In the resonance region, the resonance parameter uncertainties (given in file 32) are propagated to the groupwise resonance self-shielded cross sections using an approximate technique suggested in Ref. 17. This technique is limited to the single-level Breit-Wigner formulation of the resonance cross sections. The procedure uses simple formulae to predict the area under each resonance. By differentiating these formulae, the sensitivity coefficients of the resonance area to the individual resonances parameters are obtained. These sensitivity coefficients are then used to propagate the resonance parameter uncertainties to the resonance area, hence to the groupwise cross section. The entire resonance area, and hence its uncertainty, is assumed to be contained within a single group. The correlations between groups are assumed to be zero using this technique. A previous study[19] compared this approximate technique with direct perturbations. In that work, general agreement is seen for many cases. In some cases there are large differences seen in the predicted and actual sensitivities, even opposite signs. Improvements need to be made in the existing procedures in order to correctly treat the impact of changes in self-shielding.

Additional work is currently under way to remedy some of the limitations with respect to the resonance parameter uncertainty treatment. Some of these studies have been reported[20] and will be incorporated into the current analyses when the decision to use later cross-section libraries is made. The cross-section libraries used in this study are based on ENDF/B-V since an ENDF/B-VI multigroup cross-section library pertinent to criticality safety applications is not available, therefore the use of the data covariances based on later versions of ENDF/B are judged to be inappropriate.

Using uncertainty information for the cross sections for the nuclides and reaction processes that are available, it is possible to estimate the uncertainty in the system multiplication factor due to these data uncertainties. Denoting the matrix of uncertainty information for all of the cross sections as $C_{\alpha\alpha}$ and the sensitivity matrix relating changes in each constituent material and process to the system k_{eff} as S_k, the uncertainty matrix for the system k_{eff} values, C_{kk}, is given as:

$$C_{kk} = S_k C_{\alpha\alpha} S_k^{\dagger} . \tag{9}$$

The S_k matrix is I × N, where I is the number of critical systems being considered, N is the number of nuclear data parameters in the problem. Typically, N is the number of nuclide/reaction processes times the number of energy groups. The $C_{\alpha\alpha}$ matrix is an N × N matrix, with the resulting symmetrical C_{kk} matrix, which is I × I. The C_{kk} matrix consists of variance values, (i.e., the standard deviation squared), σ_i^2, for each of the critical systems under consideration (the diagonal elements), as well as the so-called "covariance" between systems $\sigma_{i,j}^2$ (the off-diagonal

elements). See Appendix A for a discussion of these variance and covariance definitions. These off-diagonal elements represent the shared or common variance, hence the term covariance, between any two of the various systems. For presentation, these off-diagonal elements are typically divided by the square root of the corresponding diagonal elements (i.e., the respective standard deviations) to generate a correlation coefficient matrix. Thus, the c_k coefficients are defined as, $c_k^{ij} = \sigma_{i,j}^2 / \sigma_i \sigma_j$, such that each c_k^{ij} value represents the correlation coefficient between uncertainties in system i and system j. Note that the ij notation is omitted in the remainder of this report. These correlations arise due to the fact that the k_{eff} values for two different systems are both functions of the same underlying random variables. The underlying random variables are the evaluated nuclear data for each nuclide. Systems with the same materials and similar spectra would be strongly correlated, while systems with different materials or differing spectra would be weakly correlated. The physical interpretation of the correlation matrix is the following: a value of zero represents no correlation between the systems, a value of unity represents full correlation between the systems, and a value of −1 represents a full anticorrelation. A k_{eff} correlation matrix for eight of the critical benchmarks described earlier (i.e., 6-$U(2)F_4$, 2-$U(5)_3O_8$) is given in Table 1. Since the diagonal elements are unity, each diagonal element is replaced by the corresponding fractional standard deviation representing the uncertainty in the calculated k_{eff} value.

Table 1 Cross-correlation coefficients[a] (due to cross sections) for k_{eff} of 2% and 5% systems

Critical system	2%(195)	2%(294)	2%(406)	2%(496)	2%(614)	2%(972)	5%(147)	5%(757)
2% H/X = 195	**0.0158**							
2% H/X = 294	0.9884	**0.0139**						
2% H/X = 406	0.9729	0.9896	**0.0129**					
2% H/X = 496	0.9556	0.9801	0.9908	**0.0122**				
2% H/X = 614	0.9269	0.9605	0.9782	0.9880	**0.0116**			
2% H/X = 972	0.8019	0.8560	0.8886	0.9177	0.9499	**0.0110**		
5% H/X = 147	0.8604	0.8624	0.8467	0.8383	0.8242	0.7521	**0.0128**	
5% H/X = 757	0.7276	0.7713	0.7961	0.8153	0.8335	0.8373	0.7795	**0.0093**

[a]Note the diagonal elements give the fraction standard deviation since the diagonal correlation coefficient is defined as unity.

The standard deviation values shown in Table 1 range from 0.93 to 1.58%. The highest uncertainties correspond to the lowest H/X values due to the fact that a harder spectrum enhances the sensitivity to the higher-energy cross sections, which are usually less well known than the thermal values. Note that the correlation coefficients, denoted as c_k, are all 0.71 or higher, indicating that most of these systems are similar to each other. Another way of looking at the 0.71 coefficient is that 71% or more of the variance is common to all these systems. Thus, these systems are expected to behave in a very similar manner with respect to bias and uncertainty determinations for the SCALE 44-group cross-section library on which these results are based. Shown in Table 2 is a correlation matrix for the 14 - $U(11)O_2$ artificial systems discussed earlier. The trends in standard deviation are replicated here with a peak uncertainty of 1.92% for an H/X of 0, going down to 0.87 for an H/X of 1000. Looking at these values with a c_k criterion of 0.8 or greater indicating similar systems leads to conclusions nearly identical to those based on a comparison of the sensitivity profiles. For example, the H/X of 0 system is only similar to the H/X of 3 system and then only marginally, so c_k is 0.8328. We see that for H/X values between 5 and 40, the similar systems include

Table 2 Cross-correlation coefficients[a] (due to cross sections) for k_{eff} of 11% systems

Critical system	11%-0	11%-3	11%-5	11%-10	11%-20	11%-40	11%-80	11%-200	11%-300	11%-400	11%-500	11%-600	11%-800	11%-1000
11% H/X = 0	**0.0191**													
11% H/X = 3	0.8328	**0.0185**												
11% H/X = 5	0.7379	0.9818	**0.0188**											
11% H/X = 10	0.6011	0.9205	0.9725	**0.0188**										
11% H/X = 20	0.4887	0.8409	0.9161	0.9784	**0.0176**									
11% H/X = 40	0.4067	0.7562	0.8403	0.9253	0.9763	**0.0151**								
11% H/X = 80	0.3428	0.6585	0.7392	0.8327	0.9094	0.9698	**0.0128**							
11% H/X = 200	0.2800	0.5240	0.5888	0.6760	0.7696	0.8705	0.9526	**0.0106**						
11% H/X = 300	0.2633	0.4751	0.5315	0.6115	0.7058	0.8157	0.9148	0.9832	**0.0099**					
11% H/X = 400	0.2557	0.4452	0.4953	0.5687	0.6604	0.7727	0.8798	0.9668	0.9846	**0.0095**				
11% H/X = 500	0.2517	0.4329	0.4688	0.5359	0.6235	0.7349	0.8453	0.9448	0.9717	0.9845	**0.0091**			
11% H/X = 600	0.2490	0.4076	0.4482	0.5097	0.5927	0.7014	0.8123	0.9200	0.9543	0.9742	0.9847	**0.0089**		
11% H/X = 800	0.2432	0.3755	0.4076	0.4567	0.5278	0.6265	0.7331	0.8514	0.8991	0.9330	0.9576	0.9734	**0.0087**	
11% H/X = 1000	0.2353	0.3452	0.3697	0.4071	0.4652	0.5509	0.6484	0.7702	0.8277	0.8731	0.9097	0.9367	0.9752	**0.0087**

[a]Note the diagonal elements give the fraction standard deviation since the diagonal correlation coefficient is defined as unity.

only the two or three neighboring systems with either higher or lower H/X values. For systems with H/X values of 80 to 1000, the systems are typically similar to the nearest three or four neighboring systems. Based on these observations, these systems appear to be similar if the H/X values are within about a factor 5 of each other.

The explicit comparison of sensitivity profiles performed earlier did not examine quantitatively the similarities of low-enriched systems (2–5 wt %) with the $U(11)O_2$ system. Table 3 gives a comparison of c_k values for these systems for comparison. These results give indications that the 2- and 3-wt % systems are only marginally similar to the 11-wt % systems. For systems with similar H/X values, the 2- and 3-wt % systems typically have a c_k value of only 0.75 with respect to the 11-wt % systems. For the 5-wt % systems and H/X values near to those of the 11-wt % systems, c_k values are already above 0.80, indicating similarity. Of course such a comparison is not possible for H/X values below about 100, where criticality is not possible for enrichments of 2–5 wt %.

These c_k values are judged to be most appropriate for correlation with error trends in a criticality safety validation analysis because they are essentially the sensitivities to the individual cross sections weighted by their uncertainties. Thus, the c_k values represent the systems similarity with respect to materials with highest sensitivity/uncertainty combination. For determination of the similarity of systems with respect to each material/reaction process it would be useful to have additional parameters that are more differential in nature. These additional parameters will be discussed in Section 5.

Table 3 Comparison of correlation coefficients[a] (due to cross sections) for k_{eff} of 2%, 3%, 5%, and 11% systems

Critical system	2%-294	2%-406	2%-496	2%-614	2%-972	3%-133	3%-277	5%-757	11%-200	11%-300	11%-400	11%-500	11%-600	11%-800
2% H/X = 294	**0.0139**													
2% H/X = 406	0.9896	0**.0129**												
2% H/X = 496	0.9801	0.9908	**0.0122**											
2% H/X = 614	0.9605	0.9782	0.9880	**0.0116**										
2% H/X = 972	0.8560	0.8886	0.9177	0.9499	**0.0110**									
3% H/X = 133	0.8752	0.8489	0.8341	0.8133	0.7297	**0.0157**								
3% H/X = 277	0.8564	0.8453	0.8400	0.8294	0.7666	0.8396	**0.0129**							
5% H/X = 757	0.7713	0.7961	0.8153	0.8335	0.8373	0.7137	0.7733	**0.0093**						
11% H/X = 200	0.7575	0.7596	0.7621	0.7599	0.7142	0.7440	0.7633	0.7892	**0.0106**					
11% H/X = 300	0.7391	0.7504	0.7589	0.7634	0.7330	0.7114	0.7496	0.8170	0.9832	**0.0099**				
11% H/X = 400	0.7248	0.7429	0.7561	0.7663	0.7491	0.6870	0.7383	0.8383	0.9668	0.9846	**0.0095**			
11% H/X = 500	0.7116	0.7354	0.7526	0.7675	0.7622	0.6661	0.7273	0.8544	0.9448	0.9717	0.9845	**0.0091**		
11% H/X = 600	0.6992	0.7274	0.7478	0.7667	0.7716	0.6478	0.7164	0.8652	0.9200	0.9543	0.9742	0.9847	**0.0089**	
11% H/X = 800	0.6667	0.7027	0.7290	0.7554	0.7805	0.6052	0.6858	0.8736	0.8514	0.8991	0.9330	0.9576	0.9734	**0.0087**
11% H/X = 1000	0.6282	0.6699	0.7004	0.7326	0.7747	0.5601	0.6481	0.8639	0.7702	0.8277	0.8731	0.9097	0.9367	0.9752

[a]Note the diagonal elements give the fraction standard deviation since the diagonal correlation coefficient is defined as unity.

4 GENERALIZED LINEAR-LEAST-SQUARES METHODOLOGY

The GLLSM has been referred to as a data adjustment procedure, a data consistency analysis, and even a data evaluation technique. The most appropriate description of GLLSM for this particular application would be that of a generalized trending analysis tool. Physically the GLLSM is designed to minimize differences between the measured and calculated values of k_{eff} for the entire set of experiments used in the data validation process. The "data changes" that result from the application of the GLLSM can then be used to predict the biases and associated uncertainties for *any* application determined to be similar to the benchmark area of applicability. Functionally, the GLLSM can be thought of as a trending of a suite of critical benchmarks with respect to the cross-section correlation coefficient between the various systems. The GLLSM has the capability to identify experiments that contain inconsistencies (i.e., the magnitude of the measured-to-calculated k_{eff} difference is larger than their combined uncertainties). A χ^2 consistency indicator is used to directly predict the overall consistency of the suite of benchmarks, a value of χ^2 for each experiment is also available from the GLLSM tool.

This present work utilizes GLLSM procedures based on those introduced by Gandini,[21] Dragt et al.,[22] and Barhen, Wagschal, and Yeivin.[23,24] The derivation of the GLLSM equations in this work follows the general notation from Ref. 25, however, the full derivations are included in Appendix B for completeness. The vector $m \equiv (m_i)$, i = 1, 2, ... I, represents a series of k_{eff} measurements on critical benchmark experiments that are to be used in the validation of a dataset for criticality safety computations. This vector m has a corresponding symmetric I × I uncertainty matrix associated with it, which is denoted as $C_{mm} \equiv \mathrm{cov}(m_i,m_j) \equiv \langle\delta m_i \delta m_j\rangle$. Further, the vector $k \equiv (k_i)$ is denoted as the corresponding series of calculated values of k_{eff} for each of these experiments. The vector $\alpha \equiv (\alpha_n)$, n = 1, 2, ... N, with its corresponding symmetric N × N uncertainty matrix $C_{\alpha\alpha} \equiv \mathrm{cov}(\alpha_n\alpha_m) \equiv \langle\delta\alpha_n\delta\alpha_m\rangle$, represents the differential data used in the calculations (i.e., nuclear data such as fission, capture, and scattering cross sections, the fission spectrum and other problem parameter data) and, additionally, the material densities used in the problem description. This procedure also allows for the possibility of correlations between the integral and differential quantities, which may be present at times in the analysis. These correlations are denoted by the N × I covariance matrix $C_{\alpha m} \equiv \langle\delta\alpha_n\delta m_i\rangle$.

The sensitivities of the calculated k_{eff} to the α parameters are given as $S_k \equiv \partial k_i/\partial\alpha_n$, with S_k being an I × N matrix. Representing perturbation of the α parameters as linear changes in the calculated k_{eff} value, yields the following:

$$k(\alpha') = k(\alpha + \delta\alpha) = k(\alpha) + \delta k \simeq k(\alpha) + S_k\delta\alpha \ , \tag{10}$$

with the corresponding uncertainty matrix of the calculated values of

$$C_{kk} \equiv \langle\delta k_j\delta k_j\rangle = S_k\langle\delta\alpha_n\delta\alpha_m\rangle S_k^{\dagger} = S_k C_{\alpha\alpha} S_k^{\dagger} \ . \tag{11}$$

If the deviations of the calculated values from their corresponding measured responses is denoted by the vector $d \equiv (d_i) = k(\alpha) - m$, then the uncertainty matrix for the deviation vector d, denoted by C_{dd}, is

$$\begin{aligned} C_{dd} &= C_{kk} + C_{mm} - S_k C_{\alpha m} - C_{m\alpha} S_k^{\dagger} \ , \\ &= S_k C_{\alpha\alpha} S_k^{\dagger} + C_{mm} - S_k C_{\alpha m} - C_{m\alpha} S_k^{\dagger} \ . \end{aligned} \tag{12}$$

Denoting $x = \alpha' - \alpha$, and $y = k(\alpha') - m$, we can rewrite Eq. (10) as

$$y = d + S_k x \ . \tag{13}$$

The measured k_{eff} values, m, and the measured (or evaluated from measurements) parameter values, α, both have their corresponding uncertainties. The best evaluated parameters α′ and the best evaluated values of the measurement m′ will be those values that are consistent with each other, namely $m' = k(\alpha')$, and are consistent

with their estimated values and uncertainties (i.e., in general they do not deviate more than a standard deveiation from their current best estimates m and α, respectively).

The GLLSM procedure involves minimizing the quadratic loss function

$$Q(x,y) = (y,x)^{\dagger} \begin{pmatrix} C_{mm} C_{m\alpha} \\ C_{\alpha m} C_{\alpha\alpha} \end{pmatrix}^{-1} (y,x) \ , \tag{14}$$

where $(y,x)^{\dagger} \equiv (y_1, y_2, ..., y_I, x_1, x_2, ..., x_N)$, subject to the constraint expressed by Eq. (13). Adopting the procedure of Refs. 23–25, the above conditional minimum formulation is equivalent to unconditionally minimizing the function R(x,y), where

$$R(x,y) = Q(x,y) + 2\lambda^{\dagger}(S_k x - y) \ , \tag{15}$$

and 2λ is an I-dimensional vector of Lagrange multipliers. Thus x and y satisfy the equations

$$\partial R(x,y)/\partial x = \partial R(x,y)/\partial y = 0 \ . \tag{16}$$

Solving the resulting equations for x and y, we obtain

$$\begin{aligned} \alpha' &= \alpha + (C_{\alpha m} - C_{\alpha\alpha} S_k^{\dagger}) C_{dd}^{-1} d, \text{ and} \\ m' &= m + (C_{mm} - C_{m\alpha} S_k^{\dagger}) C_{dd}^{-1} d, \end{aligned} \tag{17}$$

where C_{dd}^{-1} is the inverse of the I × I matrix C_{dd} Eq. (12) and α′ and m′ are the best estimate of the parameters and measurement within their uncertainty range.

A few observations are due here:

1. If the α′ values obtained in Eq. (17) are substituted in k(α′), using the linearity assumption of Eq. (10), the m′ value of Eq. (17) should be obtained, thus m′ = k(α′) is satisfied.

2. Moreover, not only are the new/best estimates of the cross sections and of the k_{eff} values consistent, but their uncertainties are reduced as well.

3. The minimum value of Q(x,y) is also known as χ^2, which is a measure of the consistency of the various calculated and measured responses. The value of χ^2/I should be near unity for a particular study to indicate consistency for the entire set of data.

The reduced uncertainty matrices are given by

$$C_{m'm'} = C_{mm} - C_{yy} \text{ and } C_{\alpha'\alpha'} = C_{\alpha\alpha} - C_{xx} \ , \tag{18}$$

where

$$C_{yy} = (C_{mm} - C_{m\alpha} S_k^{\dagger}) C_{dd}^{-1} (C_{mm} - S_k C_{\alpha m})$$

and

$$C_{xx} = (C_{\alpha m} - C_{\alpha\alpha} S_k^{\dagger}) C_{dd}^{-1} (C_{m\alpha} - S_k C_{\alpha\alpha}) \ . \tag{19}$$

This could of course suggest that any criticality application that is similar to the selected benchmarks should be calculated using the modified cross sections and thus have a reduced uncertainty. However, even when maintaining "conventional" criticality estimates using "established" cross sections and trend curves, the GLLSM approach can be beneficial, as will be demonstrated in the next section.

In summary, the GLLSM procedure as applied to the validation of cross-section libraries for criticality safety applications is designed to predict the data changes, x, such that the differences between measured and calculated k_{eff} values (i.e., the quantity, y) are minimized. These k_{eff} differences are the trends observed in the traditional criticality safety trending analyses. Removal of these trends and the identification of the data responsible for them are keys to the application of GLLSM techniques to criticality safety data validation.

4.1 Application of GLLSM to Validation

For a criticality safety scenario of interest (denoted the "application"), the "measurement," m_a, associated with the predicted k_{eff} values, $k(\alpha)$, does not exist. The quality of interest is the bias, which is defined as the difference between the predicted value $k(\alpha)$ and the best estimate "measurement" for the application, m_a'. Now consider rewriting Eq. (10) as:

$$k(\alpha') - m_a' = [k(\alpha) - m_a'] + S_a(\alpha' - \alpha) , \tag{20}$$

where S_a are the calculated sensitivities for the application. The solution of Eq. (17) via the GLLSM procedures allows evaluation of α'. The GLLSM theory predicts that if a sufficient number of experiments are similar to the application of interest, the calculated value of k_{eff} using the "best" cross sections, α', will indeed approach the value of the best estimate measurement for the application. Thus, $k(\alpha') \cong m_a'$ and the bias for the application can be determined to be

$$b_a = k(\alpha) - m_a' = - S_a(\alpha' - \alpha) , \tag{21}$$

where $\alpha' - \alpha$ was obtained in Eq. (17) using all similar benchmark criticality measurements.

The definitions of "similar" and "sufficient" number of experiments can now be determined by tests using actual benchmark experiments.

4.2 Testing of GLLSM with Low-Enriched U Systems

The general approach of GLLSM is the combination of information obtained in a series of integral experiments, with the aim of predicting changes in the underlying nuclear data such that differences in the calculated and measured k_{eff} values are minimized. The GLLSM techniques are useful for understanding the relative consistency of experiments in that this combination of integral experiments can be in a graded manner. An overall measure of the consistency of the GLLSM application is obtained via the use of a χ^2 analysis, thus inconsistencies between groups of experiments can be identified. Experiments in the series can also be added cumulatively in order to see the "convergence" of the technique. Using actual experiments as example "applications," trial analyses can be performed to test for convergence, where the measure of convergence is that the quantity in the left-hand side of Eq. (20) asymptotically approaches zero within the bounds of the measurement uncertainty as the number of experiments used in the GLLSM process is increased. For consistency with later applications, this absolute quantity is recast into the relative quantity (e-a)/c where e is the experimental value, m_a'; a is the adjusted calculated value, $k_a(\alpha')$; and c is the original calculated value $k_a(\alpha)$. These tests are used to help determine a minimum magnitude of c_k that represents

"similarity" or "applicability." In addition these tests help indicate the sufficient number of experiments needed for convergence by the GLLSM procedure.

4.2.1 Tests with Experimental Data

The 2 wt % and 5 wt % systems discussed earlier were chosen for further study as a demonstration application of the GLLSM procedures. For this phase of the study, the measured results from selected experiments are ignored to see if GLLSM can accurately predict observed biases, i.e., individual experiments are assumed to be the application and the process tested using an increasing number of the remaining experiments. These systems are excellent candidates since they are highly correlated with each other and consist of multiple enrichments and a fairly broad range of H/X values from 147 to 972. These systems are documented in Refs. 15 and 16 with the properties given in Tables 4 and 5. (These 3-D systems were modeled as 1-D spheres; the stated references give both the actual system dimensions and spherical model dimensions.) The uncertainties in the number densities noted in the tables were included in the analysis, along with a uniform uncertainty in the measured system multiplication factor that varied between 0.1 and 0.4% for each system.

Correlations in the material density uncertainties were established, but the measurement uncertainties of 0.1 to 0.4% were assumed to be uncorrelated between systems. The tightening of the system uncertainties (0.1%), and the loosening of the system uncertainties (0.4%) were used to test the variability of the solutions with assumptions in these quantities.

Unlike the real applications where measured values are not available, the 2% and 5% systems can serve as a good testing arena for the GLLSM predicted k_{eff} values. The convergence of the 2 wt % systems is shown in Figure 21. Here the (e-a)/c values are given as a function of the number of experiments "added" together in the GLLSM procedure. For convenience, the "0 experiments included" case assigns the calculated value to the adjusted value such that this data point gives the actual calculated-versus-experimental discrepancy. The order of adding systems into the GLLSM procedure is from low to high H/X values: the first system added has an H/X of 195, the second has an H/X of 294, and so on. The convergence toward an (e-a)/c value of 0 is seen in Figure 21, even though the convergence is incomplete. The identical situation is shown in Figure 22, except for an experimental uncertainty of 0.1%, instead of 0.4% in the results for Figure 21. The convergence is closer to 0 in Figure 22 due to the decreased flexibility in movement of the measured values, and hence greater movement of the calculated values. With the exception of the system with H/X of 972, the systems converge to approximately the same values in both Figures 21 and 22. Note that in Figures 21 and 22 the two systems with H/X values of 972 and 294 seem to have some difficulty converging. The system with an H/X value of 972 does indeed "converge" for experimental uncertainty of 0.1%, but only after the system itself is included in the adjustment. This behavior is due to the fact that this system is less correlated to the remaining systems. In Table 1, the correlation coefficients for the system with an H/X of 972 range from 0.80 – 0.95, with only two systems that have correlation coefficients greater than 0.90. While certainly these correlation coefficients should indicate similarity between these systems, it appears that they are only marginally able to produce convergence in the GLLSM scheme. The system with an H/X value of 294 is quite different, in that four of the other systems have correlation coefficients values of 0.96 or higher. The system seems to be converged, only it doesn't converge to 0. This behavior appears to be due to a slight inconsistency in this experiment (based on its χ^2 value) in relation to its companion experiments. The experiment is still valid; however, for this limited set of experiments, the system with an H/X of 294 is somewhat inconsistent with the other five systems. In Figure 23, the effect of omitting this experiment is seen, where the results are largely unchanged, thus this experiment doesn't add anything or take away any information from the combined systems.

Table 4 Properties of 2-wt % UF_4 experiments[a]

	U(2)F4-1	U(2)F4-2	U(2)F4-3	U(2)F4-4	U(2)F4-5	U(2)F4-6
Atom densities						
^{235}U (10^{20} atoms/cm^3 ± 1.2%)	1.5811	1.3303	1.1191	0.9924	0.8667	0.6232
^{238}U (10^{21} atoms/cm^3 ± 0.7%	7.6467	6.4370	5.4152	4.7998	4.1941	3.0150
H (10^{22} atoms/cm^3 ± 1.2%)	3.0864	3.9097	4.5472	4.9212	5.3187	6.0557
C (10^{22} atoms/cm^3 ± 1.2%)	1.4839	1.8797	2.1861	2.3660	2.5570	2.9114
F (10^{22} atoms/cm^3 ± 0.7%	3.1219	2.6280	2.2109	1.9596	1.7123	1.2309
Critical radius (cm)	44.91	38.50	36.38	36.36	37.67	49.65

[a]*Source*: Ref. 15.

Table 5 Properties of 5-wt % U_3O_8 experiments[a]

	$U(5)_3O_8$ H/X = 147	$U(5)_3O_8$ H/X = 245	$U(5)_3O_8$ H/X = 320	$U(5)_3O_8$ H/X = 396	$U(5)_3O_8$ H/X = 503	$U(5)_3O_8$ H/X = 757
Atom densities						
^{234}U (10^{17} atoms/cm^3 ± 0.71%	8.7460	5.8410	5.1680	4.2730	3.5050	2.3260
^{235}U (10^{20} atoms/cm^3 ± 0.71%)	2.1290	1.4220	1.2580	1.0400	0.8532	0.5663
^{238}U (10^{21} atoms/cm^3 ± 0.5%	4.0880	2.7300	2.4160	1.9970	1.6380	1.0870
H (10^{22} atoms/cm^3 ± 0.5%)	3.1220	3.4780	4.0280	4.1090	4.2960	4.2870
C (10^{22} atoms/cm^3 ± 0.5%)	1.5660	1.7440	2.0200	2.0610	2.1550	2.1500
O (10^{22} atoms/cm^3 ± 0.5%	1.3410	0.9698	0.9086	0.7926	0.6993	0.5440
Critical radius (cm)	35.563	34.106	32.383	33.158	37.67	41.214

[a]*Source*: Ref. 16.

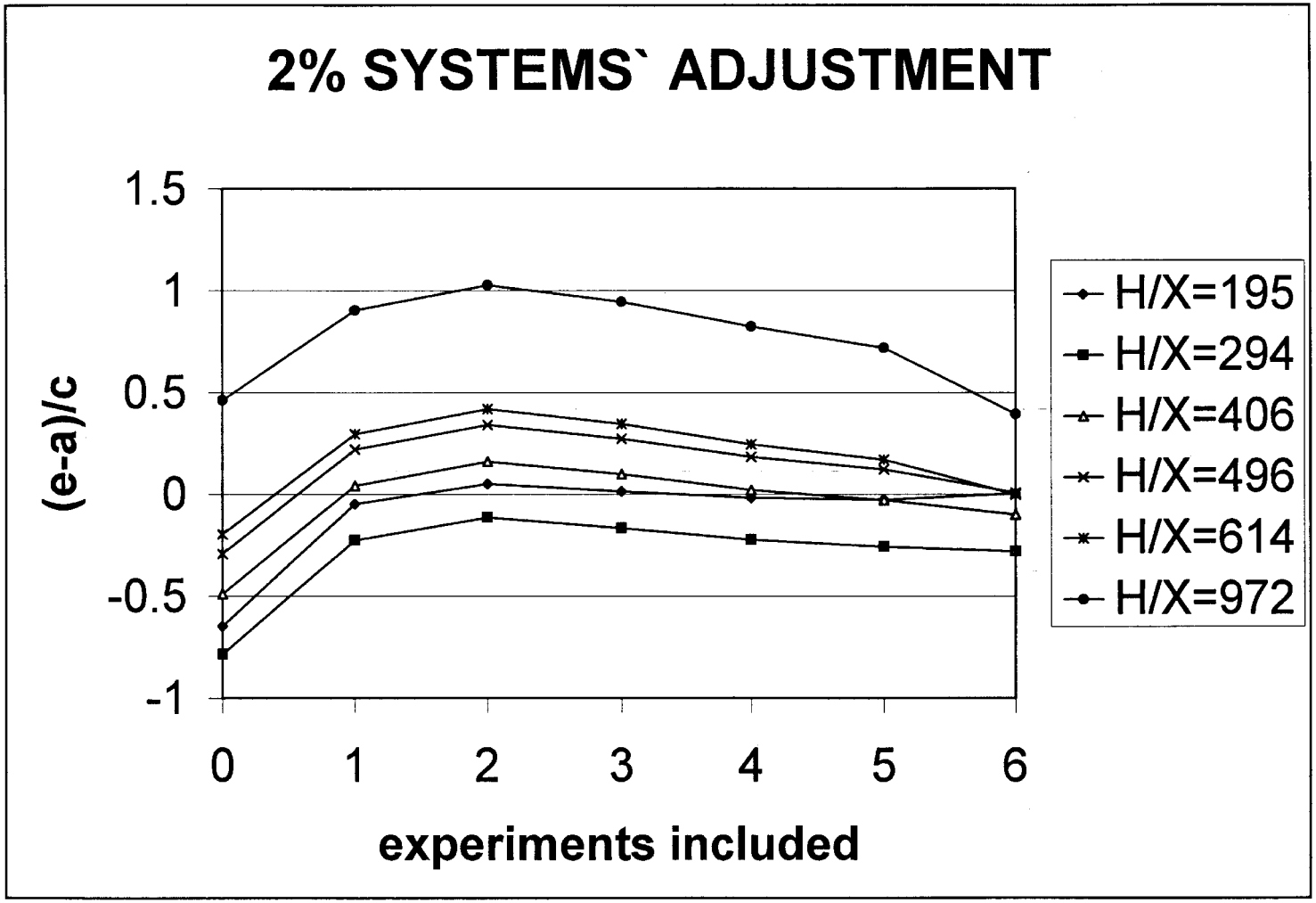

Figure 21 Predicted values of (e-a)/c as a function of the number of experiments included for 2-wt % UF_4 systems (0.4% experimental uncertainty)

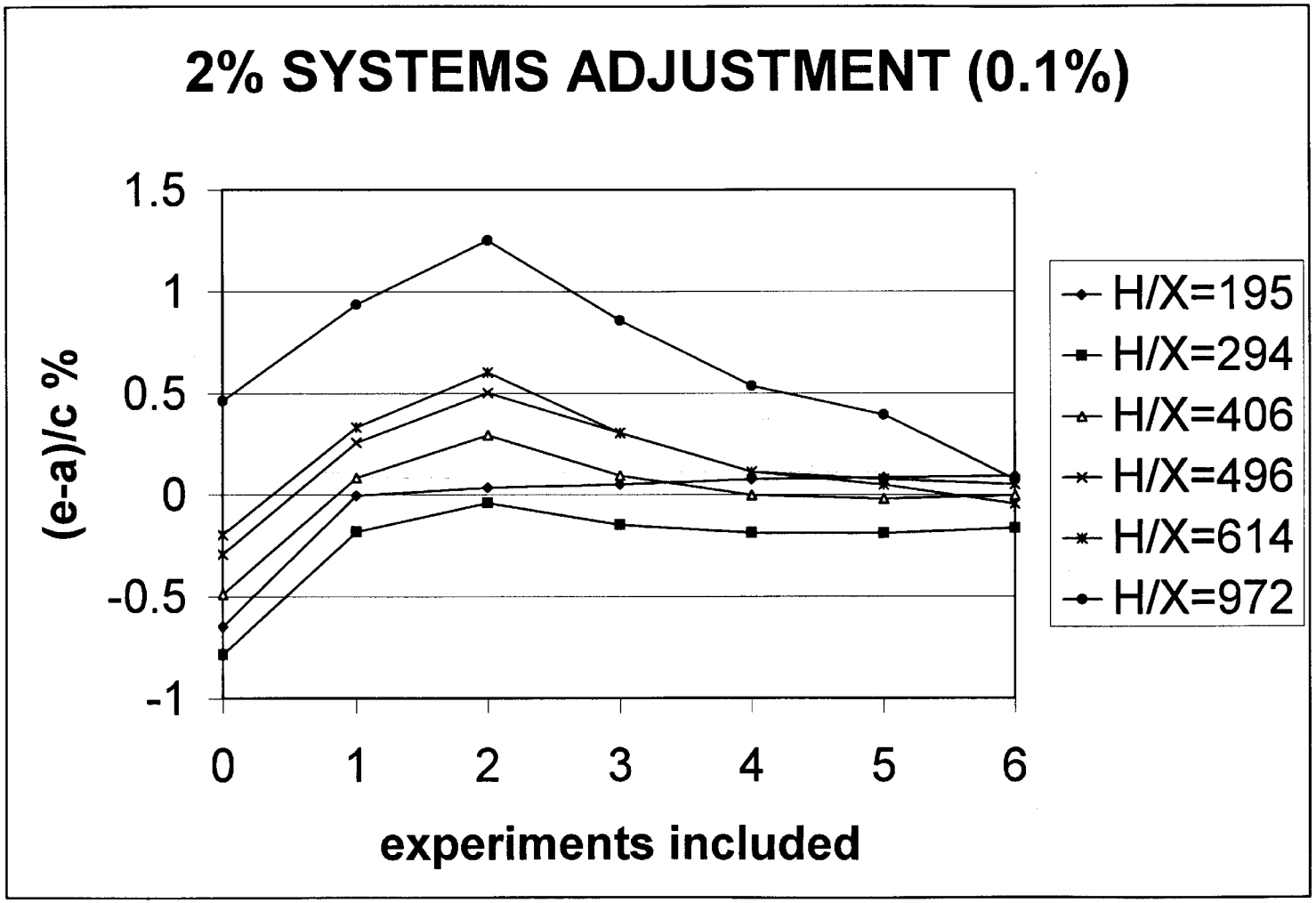

Figure 22 Predicted values of (e-a)/c as a function of the number of experiments included for 2-wt % UF_4 systems (0.1% experimental uncertainty)

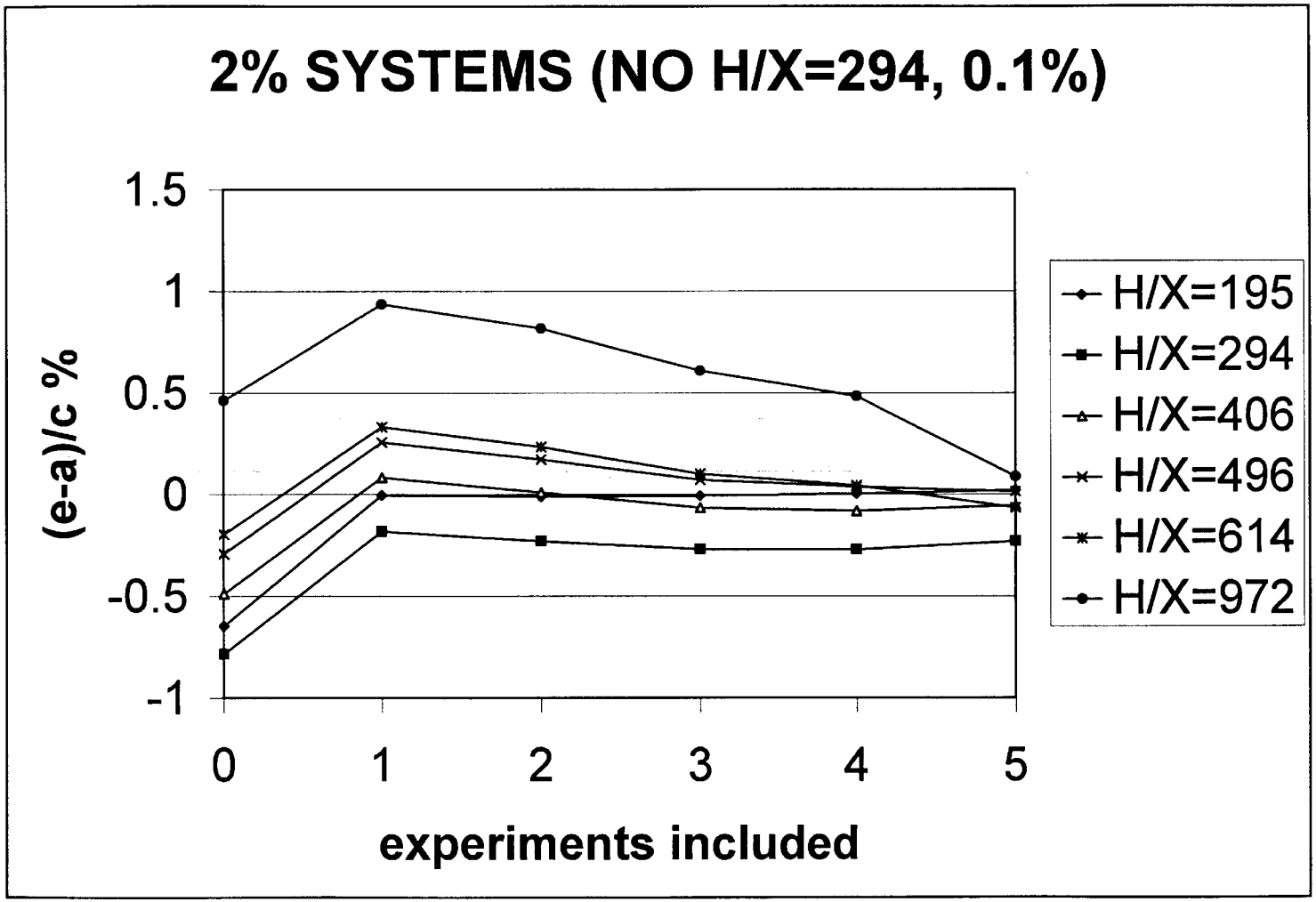

Figure 23 Predicted values of (e-a)/c as a function of the number of experiments included for 2-wt % UF_4 systems (H/X = 294 system omitted from analysis)

The examples given in Figures 21–23 for the application of GLLSM procedure to a series of 2-wt % systems are not typical for a standard analysis. They are given only to show that for very highly correlated systems, convergence can be quite rapid. The more general situation is shown in Figure 24, which shows the combined effect of the same 6 experiments, only the values to the far left of the plot correspond to the "learned" effects of some 62 other experiments. These experiments correspond to experiments 7–66, 91, 94 summarized in Table 1 of Volume 2 of this report. These 62 experiments consist of numerous low-enriched U systems, several systems with enrichments in the 10–20-wt % range and quite a few high-enriched U systems. Although this collection of critical experiments is incomplete, it is designed to demonstrate the use of GLLSM techniques on a wide variety of typical application scenarios, which will be the subject of Volume 2.

Comparison of the (e-a)/c predictions in Figure 24 between those on the far left to those of the far right reveal that for all cases, except the H/X of 972 system, the 62 other experiments are sufficient to converge the GLLSM procedure (i.e., the predicted values on the left- and right-hand sides of the figure are approximately equal to each other). In essence, there is little to no difference between the predicted differences in the 2-wt % systems, whether or not they are included in the GLLSM procedure. The H/X = 972 case does not converge.* Interestingly, the 62 other experiments do not contain a single additional system with a correlation coefficient greater than 0.9. Hence, this system still does not converge even though there are 62 systems in the procedure instead of only 6.

The key question for the H/X = 972 system is whether its failure to converge under these circumstances is due to an inconsistency or due to the lack of sufficient similar experiments in the GLLSM procedure. Even though the definitive answer to this question requires more study, the apparent answer is that with additional similar experiments included in the GLLSM procedure it would converge. This scenario is believed to be plausible since when the experiment itself is added to the GLLSM procedure, as shown in Figures 21 and 22, this case either begins to converge, or does indeed converge.

The application of the GLLSM procedure to the 5-wt % systems was also examined in a similar manner. In Figure 25, the (e-a)/c values are given for each of the 6 systems consisting of 5-wt % U_3O_8 material. Again, there is rapid convergence of the GLLSM procedure for these very highly correlated systems. In this case, 2 systems appear to be unconverged after the sequential combination of these experiments. These systems correspond to H/X values of 245 and 320. The first 3 systems (H/X of 147, 245 and 320) are all very highly correlated with correlation coefficients greater than 0.95. Thus, these 2 systems would appear to simply have inconsistencies with the remaining systems. In Figure 26, the tightening of the experimental uncertainties from 0.4% to 0.1% has little or no effect on the convergence of these experiments. Interestingly, if one assumes that the system with an H/X of 245 is inconsistent and removes it from the GLLSM procedure, the effect is shown in Figure 27, where the other 5 remaining systems converge while no effect is seen for the H/X = 245 system. Thus, it would appear from this analysis that the system with an H/X of 245 is inconsistent with the remaining systems and should be removed from the analysis if only a few experiments are available for consideration. This observation is confirmed by noting that the χ^2 value for the experiment with an H/X = 245 (its χ^2 value is much greater than unity) indicates the least consistency as compared with the remaining experiments.

The behavior of the 5-wt % systems with the inclusion of the entire 62 experimental systems was also examined. In Figure 28, the convergence of the (e-a)/c values is shown, first considering the 62-system database, followed by the addition of the 6 systems with 5-wt % enrichments. The addition of these 5-wt % systems is performed using an "optimal" procedure. The optimal sequence is defined such that the most consistent experiments are added first, followed by those which have less and less consistency. The order of inclusion from left to right is H/X

---

*Convergence is not seen for this experiment in Figure 24; however, when the experimental uncertainty is reduced to 0.1%, all of the 2% systems converge to better than 0.1% with the exception of the "troublesome" H/X = 294 which converges to only 0.15%.

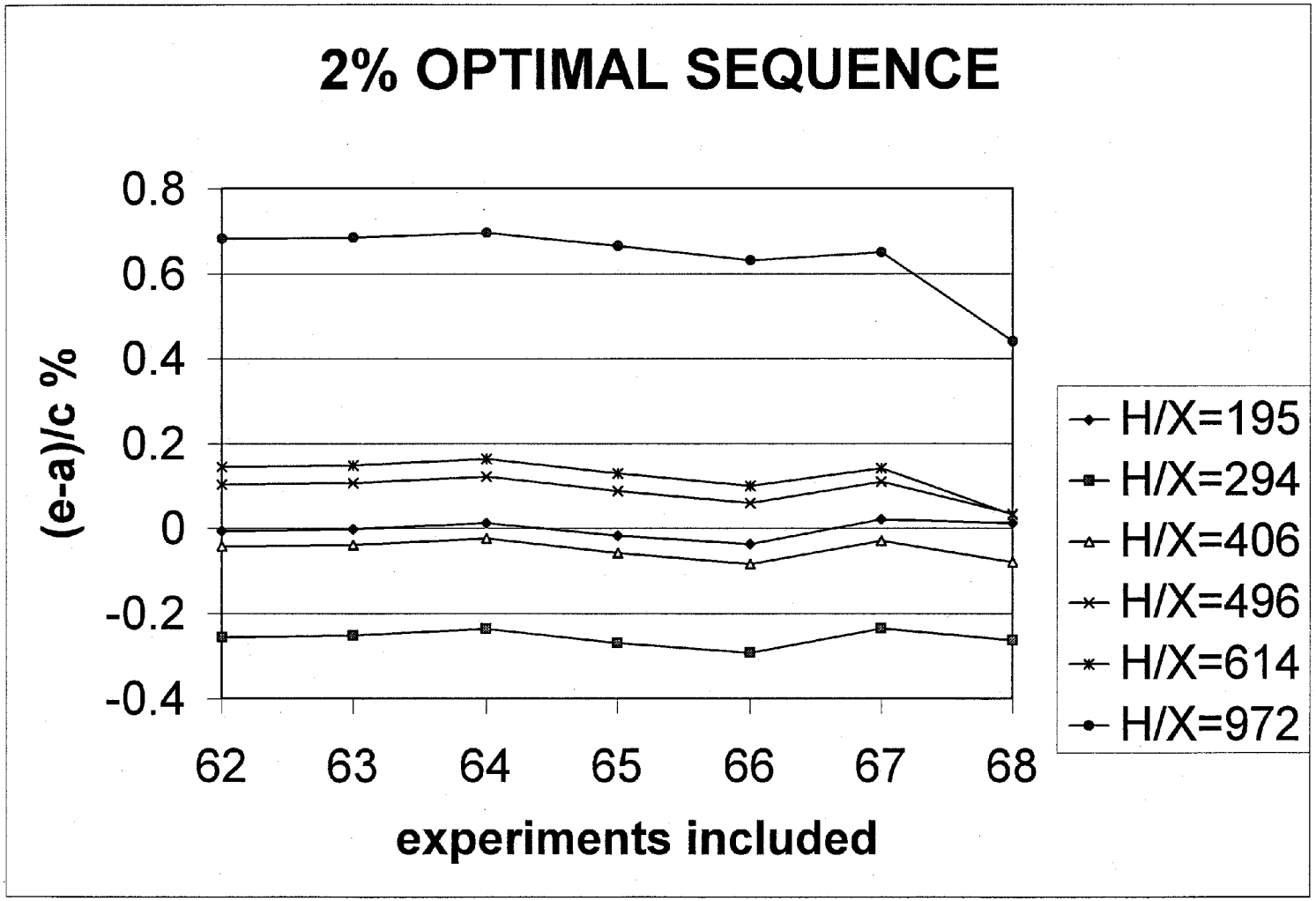

Figure 24 Predicted values of (e-a)/c as a function of the number of experiments included for 2-wt % UF_4 systems. The 2% experiments were added in the following H/X sequence: 195, 406, 496, 614, 294, 972.

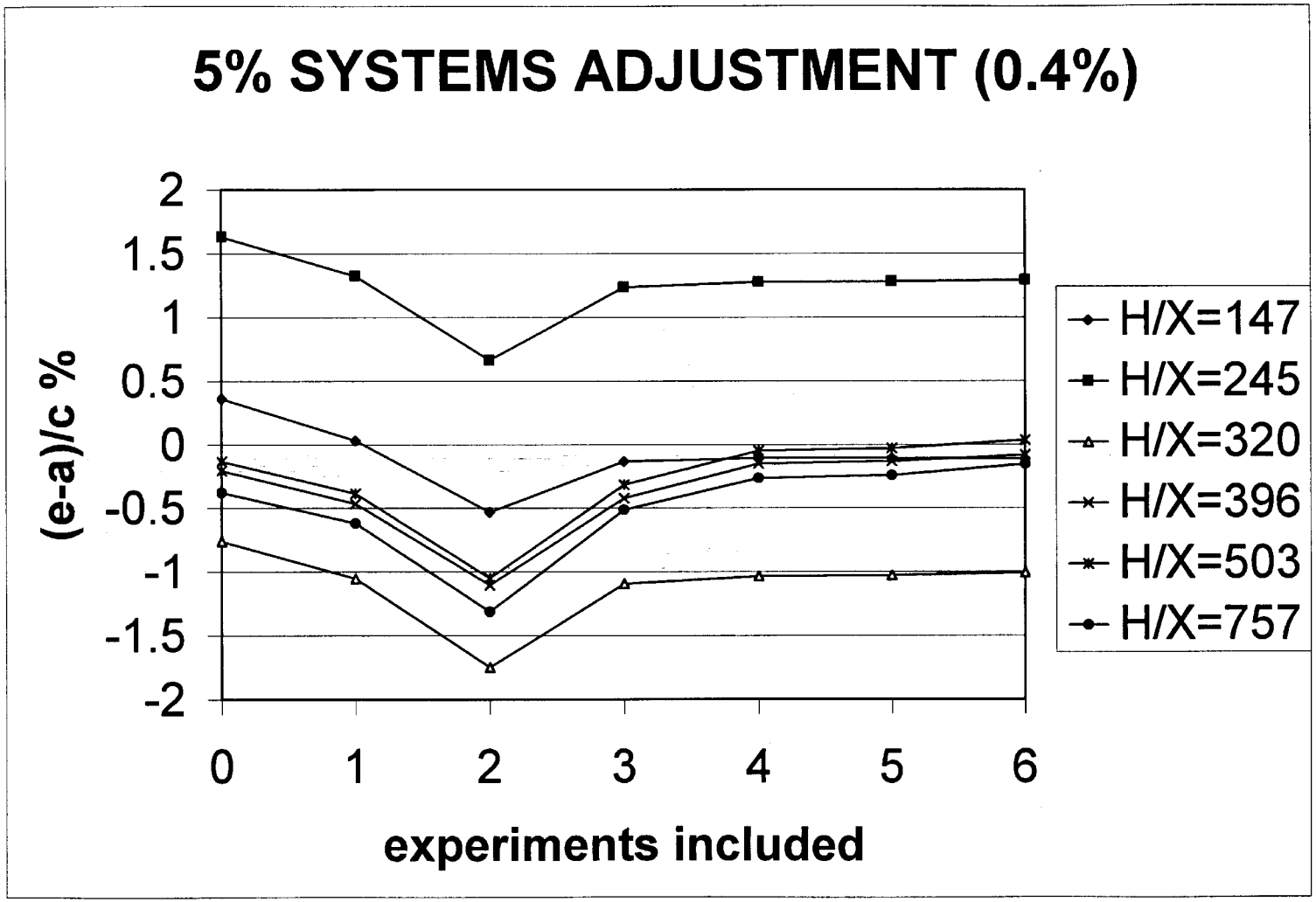

Figure 25 Predicted values of (e-a)/c as a function of the number of experiments included for 5-wt % U_3O_8 systems (0.4% experimental uncertainty)

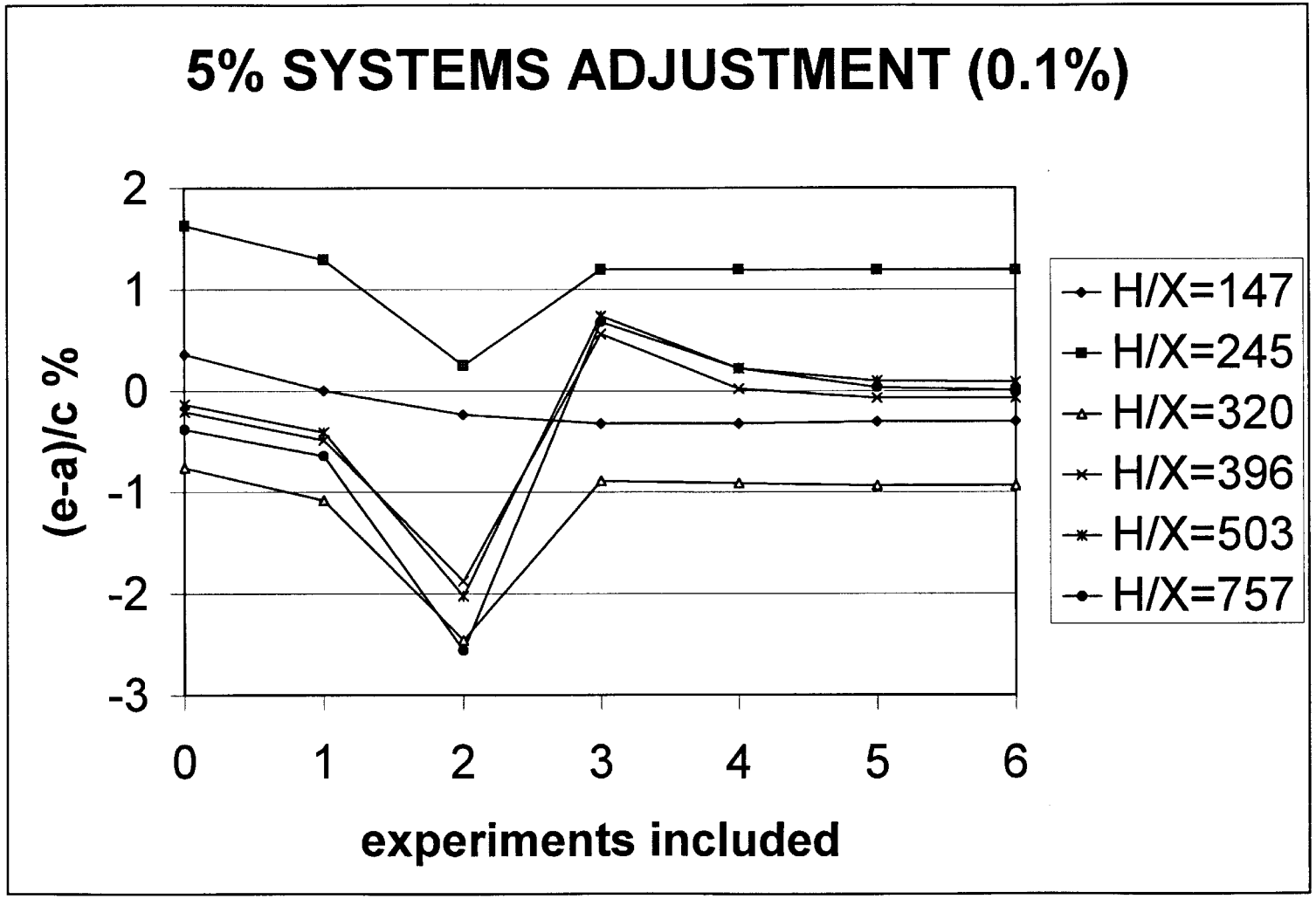

Figure 26 Predicted values of (e-a)/c as a function of the number of experiments included for 5-wt % U_3O_8 systems (0.1% experimental uncertainty)

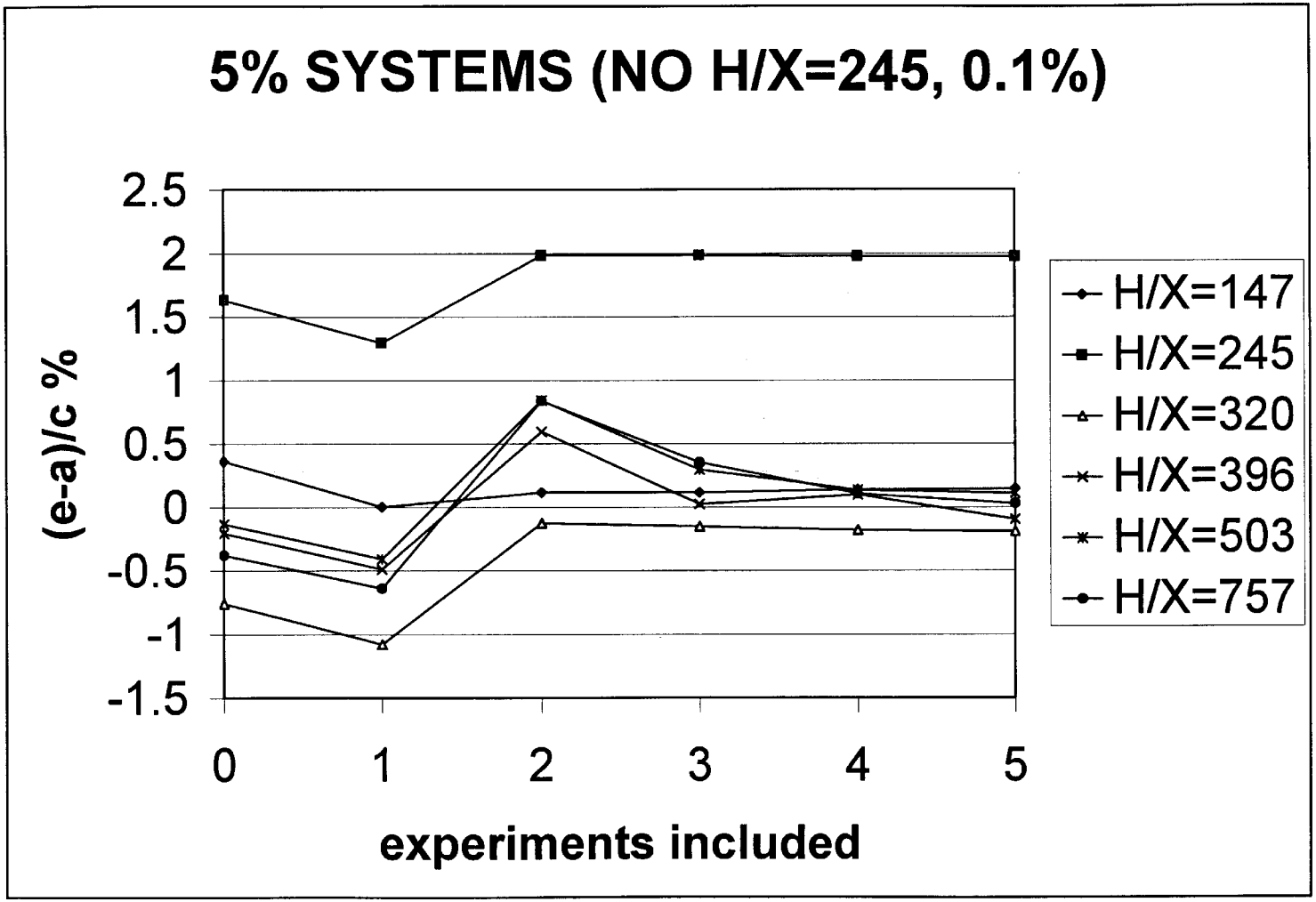

Figure 27 Predicted values of (e-a)/c as a function of the number of experiments included for 5-wt % U_3O_8 systems (0.1% experimental uncertainty, H/X = 245 system omitted)

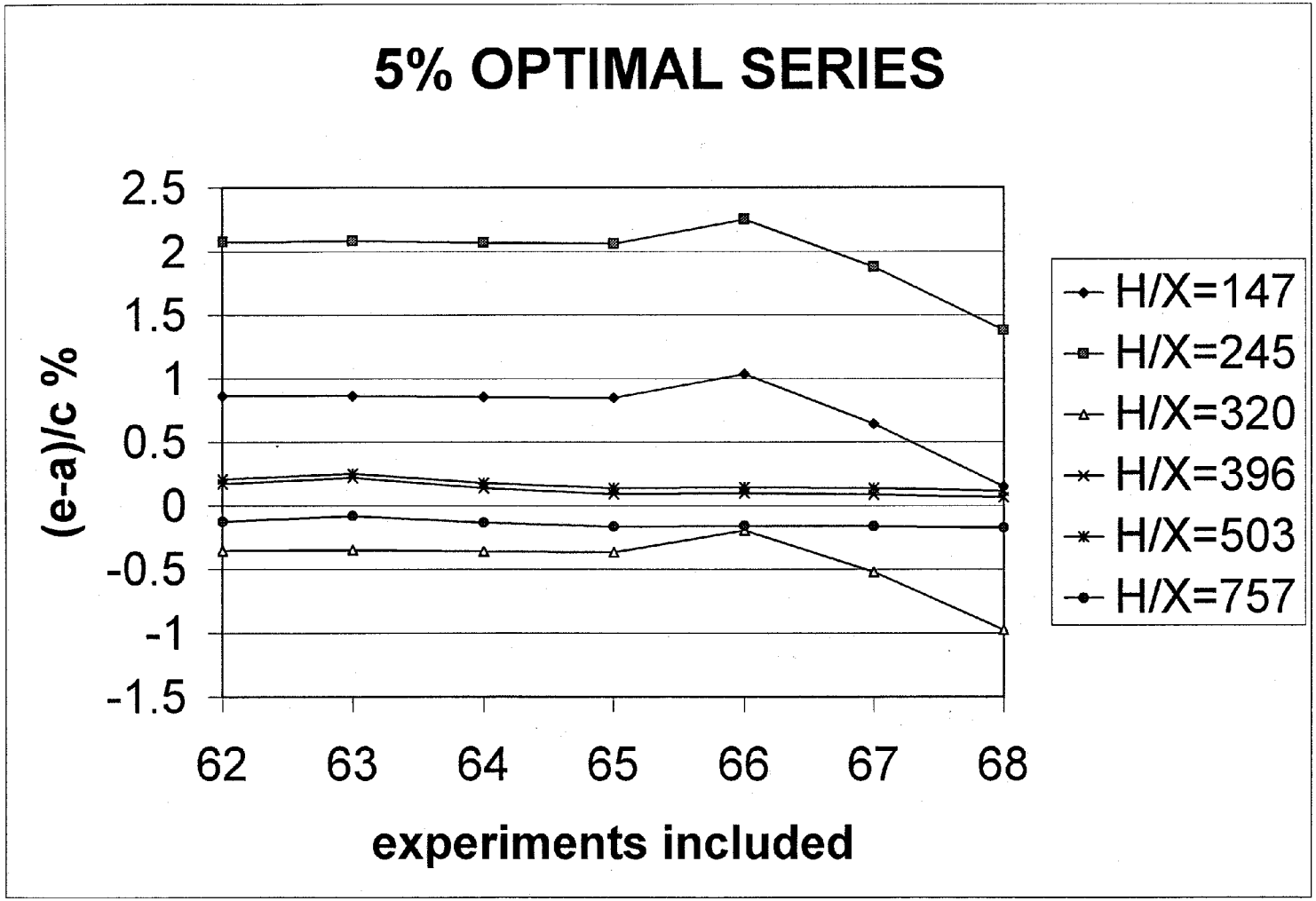

Figure 28 Predicted values of (e-a)/c as a function of the number of experiments included for 5-wt % U_3O_8 systems (0.4% experimental uncertainty)

values of 757, 396, 503, 320, 147, and 245. The divergence of the solutions near the right-hand side of the graph was expected, since the analysis of the six 5-wt % experiments alone concluded that the H/X = 245 system is inconsistent with the remaining systems. However, it appears from this analysis that the system with an H/X value of 147 is also inconsistent with the remaining systems. This finding is curious since the calculated value for this system agrees well with its measured value; however, it appears to be somewhat inconsistent with the general trends seen in the other data. For the remaining 4 systems (H/X of 320, 396, 503 and 757), it is clear that, not only are these systems converged, but the database of 62 experiments very accurately predicts the (e-a)/c values for these experiments.

4.2.2 Lessons Learned for Use of Correlation Coefficients

As stated in the introduction to this section, two of the goals of this GLLSM analysis were to predict the *number* of experiments and the *magnitude* of the correlation coefficient necessary for convergence, i.e., the similarity criteria. Obviously these two quantities are connected. It would be expected that fewer experiments are needed to ensure convergence if the correlation coefficients are larger, than if they were smaller. With this in mind, a numerical exercise was carried out using the 2-wt % experiments. In Figure 29, the values of (e-a)/c are plotted versus the correlation coefficient range for the 62 plus experiments in the benchmark database. The values plotted to the far right correspond to the inclusion of all of the experiments (i.e., correlation coefficients 0.9–1.0 and lower), followed by inclusion of experiments with correlation coefficients of 0.8–0.89 and lower, and so on. This curve is designed to estimate the correlation coefficient by which convergence is typically obtained. It appears from these results that in general correlation coefficients of 0.80 and higher can be utilized to obtain convergence. The exception is again the system with an H/X of 972, which was shown previously to be quite difficult to converge. Even though these results only correspond to the group of 2-wt % systems, there appears to be a clear break in the behaviour of the convergence for systems with correlation coefficients below 0.80. Although the actual *number* of experiments needed to ensure convergence is quite difficult to conclude precisely, it appears that for correlation coefficients equal to 0.9 or higher, about 5–10 experiments are needed. These recommendations are based on the 2 wt % and 5 wt % cases shown in the previous section which seem to indicate that convergence is seen when about 4 other highly-correlated ($c_k > 0.9$) experiments are included in a GLLSM analysis. For correlation coefficients value between 0.80 and 0.89 approximately 10–20 experiments are needed, although these are not sufficient in all cases, as seen for the system with an H/X of 972. The recommendations for less-highly correlated systems ($0.8 \leq c_k \leq 0.89$) are loosely based on the number of experiments in that range for the exercise shown in Figure 29. The primary factor in whether systems with correlation coefficients between 0.80 and 0.89 produce convergence is believed to be the "completeness" of the experiments, that is, do the other experiments provide validation of the application system for all important cross sections and energy ranges. Further development of the concept of completeness is currently ongoing.

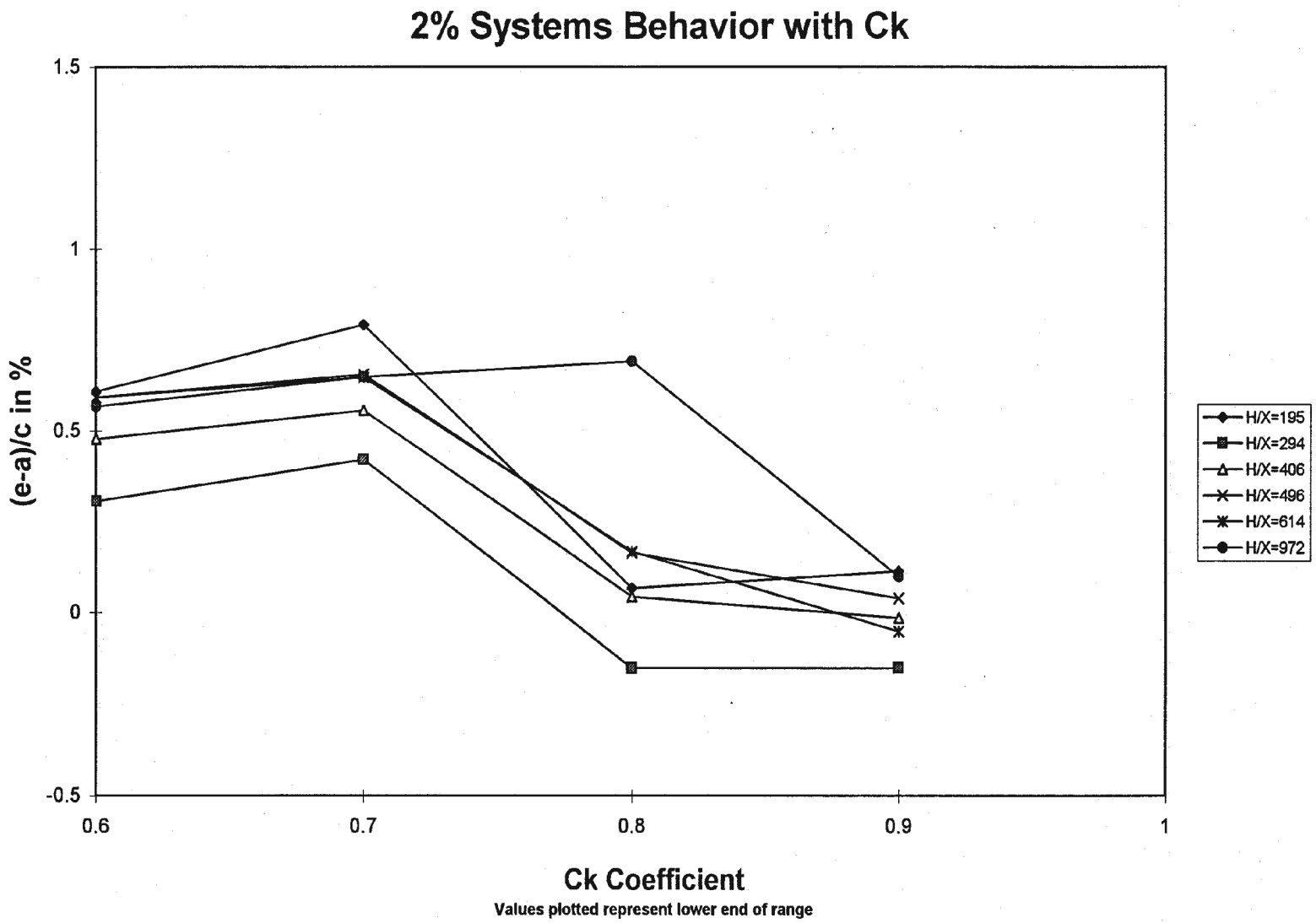

Figure 29 Dependence of the predicted (e-a)/c values on the inclusion of experiments in various ranges of correlation coefficients

5 INTEGRAL PARAMETER APPLICATIONS

Two integral parameter quantities have been discussed thus far in this report: the total sensitivities and the correlation coefficients. The total sensitivities are quite useful in identifying trends in the various systems; however, they can be quite confusing when applied to only a few disconnected systems because their uniqueness cannot be guaranteed. The correlation coefficients, c_k, on the other hand, give simple indications of the degree of commonality between the various uncertainty contributors for each system, regardless of their origin. In order to generate the correlation coefficients, cross-section uncertainty information must be available for all important systems components. In some cases, system similarity may need to be determined based solely on their respective sensitivities. A measure of similarity consisting of a single parameter or perhaps a few parameters is needed for these situations.

Tests of many different parameter types were carried out in order to determine a set of values that would best satisfy the needed similarity determination. The most promising set of parameters are a family of "D" values as defined below:

$$
\begin{aligned}
D_n &= \sum_{i=1}^{g} \left| S_{nai} - S_{nei} \right| \\
D_c &= \sum_{i=1}^{g} \left| S_{cai} - S_{cei} \right| \\
D_s &= \sum_{i=1}^{g} \left| S_{sai} - S_{sei} \right| ,
\end{aligned}
\tag{22}
$$

where S is the relative sensitivity of k_{eff} for the application, a, or experimental configuration, e, to $\bar{\nu}$ (n) or to the capture (c) and scattering (s) cross sections for energy group i. See Eq. (9) for the defining relation for the S values.

These parameters can be presented as a single quantity as defined above or as an energy-dependent profile, corresponding to the absolute value of the differences in the sensitivities by energy group. Values of D_n, D_c, and D_s are given in Table 6 for a $U(2)F_4$, H/X = 195 system versus the family of $U(11)O_2$ "artificial" systems described earlier in this report.

Table 6 D parameters for H/X = 195 $U(2)F_4 + CH_2$ as compared with $U(11)O_2 + H_2O$

H/X	D_n	D_c	D_s
0	1.7986	0.7938	0.7381
3	1.6084	0.6641	0.6030
5	1.5215	0.6125	0.5497
10	1.3241	0.5230	0.4781
20	1.0329	0.4220	0.4681
40	0.6748	0.3593	0.5140
80	0.3430	0.3220	0.5615
200	0.1261	0.3086	0.6085
300	0.2355	0.3751	0.6164
400	0.2982	0.4270	0.6123
500	0.3373	0.4694	0.6013
600	0.3633	0.5042	0.5867
800	0.4025	0.5701	0.5539
1000	0.4271	0.6201	0.5198

These coefficients are useful in making a quick determination of the similarity between pairs of systems. Since the range of D values is 0 to 2, values above 1 are certainly indicative of systems that are dissimilar. This dissimilarity is clear from Figure 30, where a D_n value of 1.7986 is represented by an energy-dependent profile. The spectra of the two systems appear to be quite different, one thermal and the other fast. Contrast Figure 30 with the Figure 31, which compares the sensitivities by group for systems of 2– and 11–wt % U with nearly identical H/X values. The D_n value in this case is 0.1261. In Figure 32, a D_n value of 0.4271 seems to indicate similar systems for an H/X value of 195 as compared with H/X of 1000. Figures 33–35 give a comparison of the same systems, but for the D_c parameter. In these figures, the D_c value of 0.3086 shown in Figure 34 certainly indicates similar systems, while the profiles representing D_c values of 0.7938 and 0.6201 (Figures 33 and 35) indicate that sizeable differences exist in these systems. The energy-dependent values for D_s corresponding to these same systems are given in Figures 36–38. These values are interesting in that none of the three are below 0.4. The D profiles indicate that while the differences in sensitivities are largely confined to two energy regions, the relative magnitudes of the sensitivities between these energy regions changes; hence the systems should not be considered similar.

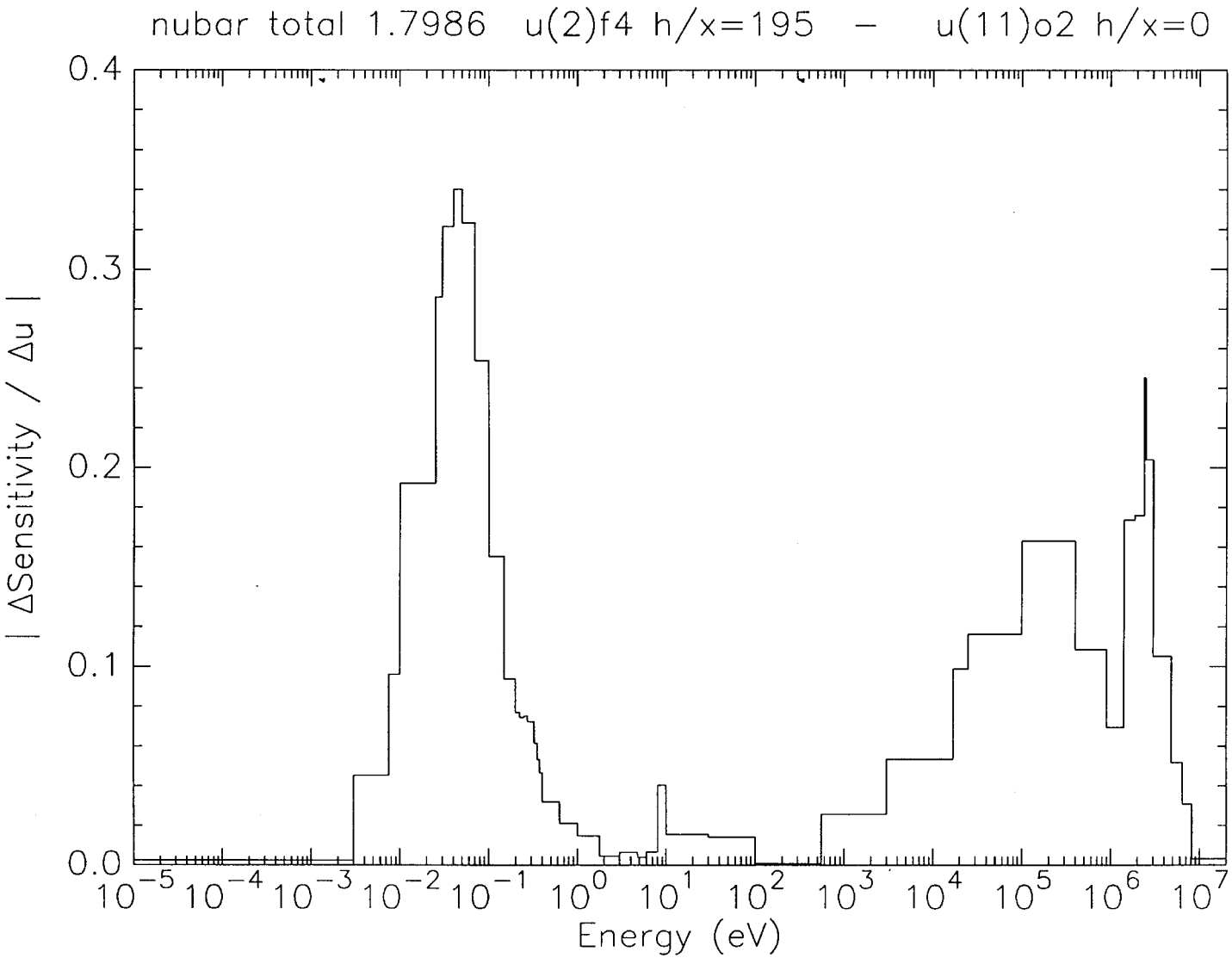

Figure 30 D_n profile for $U(2)F_4$ H/X = 195 and $U(11)O_2$ H/X = 0 systems; Total D_n = 1.7986

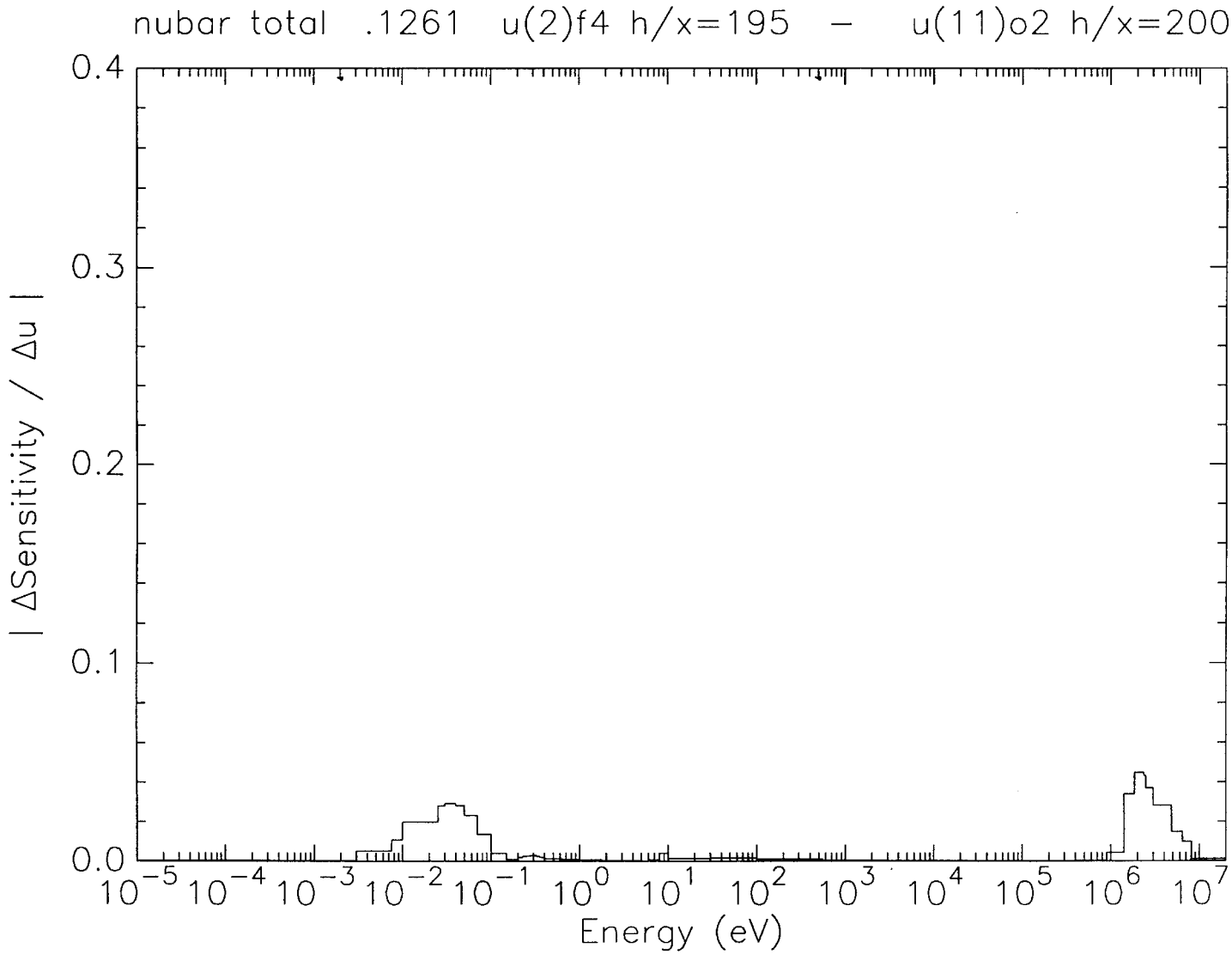

Figure 31 D_n profile for $U(2)F_4$ H/X = 195 and $U(11)O_2$ H/X = 200 systems; Total D_n = 0.1261

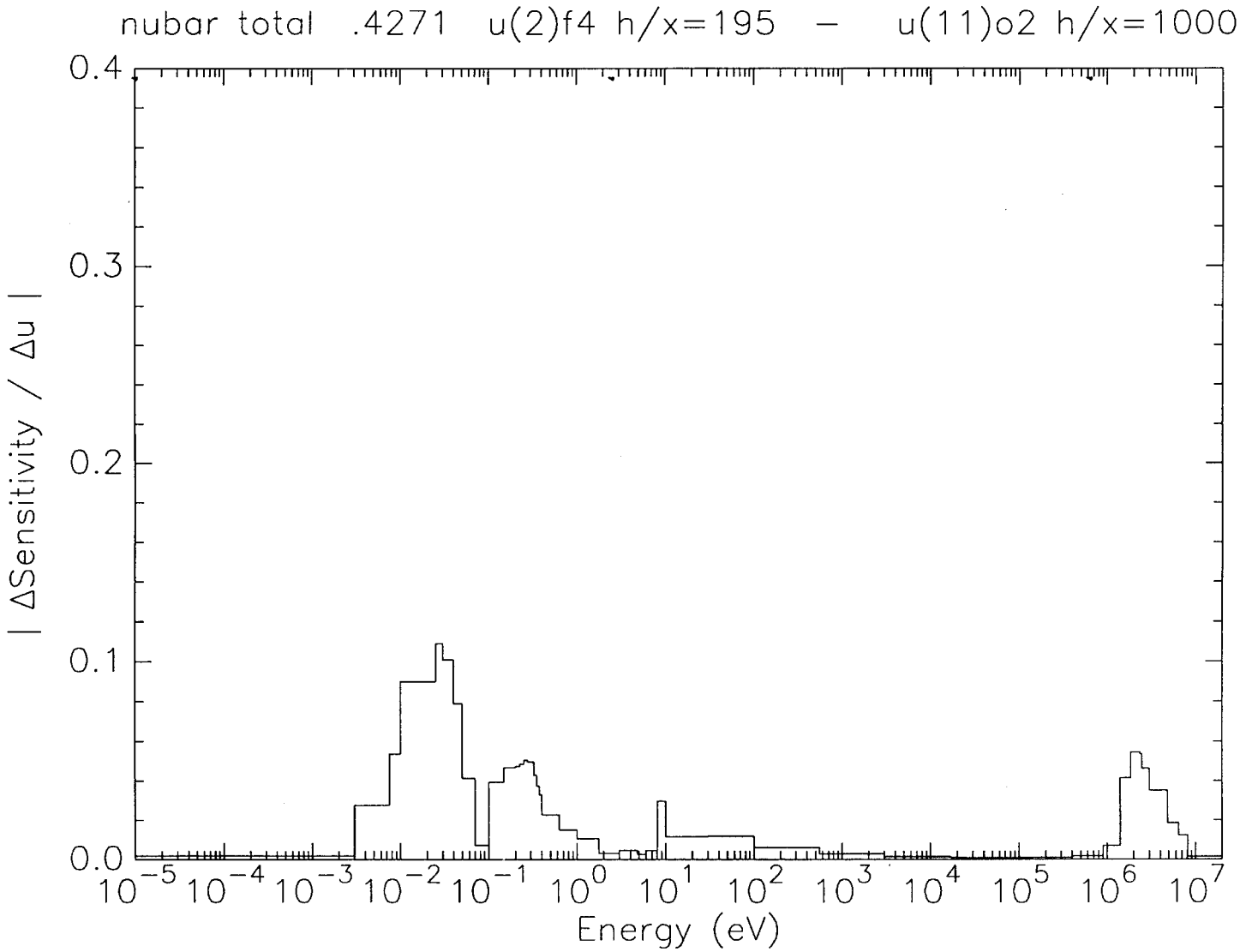

Figure 32 D_n profile for $U(2)F_4$ H/X = 195 and $U(11)O_2$ H/X = 1000 systems; Total D_n = 0.4271

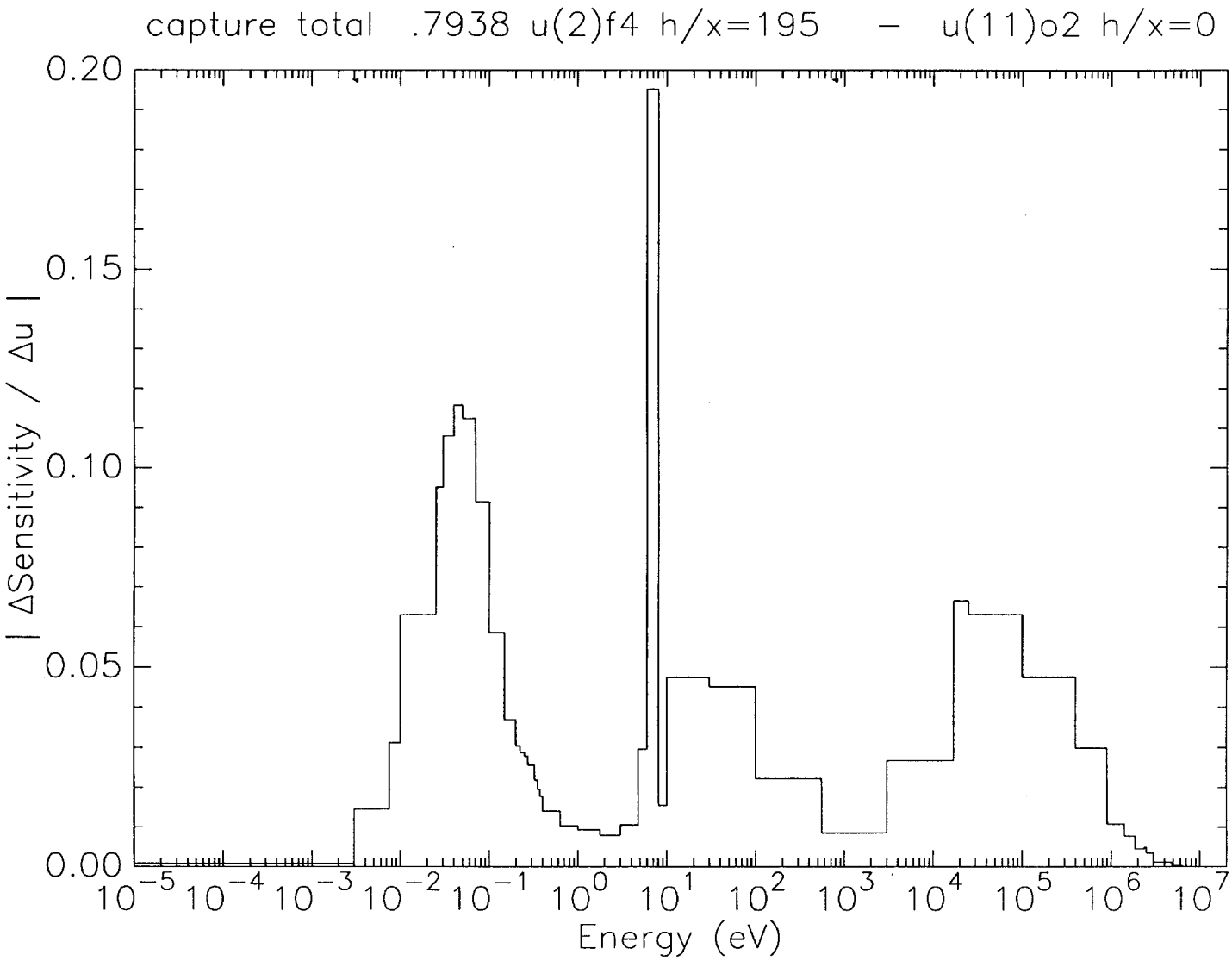

Figure 33 D_c profile for $U(2)F_4$ H/X = 195 and $U(11)O_2$ H/X = 0 systems; Total D_c = 0.7938

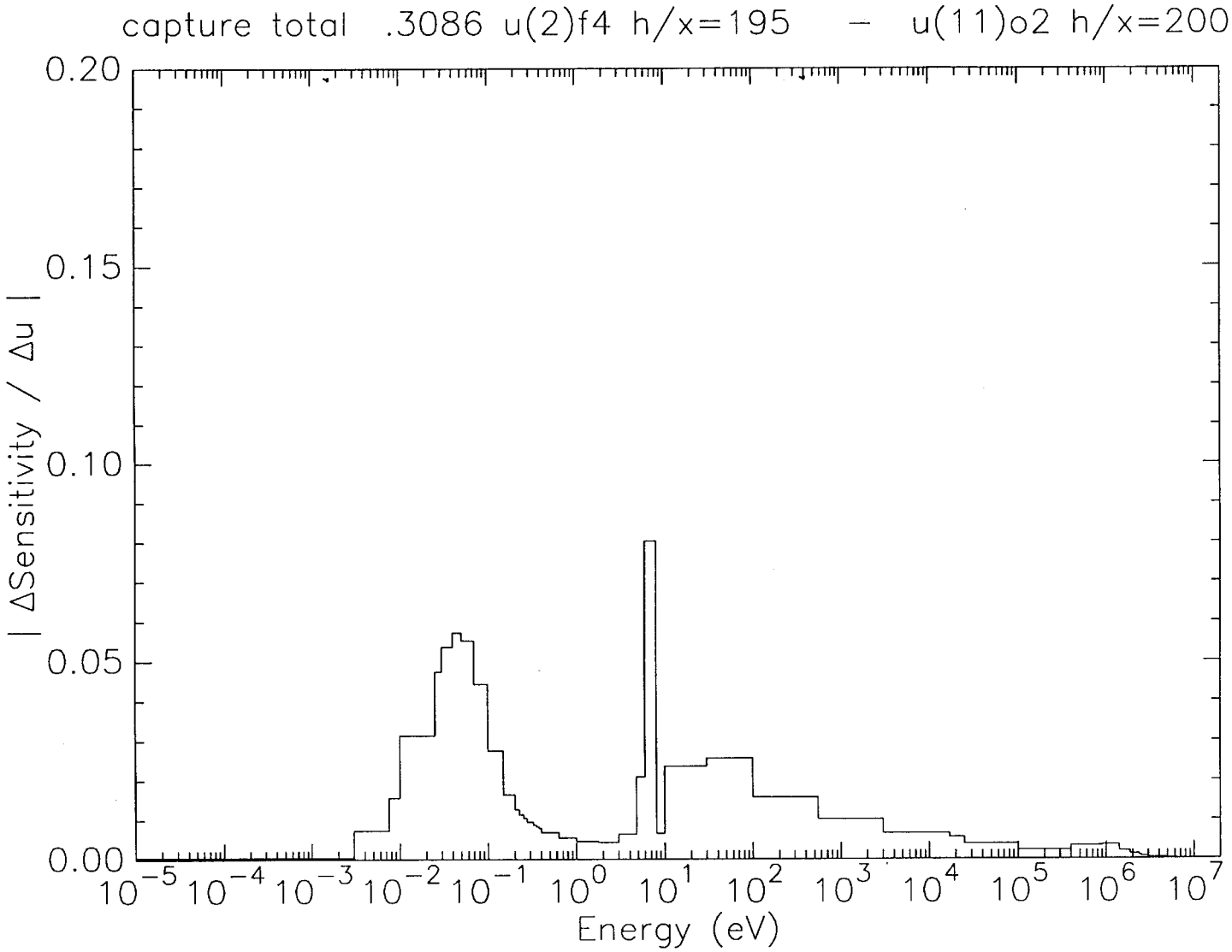

Figure 34 D_c profile for $U(2)F_4$ H/X = 195 and $U(11)O_2$ H/X = 200 systems; Total D_c = 0.3086

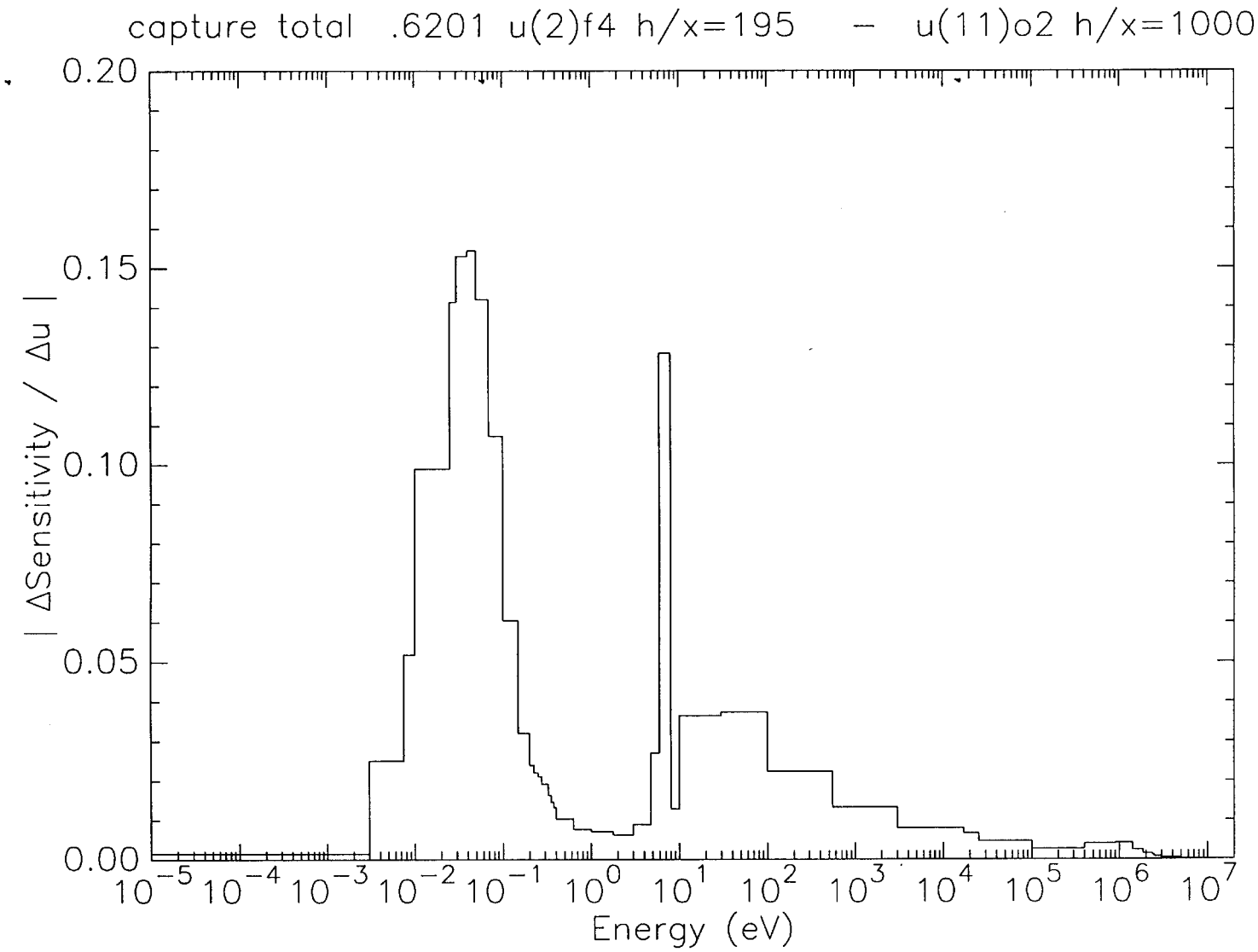

Figure 35 D_c profile for $U(2)F_4$ H/X = 195 and $U(11)O_2$ H/X = 1000 systems; Total D_c = 0.6201

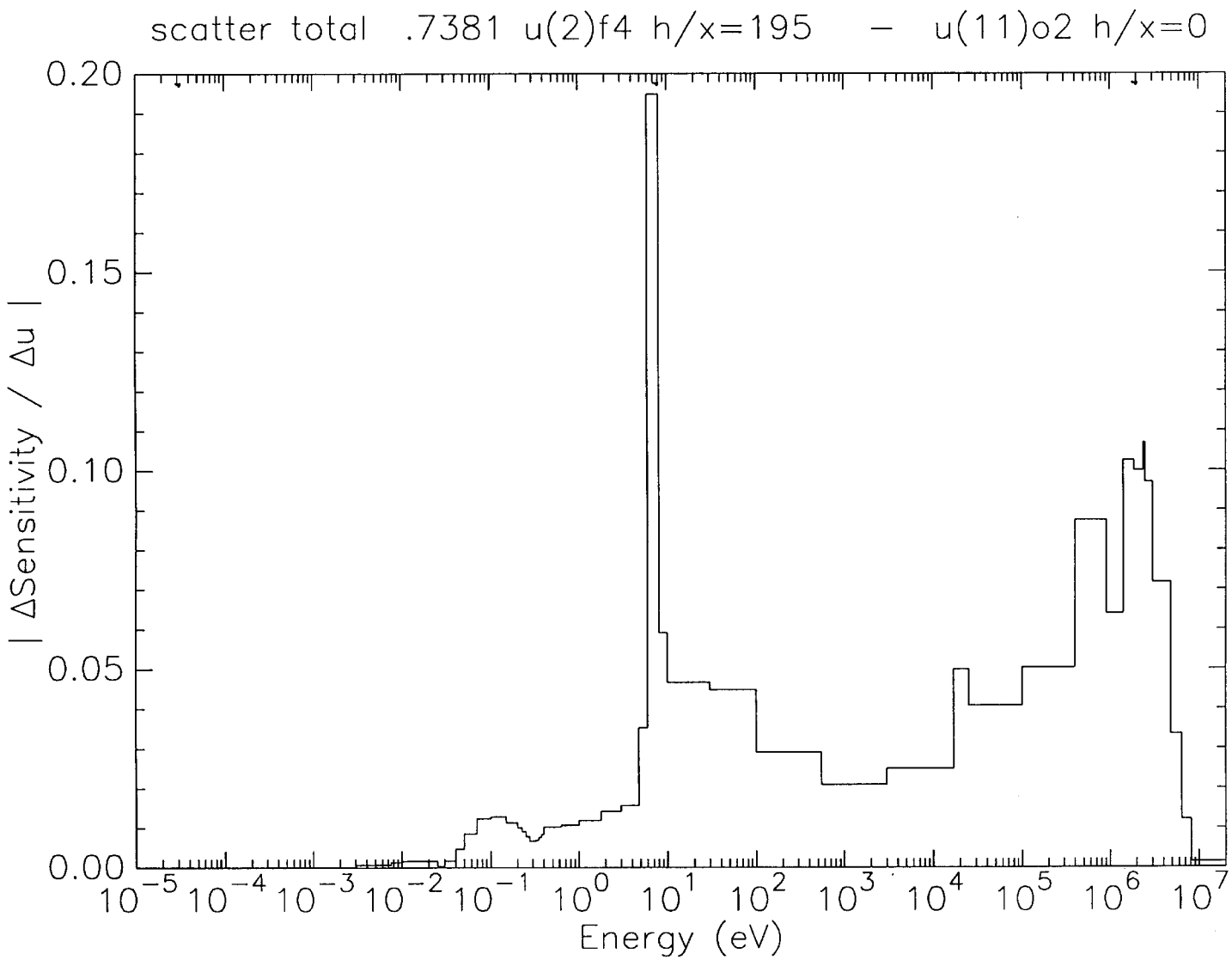

Figure 36 D_s profile for $U(2)F_4$ H/X = 195 and $U(11)O_2$ H/X = 0 systems; Total D_s = 0.7381

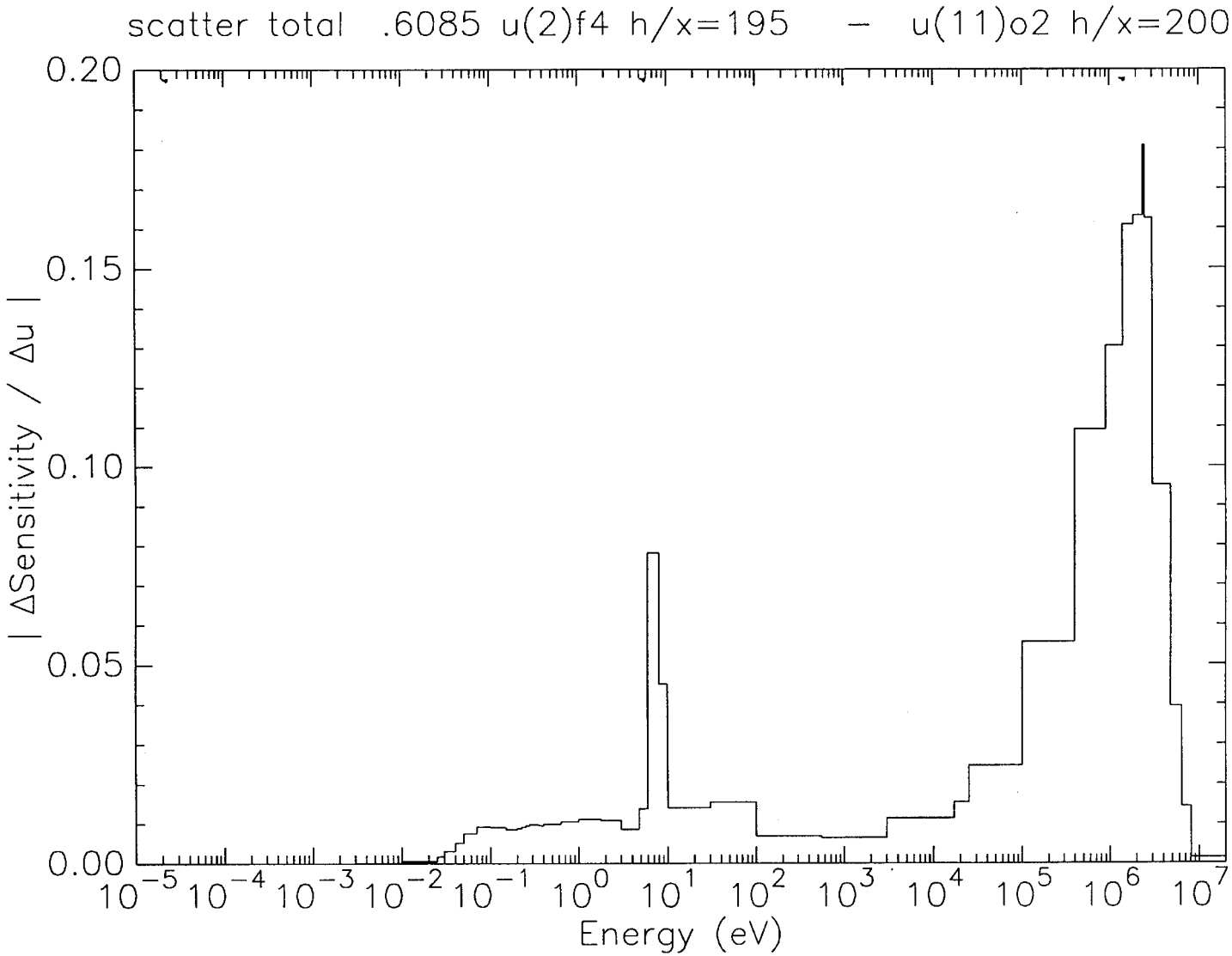

Figure 37 D_s profile for $U(2)F_4$ H/X = 195 and $U(11)O_2$ H/X = 200 systems; Total D_s = 0.6085

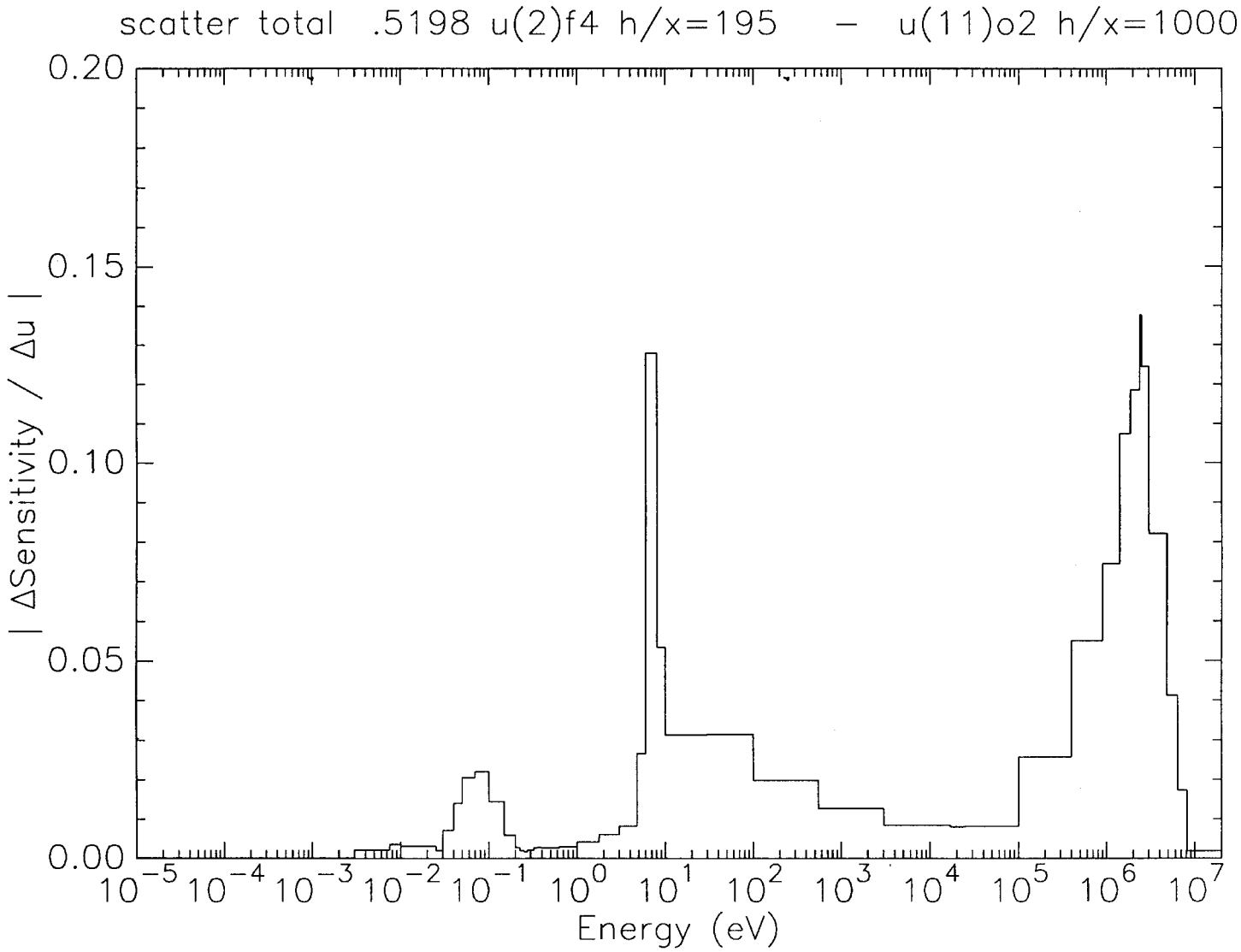

Figure 38 D_s profile for $U(2)F_4$ H/X = 195 and $U(11)O_2$ H/X = 1000 systems; Total D_s = 0.5198

The precise numerical value of these D's that determine system similarity is difficult to define, requiring some degree of expert judgement. For comparison with the c_k values presented previously, values of D_n, D_s, and D_c below about 0.4 generally correspond to systems with c_k values above about 0.8. In order to show the explicit relationship between the various c_k and D values, Figure 39 contains a plot of the values of D_n, D_c, and D_s versus c_k, corresponding to the $U(11)O_2$ H/X = 500 system with respect to the experimental benchmark data base used in Vol. 2. Linear fits to these data points are shown as a solid line for D_n vs c_k, a dotted line for D_s vs c_k, and a dashed line for D_c vs c_k. Even though the fits are somewhat fuzzy, clearly the c_k values greater than 0.8 correspond very closely to D_n, D_c, and D_s values below 0.4–0.5.

The individual values of D_n, D_c and D_s give specific similarity information relating to fission, capture and scattering. However, to be compared with the single value of c_k, an additional parameter was postulated. The parameter D_{sum} is defined as the sum of D_n, D_c and D_s. A plot of D_{sum} versus c_k is shown in Figure 40. There the c_k value of 0.8 clearly corresponds to a D_{sum} value of about 1.2. Thus, an additional indicator of system similarity would be a D_{sum} value of less than 1.2.

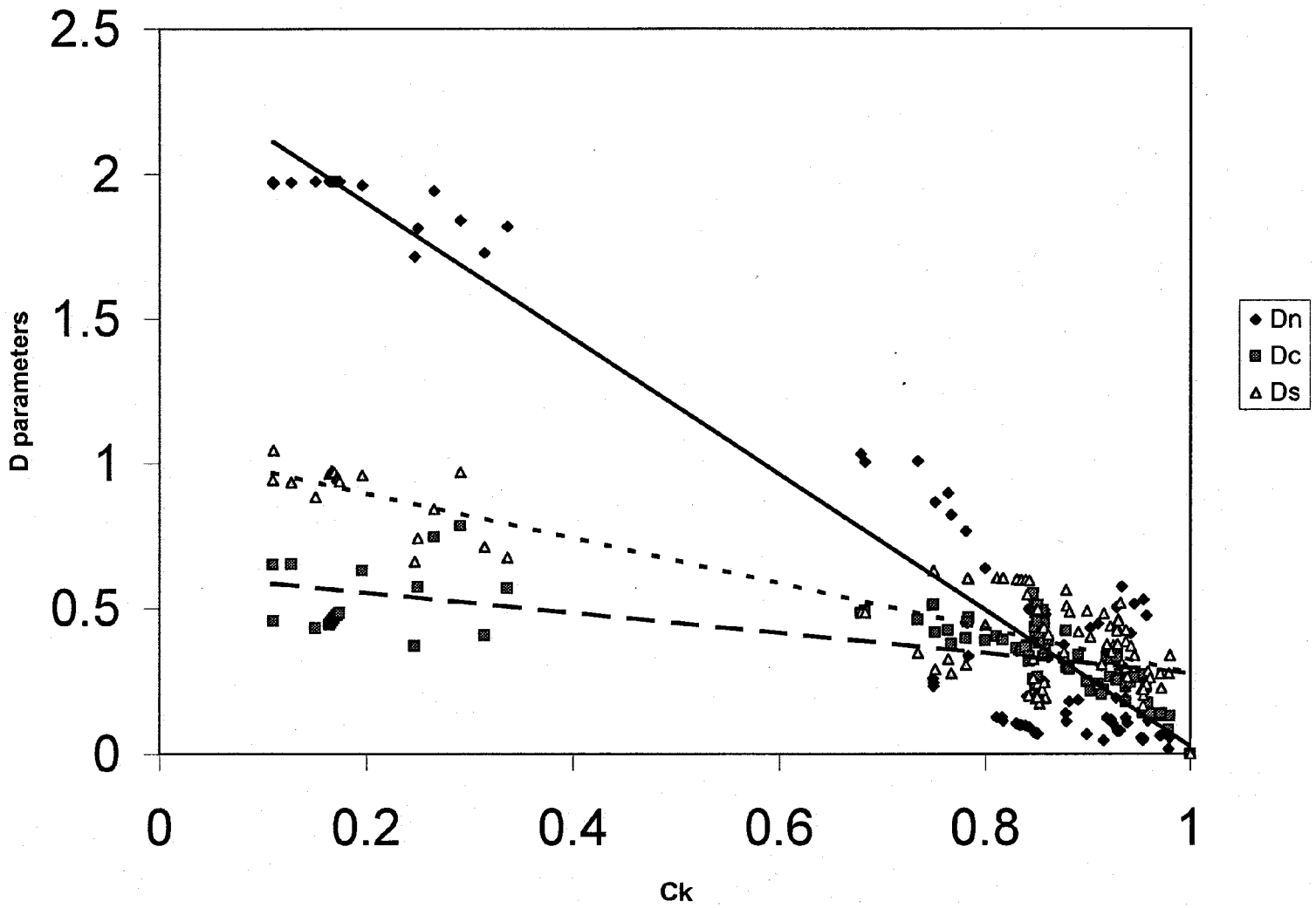

Figure 39 Comparison of D_n, D_s, D_c values with c_k values for benchmark database with respect to $U(11)O_2$ H/X = 500 system

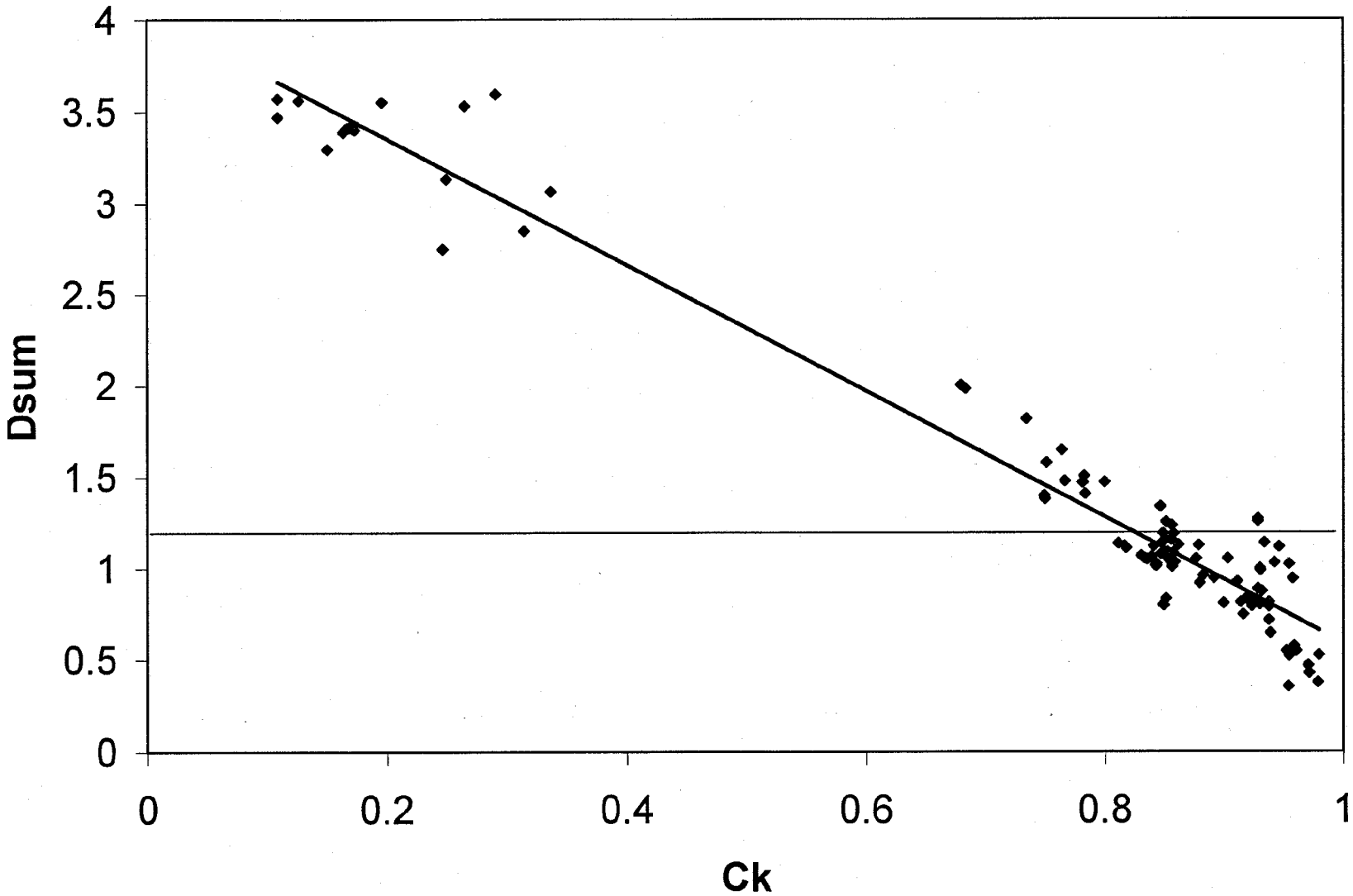

Figure 40 Comparison of D_{sum} values with c_k values for benchmark database with respect to $U(11)O_2$ H/X = 500 system

6 SUMMARY

This report has presented the theoretical basis for the application of the sensitivity and uncertainty analysis methods to the validation of data sets for use in criticality safety applications. These procedures involve standard sensitivity and uncertainty analyses that were developed in the late 1970s primarily for use in the development of fast reactor systems in the United States and abroad. The sensitivity analyses produce energy-dependent sensitivity values (sensitivity profiles) which give the change in the system k_{eff} value as a function of changes in the cross sections by energy. These analyses provide the basic understanding of the physics of each critical benchmark system in order to properly characterize similarities between systems in a consistent manner. The uncertainty analyses provide an estimate of the uncertainties in the calculated values of the system k_{eff}, as well as correlations in these uncertainties between systems. The use of both sensitivity and uncertainty analyses in the formal determination of areas (or ranges) of applicability has been developed in this work. These determinations of applicability can be accomplished via parameters, which represent the differences in $\bar{\nu}$, capture, and scattering sensitivity profile values (i.e., D_n, D_c, and D_s, respectively) and the correlation coefficients, c_k. Ranges of these parameters, proposed to formally define the applicability of a series of critical benchmark experiments to a particular application area, are c_k values that are 0.80 or higher, D_{sum} values that 1.2 or less and values of D_n, D_c, and D_s that are 0.40 or less. These parameters relate directly to the applicability or similarity between pairs of systems — one of which is assumed to be a benchmark; the other, an application.

The sensitivity and uncertainty analysis results, along with the calculated and measured k_{eff} values and estimates of uncertainties in the measurements, were used in this work to demonstrate application of the full GLLSM procedure to data validation for criticality safety studies. The primary goal of the GLLSM analysis is the prediction of the calculated-versus-measured differences for systems that have not been measured. These calculated-versus-measured differences are the so-called calculational biases. Application of the GLLSM procedures to a series of critical experiments is designed to identify "changes" in the underlying nuclear data such that the calculated-versus-measured differences are minimal. This work has identified the relationship between these predicted data changes and the calculational bias for systems that have not been measured, and hence correspond to interpolations or extrapolations in the vector space corresponding to the original set of benchmark experiments. Uncertainties in the bias can be estimated based on the standard deviation provided by the GLLSM procedure.

To demonstrate the basic concepts and usefulness of the GLLSM procedure and to estimate the required magnitude of the c_k and D parameters and number of systems needed for a meaningful estimate of bias, the GLLSM procedure was applied to a set of 2-wt % and 5-wt % uranium oxide and uranium fluoride critical benchmarks, which consisted of 6 experiments each. Initial studies were performed on the 2-wt % and 5-wt % systems in isolation to demonstrate that for highly correlated systems, the GLLSM procedure can produce rapid convergence on the predicted bias for such systems. These studies were unique in that omission of one of the experiments from the GLLSM procedure allowed simulation of the prediction of bias for that experiment as if it had never been performed. These predictions can then be compared directly to the actual biases, because the measured and calculated values of k_{eff} are known.

Results using this limited number of highly correlated experiments show that convergence can be quite rapid. However, the use of a large number of experiments in the GLLSM procedure is recommended since they place additional constraints on the cross-section data changes that are not present in a case with few experiments. The use of a large number of experiments in the GLLSM procedure was also demonstrated in this work. The results show that the large database is quite effective in producing convergence for the 2-wt % and 5-wt % sets without including any of the 2-wt % and 5-wt % data directly in the GLLSM combination procedure. This method is the desired operation of the GLLSM for applications in which no direct measurements are available.

This work also demonstrates approximate values of the c_k parameter and the associated number of experiments for which convergence of the GLLSM procedure can be expected. These results are expected to be useful for non-GLLSM analyses as well, in that these guidelines should also apply to more traditional trending procedures as well.

An estimated 5–10 benchmarks with values of c_k equal to 0.9 or higher are needed to ensure convergence in a GLLSM procedure. Therefore, a corresponding number and type of systems should be considered a minimum for standard validation analyses. Under certain conditions, convergence can also be expected for 10–20 systems with c_k values between 0.8 and 0.9. The type of conditions under which convergence can be produced with systems with a c_k value less than 0.8 (even much less than 0.8) is the subject of current research.

Further comparison of the use of c_k and D values indicate that D values less than 0.4 (or sum of the D values less than 1.2) match the area of applicability criteria associated with $c_k > 0.8$.

7 REFERENCES

1. *American National Standard for Nuclear Criticality Safety in Operations with Fissionable Material Outside Reactors*, ANSI/ANS-8.1-1998, American Nuclear Society (1998).

2. R. L. Murray, *Nuclear Reactor Physics*, Prentice-Hall, Englewood Cliffs, NJ, 1957.

3. J. R. Lamarsh, *Nuclear Reactor Theory*, Addison-Wesley, Reading, MA, 1966.

4. A. Henry, *Nuclear-Reactor Analysis*, MIT Press, Cambridge, MA, 1975.

5. E. M. Oblow, "Sensitivity Theory from a Differential Viewpoint," *Nucl. Sci. Eng.* **59**, 187 (1976).

6. W. M. Stacey, Jr., "Variational Estimates and generalized Perturbation Theory for the Ratios of Linear and Bilinear Functionals," *J. Math. Phys.*, **13**, 1119 (1972); see also W. M. Stacey, Jr., "Variational Estimates of Reactivity Worths and Reaction Rate Ratios in Critical Nuclear Reactors," *Nucl. Sci. Eng.* **48**, 444 (1972).

7. L. N. Usachev, "Perturbation Theory for the Breeding Ratio and for Other Number Ratios Pertaining to Various Reactor Processes," *J. Nucl. Energy* Pts. A/B, **18**, 571 (1964).

8. A. Gandini, "A Generalized Perturbation Method for Bilinear Functionals of the Real and Adjoint Neutron Fluxes," *J. Nucl. Energy* **21**, 755 (1967).

9. C. R. Weisbin, J. H. Marable, J. L. Lucius, E. M. Oblow, F. R. Mynatt, R. W. Peelle, and F. G. Perey, *Application of FORSS Sensitivity and Uncertainty Methodology to Fast Reactor Benchmark Analysis*, ORNL/TM-5563, Union Carbide Corp., Oak Ridge National Lab., December 1976. See also, *Nucl. Sci. Eng.*, **66**, 307 (1978).

10. J. L. Lucius, C. R. Weisbin, J. H. Marable, J. D. Drischler, R. Q. Wright, and J. E. White, *A Users Manual for the FORSS Sensitivity and Uncertainty Analysis Code System*, ORNL-5316, Martin Marietta Energy Systems, Oak Ridge National Lab., January 1981.

11. *SCALE: A Modular Code System for Performing Standardized Computer Analyses for Licensing Evaluations*, NUREG/CR-0200, Rev. 5 (ORNL/NUREG/CSD-2/R5), Vols. I–III, March 1997. Available from Radiation Safety Information ComputationalCenter at Oak Ridge National Laboratory as CCC-545.

12. R. L. Childs, *SEN1: A One-Dimensional Cross-Section Sensitivity and Uncertainty Module for Criticality Safety Analysis*, NUREG/CR-5719 (ORNL/TM-13738), U.S. Nuclear Regulatory Commission, Oak Ridge National Lab., July 1999.

13. W. A. Rhodes, and R. L. Childs, *An Updated Version of the DOT 4 One- and Two-Dimensional Neutron/Photon Transport Code*, ORNL-5851, Union Carbide Corp., Oak Ridge National Lab., 1982.

14. B. L. Broadhead, and B. T. Rearden, *Exploratory Studies for Three-Dimensional Sensitivity Methods*, ORNL/M-6583, Lockheed Martin Energy Research Corp., Oak Ridge National Lab., 1998.

15. S. J. Raffety and J. T. Mihalczo, *Homogenized Critical Assemblies of 2 and 3% Enriched Uranium in Paraffin*, Y-DR-14, Union Carbide Corp., Nuclear Division, Oak Ridge Y-12 Plant, 1969.

16. D. F. Cronin, *Critical Mass Studies, Part X*, ORNL-2968, Union Carbide Nuclear Corp., Oak Ridge National Lab., 1960.

17. J. D. Smith, III and B. L. Broadhead, *Multigroup Covariance Matrices for Fast Reactor Studies*, ORNL/TM-7389, Martin Marietta Energy Systems, Oak Ridge National Lab., 1981.

18. R. E. McFarlane, R. J. Barrett, D. W. Muir, and R. M. Boicourt, *The NJOY Nuclear Data Processing System: User's Manual*, LA-7584-M, Los Alamos National Lab., 1978.

19. B. L. Broadhead, *A Nuclear Data Adjustment Methodology Utilizing Resonance Parameter Sensitivities and Uncertainties*, ORNL/CSD/TM-212, Martin Marietta Energy Systems, Oak Ridge National Lab., 1984.

20. H. Derrien, N. M. Larson, and L. C. Leal, *Covariance Matrices for Use in Criticality Safety Predictability Studies*, ORNL/TM-13492, Lockheed Martin Energy Research Corp., Oak Ridge National Lab., 1997.

21. A. Gandini, *Nuclear Data and Integral Measurements Correlation for Fast Reactors, Part 1: Statistical Formulation*, RT/FI(73)5, Comitato Nazionale Energia Nucleare, 1973.

22. J. B. Dragt, J. W. M. Dekker, H. Gruppelaar, and A. J. Janssen, "Methods of Adjustment and Error Evaluation of Neutron Capture Cross Sections; Application to Fission Product Nuclides," *Nucl. Sci. Eng.* **62**, 117 (1977).

23. J. J. Wagschal, and Y. Yeivin, "The Significance of Lagrange Multipliers in Cross-Section Adjustment," *Trans. Am. Nucl. Soc.* **34**, 776 (1980).

24. J. Barhen, J. J. Wagschal, and Y. Yeivin, "Response-Parameter Correlations in Uncertainty Analysis," *Trans. Am. Nucl. Soc.* **35** (1980).

25. R. E. Maerker, B. L. Broadhead, and J. J. Wagschal, "Theory of an New Unfolding Procedure in Pressurized Water Reactor Pressure Vessel Dosimetry and Development of an Associated Benchmark Data Base," *Nucl. Sci. Eng.* **91**, 369 (1985). See also *Development and Demonstration of an Advanced Methodology for LWR Dosimetry Applications*, EPRI NP-2188, Electric Power Research Institute, Palo Alto, Calif., December 1981.

APPENDIX A

Covariance Concepts

APPENDIX A

Covariance Concepts†

Let the variable y represent measurements taken with some instrument or device that will not yield an exact result, but will give a variety of numbers with some spread. If a very large number of measurements were made, a probability distribution such as a Gaussian could be developed. A related expression is the probability density, labeled f(y), having the property that its integral over all values of y is 1, i.e,

$$\int f(y)dy = 1.$$

The average value of y is

$$\overline{y} = \int y\, f(y)\, dy$$

For a finite number of measurements, y_i, where i = 1, 2, 3, ...,N,

$$\overline{y} = (1/N)\Sigma\, y_i\, f(y_i).$$

These are examples of an expectation value (or expected value), written either as E(y) or as <y>. More generally, we can find the expectation value of a function of y, e.g., g(y), by forming

$$E[g(y)] = \int g(y)f(y)dy.$$

A measure of the width of the distribution is sought. We take note of the differences between each observation and the average,

$$\delta y = y - \overline{y}.$$

Form the square of that difference and evaluate the expectation value

$$E[(\delta y)^2] = E[(y - \overline{y})^2] = \int (y - \overline{y})^2\, f(y)dy.$$

This is called the *variance*, often symbolized by var(y) or simply v(y). The square root of the variance is the standard deviation,

$$\sigma(y) = [\mathrm{var}(y)]^{1/2}$$

having the same units as y and a measure of the width of the distribution. Related parameters often used are the relative variance, $\mathrm{var}(y)/[\overline{y}]^2$ and the relative standard deviation, $\sigma(y)/[\overline{y}]$. All of these quantities may be found for other variables such as u, v, w, z, etc.

There are several distributions that are appropriate for certain processes, but the *standard distribution* (or Gaussian) is most often applied. One calculates the average of the measured data, $\overline{y}$, and also the standard deviation, σ, and inserts them in the theoretical expression,

---

†Used with permission from Dr. R. L. Murray, North Carolina State University, Raleigh, NC.

$$f(y) = 1/[\sigma(2\pi)^{1/2}] \exp\{-1/2\, [(y - \overline{y})/\sigma]^2\},$$

which is used for evaluation of expectation values.

When a measured variable depends on two or more parameters, for example, r(x,y), each of the variables x and y has its own expectation value

$$E(x) = E(\overline{x} + \delta x) = \overline{x}$$

$$E(y) = E(\overline{y} + \delta y) = \overline{y}.$$

A joint probability density function is needed, f(x,y). To obtain the f(x) needed to find E(x), it is required to integrate f(x,y) over all y, and similarly for f(y).

It is possible that there is some relationship between x and y. To check that, a new quantity is introduced, the *covariance.* For the two-variable case, it is written as

$$\mathrm{cov}(x,y) = \sigma^2_{x,y} = E(\delta x\, \delta y) = \int (x - \overline{x})(y - \overline{y})\, f(x,y)\, dx\, dy$$

It is seen to be the weighted product of the error in x and the error in y. A related quantity is the correlation coefficient, defined by

$$\rho\,(x,y) = \mathrm{cov}(x,y)/\sigma_x\, \sigma_y$$

with $\rho\,(y,y) = 1$. It can be shown that if there is direct dependence of x on y the correlation coefficient ρ is +1, if there is no dependence, ρ is zero.

To be more specific, let us consider a critical assembly similar to the Los Alamos Godiva, but composed of pure U-235 as metal. To a rough approximation the neutron flux can be described by a one-group diffusion model,

$$D\nabla^2\phi - \phi\Sigma_a + \lambda\phi\Sigma_f\nu = 0$$

where $\lambda = 1/k_{eff}$. Ignoring variations in the diffusion coefficient D and the number density N for uranium, the value of k_{eff} depends on ν, σ_a, and σ_f. The method of measuring the number of neutrons per fission is generally different from that used to measure cross sections. However, the methods of measuring the two cross sections may be similar so that σ_a and σ_f are correlated, and there is a non-zero value of the covariance $\mathrm{cov}(\sigma_a, \sigma_f)$.

Let us derive a formula for the variance of a function of two variables, assuming a linear relationship

$$r(x,y) = ax + by.$$

where a and b are constants. The expectation value of r is clearly

$$\overline{r} = a\,\overline{x} + b\,\overline{y}.$$

The variance of r is

$$v(r) = E[(r - \overline{r})^2].$$

Form the quantity

$$r - \overline{r} = a(x - \overline{x}) + b(y - \overline{y})$$

$$= a\,\delta x + b\,\delta y.$$

Thus

$$(r - \overline{r})^2 = a^2\,(\delta x)^2 + b^2\,(\delta y)^2 + 2\,a\,b\,\delta x\,\delta y.$$

Form the expectation value to obtain the variance

$$v(r) = a^2\,v(x) + b^2\,v(y) + 2\,a\,b\,\mathrm{cov}(x,y),$$

which says in words that the variance of r as a linear function of x and y is composed of the variances of x and y plus a covariance term. If x and y are not related, the last term is zero, and the variance is merely the sum of those for x and y.

A more general case is where r depends on a number of variables, i.e.,

$$r(x_1, x_2, x_3,\ldots,x_N).$$

It is very convenient to turn to a matrix representation of r,

$$\mathbf{r} = \begin{matrix} x_1 \\ x_2 \\ x_3 \\ \cdot \\ \cdot \\ \cdot \\ x_N \end{matrix}$$

There may be relationships between pairs of variables x_i and x_j, leading to a set of variances $v_{i,j} = E(\delta x_i, \delta x_j)$ that form a matrix array as follows:

$$\mathbf{v}(r) = \begin{matrix} v_{11} & v_{12} & v_{13} \ldots \\ v_{21} & v_{22} & v_{23} \ldots \\ v_{31} & v_{32} & v_{33} \ldots \\ \cdot & \cdot & \cdot \end{matrix}$$

This matrix is called the covariance matrix, even though the main diagonal consists of variances. It is symmetric about that diagonal, because $v_{i,j}$ is the same as $v_{j,i}$. It is also known as the error matrix.

To illustrate the benefits of the matrix method, we now derive a compact relation involving the way the variable r changes with the various x_i. Propose that the variations are small, so that the first two terms of a Taylor series are sufficient. Thus write

$$r(x) = r(\overline{x}) + (dr/dx_1)dx_1 + (dr/dx_2)dx_2 + (dr/dx_3)dx_3 + \ldots + (dr/dx_N)dx_N$$

where, strictly speaking, partial derivative symbols should be used. Let r'_i stand for the rate of change or slope dr/dx_i, directly related to sensitivity. Then a compact expression for $\delta r = r - \overline{r}$ can be written,

$$\delta r = r'_1\, \delta x_1 + r'_2\, \delta x_2 + r'_3\, \delta x_3 + \ldots$$

Write out the square of δr for a case of three variables,

$$(\delta r)^2 = (r'_1 \delta x_1 + r'_2\, \delta x_2 + r'_3\, \delta x_3)(r'_1\, \delta x_1 + r'_2\, \delta x_2 + r'_3\, \delta x_3)$$

$$= r'_1(\delta x_1)^2\, r'_1 + r'_1(\delta x_1)(\delta x_2) r'_2 + r'_1(\delta x_1)(\delta x_3)\, r'_3$$

$$+ r'_2\, (\delta x_2)(\delta x_1)^2\, r'_1 + r'_2(\delta x_2)^2\, r'_2 + r'_2(\delta x_2)(\delta x_3) r'_3$$

$$+ r'_3(\delta x_3)(\delta x_1)\, r'_1 + r'_3(\delta x_3)(\delta x_2) r'_2 + r'_3(\delta x_3)^2 r'_3.$$

Take the expectation value of the sum to produce variances and covariances. The expression can be written in matrix notation as

$$v(\mathbf{r}) = E[(\delta r)^2] = \mathbf{r}'\, \mathbf{v}\, (\mathbf{r}')^T$$

where T stands for transposed, i.e. interchanged rows and columns. The two r matrices are

$$\mathbf{r}' = \begin{matrix} r'_1 \\ r'_2 \\ r'_3 \end{matrix} \qquad (\mathbf{r}')^T = \begin{matrix} r'_1 & r'_2 & r'_3 \end{matrix}$$

The compact formula expresses the total variance due to the variations δx_1, δx_2, and δx_3 including all possible interactions, weighted by the sensitivities of the function r to changes. The virtue of the matrix method is the ability to perform algebraic operations conveniently.

APPENDIX B

Derivation of the Generalized Linear-Least-Squares Equations

APPENDIX B

Derivation of the Generalized Linear-Least-Squares Equations

The derivation of the generalized linear least squares methods is taken from ref. 25 with only minor variations.

Let the vector $m \equiv (m_i)$, $i = 1,2, \ldots I$ represent a series of critical benchmark measurements (i.e., responses) for all of which calculations are available. This vector m has a corresponding symmetric $I \times I$ uncertainty matrix associated with it which we denote as $C_{mm} \equiv \mathrm{cov}(m_i, m_j) \equiv \langle \delta m_i \, \delta m_j \rangle \equiv \langle (\delta m)(\delta m)^\dagger \rangle$.* Let the vector $k \equiv (k_i)$ represent a calculation of the k_{eff} values for each experiment. Further, let the vector $\alpha \equiv (\alpha_i)$, $i = 1,2, \ldots N$, with its corresponding symmetric $N \times N$ uncertainty matrix $C_{\alpha\alpha} \equiv \langle \delta\alpha_i \, \delta\alpha_j \rangle$, represent the differential data used in the calculations (i.e., nuclear data such as fission cross sections, partial cross sections used in the transport calculation and the fission spectrum, and nonnuclear data such as corrections (biases) arising from methods approximations). We shall also allow for the possibility of correlations between the integral and differential data, which although may often be neglected in a first iteration of the adjustment procedure, are present in any subsequent iteration because of the nature of the combining process. These covariances are denoted by the $N \times I$ matrix $C_{\alpha m} \equiv \langle \delta\alpha_n \, \delta m_i \rangle$.

If we define the sensitivities of the calculated responses to each of the parameters α as $S_k \equiv (\partial k_i / \partial \alpha_n)$, with S_k being an $I \times N$ matrix, and if we impose the linearity restriction,

$$k(\alpha + \delta\alpha) = k(\alpha) + \delta k \simeq k(\alpha) + S_k \delta\alpha \ , \tag{1}$$

$$C_{kk} \equiv \langle (\delta k)\ (\delta k)^\dagger \rangle = S_k \langle (\delta\alpha)\ (\delta\alpha)^\dagger \rangle S_k^\dagger = S_k C_{\alpha\alpha} S_k^\dagger \tag{2}$$

then the uncertainty matrix corresponding to the calculated responses becomes

which reflects the propagation of the uncertainties in α through the calculation of k.

If we denote the deviations of the measured responses from their corresponding calculated values by the vector $d \equiv$

$$\begin{aligned} C_{dd} &= \langle \delta(k - m)\ \delta(k - m)^\dagger \rangle = \langle \delta k \delta k^\dagger \rangle + \langle \delta m \delta m^\dagger \rangle - \langle \delta k \delta m^\dagger \rangle - \langle \delta m \delta k^\dagger \rangle \\ &= C_{kk} + C_{mm} - S_k C_{\alpha m} - C_{m\alpha} S_k^\dagger \\ &= S_k C_{\alpha\alpha} S_k^\dagger + C_{mm} - S_k C_{\alpha m} - C_{m\alpha} S_k^\dagger \end{aligned} \tag{3}$$

$(d_i) \equiv k - m$, then the uncertainty matrix for d, denoted by C_{dd}, is

Let the (unknown) adjusted parameter vector be $\alpha' \equiv (\alpha_i')$, and the adjusted calculated response vector be $k'(\alpha')$. By imposing the condition $m' = k'(\alpha')$, we are forcing the adjusted values α' and m' to be consistent within the limits of linearity of the theory. If we further denote the actual adjustments by $x = \alpha' - \alpha$ and $y = m' - m$, then the linear approximation expressed by Eq. (1) becomes

---

*The symbol "†" is used to denote the transpose, and the brackets "< >" are used to designate an expectation value, i.e., an average over a probability distribution, of possible deviations (δ) from the mean value.

$$m' = k + S_k x$$

or

$$m' - m = k - m + S_k x$$

thus leading to

$$y = d + S_k x \; . \tag{4}$$

The generalized linear least squares procedure involves minimizing the quadratic loss function

$$Q(x,y) = (y,x)^{\dagger} \begin{pmatrix} C_{mm} & C_{m\alpha} \\ C_{\alpha m} & C_{\alpha\alpha} \end{pmatrix}^{-1} (y,x) \; , \tag{5*}$$

where $(y,x)^{\dagger} \equiv (y_1,\ldots,y_I, x_1,\ldots,x_N)$, subject to the constraint expressed by Eq. (4). Adopting the procedure of Refs. 23–24, the above conditional minimum formulation is equivalent to unconditionally minimizing the function R(x,y), where

$$R(x,y) = Q(x,y) + 2\lambda^{\dagger}(S_k x - y) \; , \tag{6}$$

and 2λ is an I-dimensional vector of Lagrange multipliers. Thus, x and y satisfy the equations

$$\partial R(x,y)/\partial x = \partial R(x,y)/\partial y = 0 \; . \tag{7}$$

The matrix in Eq. (5) can be expressed as the following identity

$$\begin{pmatrix} C_{mm} & C_{m\alpha} \\ C_{\alpha m} & C_{\alpha\alpha} \end{pmatrix}^{-1} \equiv \begin{pmatrix} C_{mm}^{-1} + C_{mm}^{-1} C_{m\alpha} A^{-1} C_{\alpha m} C_{mm}^{-1} & -C_{mm}^{-1} C_{m\alpha} A^{-1} \\ -A^{-1} C_{\alpha m} C_{mm}^{-1} & A^{-1} \end{pmatrix} \; , \tag{8}$$

in which $A = C_{\alpha\alpha} - C_{\alpha m} C_{mm}^{-1} C_{m\alpha}$. Thus, Eq. (6) becomes

$$\begin{aligned} R(x,y) = {} & y^{\dagger}(C_{mm}^{-1} + C_{mm}^{-1} C_{m\alpha} A^{-1} C_{\alpha m} C_{mm}^{-1} \; y - x^{\dagger}(A^{-1} C_{\alpha m} C_{mm}^{-1}) y \\ & - y^{\dagger}(C_{mm}^{-1} C_{m\alpha} A^{-1}) \; x + x^{\dagger} A^{-1} x + 2\lambda^{\dagger}(S_k x - y) \; , \end{aligned} \tag{9}$$

---

*The symbol "−1" refers to the inverse of a matrix.

and the Eqs. (7) become

$$\partial R(x,y)/\partial x = 0 = -1^{\dagger}(A^{-1}C_{\alpha m}C_{mm}^{-1})\ y - y^{\dagger}(C_{mm}^{-1}C_{m\alpha}A^{-1})\ 1 - 1^{\dagger}A^{-1}\ x + x^{\dagger}A^{-1}1 + 2\lambda^{\dagger}S_k 1\ , \tag{10a}$$

$$\begin{aligned}\partial R(x,y)/\partial y = 0 = {} & 1^{\dagger}(C_{mm}^{-1} + C_{mm}^{-1}C_{m\alpha}A^{-1}C_{\alpha m}C_{mm}^{-1})\ y \\ & + y^{\dagger}(C_{mm}^{-1} + C_{mm}^{-1}C_{m\alpha}A^{-1}C_{\alpha m}C_{mm}^{-1})\ 1 \\ & - x^{\dagger}(A^{-1}C_{\alpha m}C_{mm}^{-1})\ 1 - 1^{\dagger}\ (C_{mm}^{-1}C_{m\alpha}A^{-1})\ x - 2\lambda^{\dagger}1\ ,\end{aligned} \tag{10b}$$

where we have introduced the symbols "1" and "0" to represent unit and zero vectors of dimensions $N \times 1$ in Eq. (10a) and of dimensions $I \times 1$ in Eq. (10b). The symbols "$1^{\dagger}$" and "$0^{\dagger}$" denote the corresponding row vectors. Since A^{-1} is symmetric and the transpose of a scalar and the scalar are the same, Eqs. (10) may be simplified to

$$S_k^{\dagger}\lambda + A^{-1}x - A^{-1}C_{\alpha m}C_{mm}^{-1}y = 0 \tag{10′a}$$

and

$$-\lambda + (C_{mm}^{-1} + C_{mm}^{-1}C_{m\alpha}A^{-1}C_{\alpha m}C_{mm}^{-1})\ y - (C_{mm}^{-1}C_{m\alpha}A^{-1})\ x = 0\ . \tag{10′b}$$

Solving for x and y yields

$$x = (C_{\alpha m} - C_{\alpha\alpha}S_k^{\dagger})\ \lambda \tag{11a}$$

and

$$y = (C_{mm} - C_{m\alpha}S_k^{\dagger})\ \lambda\ , \tag{11b}$$

which reflect the driving influence of the vector λ and the independence of the solution on A^{-1}. Substituting the values of x and y into Eq. (4) yields

$$\lambda = C_{dd}^{-1}d\ , \tag{12}$$

with

$$C_{\lambda\lambda} = <(\delta\lambda)\ (\delta\lambda)^{\dagger}> = C_{dd}^{-1}<(\delta d)\ (\delta d)^{\dagger}>\ C_{dd}^{-1} = C_{dd}^{-1}\ . \tag{13}$$

The adjusted values α' and m' are found from the adjustments in Eqs. (11) to be

$$\alpha' = \alpha + (C_{\alpha m} - C_{\alpha\alpha}S_k^{\dagger})\ C_{dd}^{-1}d \tag{14a}$$

and

$$r' = r + (C_{mm} - C_{m\alpha}S_k^{\dagger})\ C_{dd}^{-1}d\ , \tag{14b}$$

where C_{dd}^{-1} is obtained by taking the inverse of Eq. (3) and is a matrix of dimensions I × I. It should be noticed that in order to obtain α' and m' <u>only</u> C_{dd} has to be inverted, although A^{-1} appears in Eqs. (8)–(10).

The covariances of the adjusted differential values are readily obtained from the first of Eqs. (14):

$$C_{\alpha'\alpha'} = <(\delta\alpha')\ (\delta\alpha')^{\dagger}> = C_{\alpha\alpha} + (C_{\alpha m} - C_{\alpha\alpha}S_k^{\dagger})\ C_{dd}^{-1} <(\delta d)\ (\delta d)^{\dagger}> C_{dd}^{-1}(C_{m\alpha} - S_k C_{\alpha\alpha})$$
$$+ (C_{\alpha m} - C_{\alpha\alpha}S_k^{\dagger})\ C_{dd}^{-1} <(\delta d)\ (\delta\alpha)^{\dagger}> + <(\delta\alpha)\ (\delta d)^{\dagger}> C_{dd}^{-1}(C_{m\alpha} - S_k C_{\alpha\alpha})\ ,$$

and since

$$<(\delta d)\ (\delta\alpha)^{\dagger}> = <(\delta k - \delta m)\ (\delta\alpha)^{\dagger}> = S_k <(\delta\alpha)\ (\delta\alpha)^{\dagger}> - <(\delta m)\ (\delta\alpha)^{\dagger}> = S_k C_{\alpha\alpha} - C_{m\alpha}$$

then

$$C_{\alpha'\alpha'} = C_{\alpha\alpha} + (C_{\alpha m} - C_{\alpha\alpha}S_k^{\dagger})\, C_{dd}^{-1}(C_{m\alpha} - S_k C_{\alpha\alpha}) - 2(C_{\alpha m} - C_{\alpha\alpha}S_k^{\dagger})\, C_{dd}^{-1}(C_{m\alpha} - S_k C_{\alpha\alpha})\ ,$$

or

$$C_{\alpha'\alpha'} = C_{\alpha\alpha} - (C_{\alpha m} - C_{\alpha\alpha}S_k^{\dagger})\, C_{dd}^{-1}(C_{m\alpha} - S_k C_{\alpha\alpha})\ . \tag{15}$$

Similarly,

$$C_{m'm'} = C_{mm} + (C_{mm} - C_{m\alpha}S_k^{\dagger})\ C_{dd}^{-1} <(\delta d)\ (\delta d)^{\dagger}> C_{dd}^{-1}(C_{mm} - S_k C_{\alpha m})$$
$$+ (C_{mm} - C_{m\alpha}S_k^{\dagger})\ C_{dd}^{-1} <(\delta d)\ (\delta m)^{\dagger}> + <(\delta m)\ (\delta d)^{\dagger}> C_{dd}^{-1}(C_{mm} - S_k C_{\alpha m})\ ,$$

with

$$<(\delta d)\,(\delta m)^{\dagger}> = <(\delta k - \delta m)\,(\delta m)^{\dagger}> = S_k <(\delta\alpha)\,(\delta m)^{\dagger}> - <(\delta m)\,(\delta m)^{\dagger}> = S_k C_{\alpha m} - C_{mm}$$

leads to

$$C_{m'm'} = C_{mm} - (C_{mm} - C_{m\alpha}S_k^{\dagger})\ C_{dd}^{-1}(C_{mm} - S_k C_{\alpha m})\ . \tag{16}$$

Finally, the cross covariances of the adjusted integral and differential data become

$$C_{\alpha'm'} = <(\delta\alpha')\,(\delta m')^{\dagger}> = C_{\alpha m} + (C_{\alpha m} - C_{\alpha\alpha}S_k^{\dagger})\ C_{dd}^{-1} <(\delta d)\ (\delta d)^{\dagger}> C_{dd}^{-1}(C_{mm} - S_k C_{\alpha m})$$
$$+ (C_{\alpha m} - C_{\alpha\alpha}S_k^{\dagger})\ C_{dd}^{-1} <(\delta d)\ (\delta m)^{\dagger}> + <(\delta\alpha)\ (\delta d)^{\dagger}> C_{dd}^{-1}(C_{mm} - S_k C_{\alpha m})\ ,$$

which reduces to

$$C_{\alpha'm'} = C_{\alpha m} - (C_{\alpha m} - C_{\alpha\alpha}S_k^{\dagger})\ C_{dd}^{-1}(C_{mm} - S_k C_{\alpha m})\ . \tag{17}$$

Thus, from Eq. (17), even if no *a priori* correlation between the differential and integral data existed, by virtue of the combination (adjustment) procedure an *a posteriori* correlation does exist and must be considered in any further iteration or in the covariance representation of the adjusted data for future use.

The minimum value of Q in Eq. (5), found by substituting the expressions for x and y from Eqs. (11), is denoted by the symbol χ^2:

$$\chi^2 \equiv Q_{min}(x,y) = d^{\dagger} C_{dd}^{-1} d = d^{\dagger} (C_{mm} + S_k C_{\alpha\alpha} S_k^{\dagger} - S_k C_{\alpha m} - C_{m\alpha} S_k^{\dagger})^{-1} d \ . \tag{18}$$

The quantity χ^2 is a measure of the adjustments made in units of (combined) standard deviations summed over all participating integral experiments.

Thus χ^2/I should be of the order of 1 or less (i.e., on the average, the adjustment in each integral experiment should be within about one combined standard deviation). This quantity, which is a figure of merit for the proposed adjustment, can be calculated without actually performing the adjustment, since all the ingredients of Eq. (18) are known *á priori* and just reflect the consistency status of the available data considered.

For the particular case of a single measurement in which there is no correlation between the integral and differential data, Eq. (18) reduces to

$$\chi^2 = (k - m)^2/(C_{mm} + S_k C_{\alpha\alpha} S_k^{\dagger}) \ , \tag{18$'$}$$

which is just the square of the discrepancy between the calculated quantity k (using the available differential data α) and the corresponding measured quantity m expressed in units of the combined variance of m (i.e., C_{mm}) and k (i.e., $S_k C_{\alpha\alpha} S_k^{\dagger}$).

The Translation or Extrapolation Problem

The calculation of k_{eff} for an criticality safety scenario, denoted the "application," involves the use of cross sections. The calculated value of k_{eff}, k_a, will generally deviate from the value that would have been measured. Our purpose is to calculate an adjusted k_{eff} value in such a way that its deviation from a projected measured value will be minimal and that the uncertainty in this calculated value be as small as possible. This adjusted calculated k_{eff} value, k_a' can be recomputed based on the suggested data adjustments, $\alpha' - \alpha$, or a Δk bias can simply be estimated using the benchmark data. The value of k_a' can be computed as:

$$k_a' = k_a + S_a(\alpha' - \alpha) = k_a + S_a(C_{\alpha m} - C_{\alpha\alpha} S_k^{\dagger}) \ C_{dd}^{-1} d \ , \tag{19}$$

or alternatively the adjusted k_a value can be written in terms of a bias, b_a;

$$k_a' = k_a + b_a \ . \tag{20}$$

from this comparison, it is clear that

$$b_a = - S_a(\alpha' - \alpha) \ .$$

Taking the covariance of both sides of Eq. (19) and noting that the uncertainty in k_a denoted C_{aa} is:

$$C_{aa} \equiv \langle(\delta k_a)\ (\delta k_a)^{\dagger}\rangle = S_a \langle(\delta\alpha)\ (\delta\alpha)^{\dagger}\rangle\ S_a^{\dagger} = S_a C_{\alpha\alpha} S_a^{\dagger} \ , \tag{21}$$

we obtain for the covariance matrix of the $k_a^{'}$ values as

$$\begin{aligned} C_{a'a'} \equiv & <(\delta k_a^{'})\ (\delta k_a^{'})^{\dagger}> S_a C_{\alpha\alpha} S_a^{\dagger} + S_a (C_{\alpha m} - C_{\alpha\alpha} S_k^{\dagger}) \\ & C_{dd}^{-1} <(\delta d)\ (\delta d)^{\dagger}> C_{dd}^{-1}\ (C_{m\alpha} - S_k C_{\alpha\alpha})\ S_a^{\dagger} \\ & + 2S_a\ (C_{\alpha m} - C_{\alpha\alpha} S_k^{\dagger})\ C_{dd}^{-1} <(\delta d)\ (\delta k_a)^{\dagger}> . \end{aligned} \tag{22}$$

Since

$$\begin{aligned} <(\delta d)\ (\delta k_a)^{\dagger}> = & <(\delta k)\ (\delta k_a)^{\dagger}> - <(\delta m)\ (\delta k_a)^{\dagger}> = S_k <(\delta\alpha)\ (\delta\alpha)^{\dagger}> S_a^{\dagger} \\ & - <(\delta m)\ (\delta\alpha)^{\dagger}> S_a^{\dagger} = S_k C_{\alpha\alpha}\ S_a^{\dagger} - C_{m\alpha} S_a^{\dagger} , \end{aligned}$$

Equation (21) becomes

$$C_{a'a'} = S_a C_{\alpha\alpha} S_a^{\dagger} - S_a (C_{\alpha m} - C_{\alpha\alpha} S_k^{\dagger})\ C_{dd}^{-1} (C_{m\alpha} - S_k C_{\alpha\alpha})\ S_a^{\dagger} . \tag{23}$$

Equations (19) and (23) represent the adjusted k_a value and its uncertainty. Again, the calculations involve only the inversion of a small I × I matrix together with some matrix multiplication.

---

*Equation (23) can be alternatively derived by substituting $C_{\alpha'\alpha'}$ directly from Eq. (15) into the following equation:

$$C_{a'a'} = S_a C_{\alpha'\alpha'} S_a^{\dagger} = S_a [C_{\alpha\alpha} - (C_{\alpha m} - C_{\alpha\alpha} S_k^{\dagger})\ C_{dd}^{-1}\ (C_{m\alpha} - S_k C_{\alpha\alpha})] S_a^{\dagger} .$$

INTERNAL DISTRIBUTION

1. S. M. Bowman
2–6. B. L. Broadhead (5)
7–11. W. C. Carter (5)
12–13. R. L. Childs (2)
14. M. E. Dunn
15. M. D. DeHart
16. K. R. Elam
17. M. B. Emmett
18. I. C. Gauld
19. N. M. Greene
20. G. R. Handley
21. O. W. Hermann
22. D. F. Hollenbach
23–24. C. M. Hopper (2)
25. W. C. Jordan
26. M. A. Kuliasha
27. L. C. Leal
28–32. C. V. Parks (5)
33. L. M. Petrie
34. R. T. Primm
35. C. E. Pugh
36. B. T. Rearden
37. R. C. Robinson
38. R. W. Roussin
39. C. H. Shappert
40. R. G. Taylor
41. T. E. Valentine
42. J. C. Wagner
43. R. M. Westfall
44. R. Q. Wright
45. Central Research Library, Document Reference Section
46. ORNL-Y-12 Technical Library
47–48. ORNL Laboratory Records (2) (for submission to OSTI)
49. ORNL Laboratory Records - RC
50. ORNL Patent Section

EXTERNAL DISTRIBUTION

51. F. M. Alcorn, BWX Technologies, Inc., Naval Nuclear Fuel, 212 Windsor Rd., Lynchburg, VA 24502
52. S. Almodovar, Fluor Daniel Hanford, P.O. Box 1000, Mail Stop A3-02, Richland, WA 99352-1000
53. S. Altschuler, U.S. Department of Energy, Richland Operations, 825 Jadwin, R3-79, Richland, WA 99352
54. R. E. Anderson, Los Alamos National Laboratory, P.O. Box 1663, NIS-6, MS J562, Los Alamos, NM 87545
55. W. L. Andrews, Defense Nuclear Facilities Safety Board, 625 Indiana Ave., Washington, DC 20004
56. C. Apperson, Westinghouse Savannah River Company, Savannah River Site, Bldg. 773-11A, Aiken, SC 29808-0001
57. M. G. Bailey, U.S. Nuclear Regulatory Commission, MS O6-G22, Washington, DC 20555
58. G. H. Bidinger, Nuclear Criticality Safety, 17016 Cashell Road, Rockville, MD 20853

59. R. N. Blomquist, Argonne National Laboratory, RA/208, 9700 S. Case Ave., Argonne, IL 60439-4842
60. C. Boman, BWX Technologies, Inc., Naval Nuclear Fuel, P.O. Box 785, Lynchburg, VA 24505
61. M. C. Brady Raap, Duke Engineering Services, 10503 W. Williams Road, Benton City, WA 99320
62. J. B. Briggs, INEEL, P.O. Box 1625, MS-3855, Idaho Falls, ID 83402
63. T. Burns, Defense Nuclear Facilities Safety Board, 625 Indiana Ave., Washington, DC 20004
64. R. D. Busch, University of New Mexico, Chemical and Nuclear Engineering Department, FEC 209, Albuquerque, NM 87131-1341
65. D. E. Cabrilla, U.S. DOE EM-66, Nuclear Material Stabilization, 19901 Germantown Road, Germantown, MD 20874-1290
66. D. E. Carlson, U.S. Nuclear Regulatory Commission, MS O6-F18, Washington, DC 20555
67. K. J. Carroll, Lockheed Martin Energy Systems, Y-12 Plant, P.O. Box 2009, Oak Ridge, TN 37831-8238
68. P. Cousinou, Institute of Protection and Nuclear Safety, B. P. 6 - 92265 Fontenay-Aux-Roses, Cedex, France
69. D. R. Damon, U.S. Nuclear Regulatory Commission, MS T8-H7, Washington, DC 20555
70. J. R. Davis, U.S. Nuclear Regulatory Commission, MS T8-A33, Washington, DC 20555
71. J. W. Davis, Framatome Cogema Fuels, CRWMS M&O, 1261 Town Center Dr., Las Vegas, NV 89134
72. R. L. Dintaman, U.S. Department of Energy, DP-13, 19901 Germantown Rd., Germantown, MD 20874-1290
73. H. L. Dodds, University of Tennessee, Nuclear Engineering Dept., 214 Pasqua Engineering Bldg., Knoxville, TN 37922
74. T. W. Doering, Framatome Cogema Fuels, 1261 Town Center Drive, Las Vegas, NV 89124
75. F. Eltawila, U.S. Nuclear Regulatory Commission, MS T10-E46, Washington, DC 20555
76. J. D. Evans, U.S. Department of Energy, S-3.1/VISTA, 1000 Independence Ave., S.W., Washington, DC 22085
77. H. D. Felsher, U.S. Nuclear Regulatory Commission, MS T8-H7, Washington, DC 20555
78. P. Felsher, Rocky Flats Environment Technology Site, Bldg. T886B, P.O. Box 464, Golden, CO 80402-0464
79. J. R. Felty, Science Applications Int'l Corp., 2418 N. Dickerson St., Arlington, VA 22207
80. I. E. Fergus, U.S. Department of Energy, EH-22, 20300 Century Blvd., Germantown, MD 20874
81. P. Finck, Argonne National Laboratory, 9700 South Cass Avenue, RA/208, Argonne, IL 60439-4842
82. E. K. Fujita, Argonne National Laboratory, 9700 South Cass Avenue, RA/208, Argonne, IL 60439-4842
83. A. S. Garcia, U.S. Department of Energy, Idaho Operations Office, 850 Energy Dr., MS 1154, Idaho Falls, ID 83401-1563
84. E. Greenspan, University of California, 4101 Etchevenny Hall, Berkeley, CA 94720
85. J. Gulliford, Winfrith Technology Centre, 306/A32, AEA Technology PLC, Winfrith, Dorchester, Dorset DT2 8DH
86. D. K. Hays, Los Alamos National Laboratory, P.O. Box 1663, Los Alamos, NM 87545

87. D. Heinrichs, Lawrence Livermore National Laboratory, P.O. Box 808, MS L-128, Livermore, CA 94551
88. A. B. Hoffman, Lockheed Martin Idaho Tech. Co., P.O. Box 1625, MS 3458, Idaho Falls, ID 83415-3458
89. S. T. Huang, Lawrence Livermore National Laboratory, MS L-128, P.O. Box 808, Livermore, CA 94551
90. J. C. Ingram, Bechtel Jacobs Company LLC, P. O. Box 4699, Bldg. K-1320, MS-7592, Oak Ridge, TN 37831-7592
91. E. F. Kendall, U.S. Department of Energy, Oak Ridge Operations Office, YSO, P.O. Box 2001, Oak Ridge, TN 37831
92. K. D. Kimball, NISYS Corporation, 6055 Atlantic Blvd., Suite G-2, Norcross, GA 30071
93. R. P. Koopman, Lawrence Livermore National Lab., P.O. Box 808, L-467, Livermore, CA 94551
94. M. A. Lee, U.S. Department of Energy, Livermore Operations, 7000 East St., P.O. Box 808, L-293, Livermore, CA 94551-0808
95. R. Libby, Pacific Northwest National Laboratory, P.O. Box 999, M/S K7-74, Richland, WA 99352
96. J. J. Lichtenwalter, Bechtel Jacobs Company LLC, P.O. Box 4699, Bldg. K-1320, MS-7592, Oak Ridge, TN 37831-7592
97. R. C. Little, Los Alamos National Laboratory, MS F663, P.O. Box 1663, Los Alamos, NM 87545
98. C. D. Manning, Siemens Power Corporation, 2101 Horn Rapids Road, P.O. Box 130, Richland, WA 99352-0130
99. R. McBroom, U.S. Department of Energy, Oak Ridge Operations Office, YSO, P.O. Box 2001, Oak Ridge, TN 37831
100. J. McKamy, U.S. Department of Energy, EH-34, 19901 Germantown Road, Germantown, MD 20874-1290
101. R. D. McKnight, Argonne National Laboratory, 9700 S. Cass Ave., Argonne, IL 60439-4842
102. T. P. McLaughlin, Los Alamos National Laboratory, P.O. Box 1663, Los Alamos, NM 87545
103. D. E.I. Mennerdal, E M Systems, Starvãgen 12, Täby, SWEDEN S-18357
104. R. D. Montgomery, Nuclear Fuel Services, Inc., 1205 Banner Hill Rd., Erwin, TN 37650
105. D. C. Morey, U.S. Nuclear Regulatory Commission, MS T8-A33, Washington, DC 20555
106. L. Mantierth, GE Nuclear Energy, P.O. Box 780, Castle Hayne Road, Wilmington, NC 28402
107. J. A. Morman, Argonne National Laboratory, 9700 S. Cass Ave., Bldg. 208, C237B, Argonne, IL 60439-4842
108. R. D. Mosteller, Los Alamos National Laboratory, MS J562, Los Alamos, NM 87545
109. K. A. Niemer, Duke Engineering & Services, 400 S. Tryon St., WC26B, P.O. Box 1004, Charlotte, NC 28201-1004
110. C. W. Nilsen, U.S. Nuclear Regulatory Commission, MS T9-F31, Washington, DC 20555
111. H. Okuno, Japan Atomic Energy Research Institute, 2-4 Shirakara-shirane, Tokai-mura, Ibaraki-ken, JAPAN 319-1195
112. S. A. Parra, Lawrence Livermore National Laboratory, P.O. Box 808, MS L-128, Livermore, CA 94551
113. L. E. Paulson, Manager, Nuclear Safety, GE Nuclear Energy, P.O. Box 780, Castle Hayne Road, Wilmington, NC 28405
114. S. Payne, U.S. DOE/AL/SASD, P.O. Box 5400, Albuquerque, NM 87185-5400

115. V. A. Perin, U.S. Nuclear Regulatory Commission, NMSS/DWM, MS T7-F3, Washington, DC 20555
116. J. Person, Lawrence Livermore National Laboratory, P.O. Box 808, MS L-128, Livermore, CA 94551
117. R. E. Pevey, University of Tennessee, Nuclear Engineering Dept., 214 Pasqua Engineering Bldg., Knoxville, TN 37922
118. J. Philbin, Sandia National Laboratory, P.O. Box 5800, Albuquerque, NM 87185-1143
119. A. W. Prichard, Pacific Northwest National Laboratory, P.O. Box 999, MSIN: K8-34, Richland, WA 99352
120. M. Rahimi, U.S. Nuclear Regulatory Commission, M/S T7F3, Washington, DC 20555
121. T. A. Reilly, Westinghouse Safety Management Solutions, 1993 South Centennial Dr., Aiken, SC 29803
122. J. D. Roarty, Defense Nuclear Facilities Safety Board, 625 Indiana Ave., N.W., Suite 700, Washington, DC 2004
123. C. Rogers, Duke Engineering Services, 10503 W. Williams Road, Benton City, WA 99320
124. C. T. Rombough, CTR Technical Services, Inc., 950 Sugarloaf Rd., Manitou Springs, CO 80829
125. B. Rothleder, U.S. Department of Energy, EH-31, 19901 Germantown Rd., Germantown, MD 20874-1290
126. M. K. Sheaffer, Lawrence Livermore National Laboratory, P.O. Box 808, L-634, Livermore, CA 94550
127. G. L. Stimmell, Manager, General Electric Co., Vallecitos Nuclear Center, P.O. Box 460, Vallecitos Road, Pleasanton, CA 94566
128. J. T. Taylor, Principle Engineer - CSE, GE Nuclear Energy, P.O. Box 780, Castle Hayne Road, Wilmington, NC 28402
129. T. Taylor, Lockheed Martin Idaho Tech. Co., P.O. Box 1625, MS 3458, Idaho Falls, ID 83415-3458
130. D. A. Thomas, Framatome Cogema Fuels, 1261 Town Center Drive, Las Vegas, NV 89124
131. C. Tripp, U.S. Nuclear Regulatory Commission, MS T8-A33, Washington, DC 20555
132. J. A. Thornton, Duke Engineering & Services, 400 S. Tryon St., WC26B, P.O. Box 1004, Charlotte, NC 28201-1004
133. H. Toffer, Fluor Daniel Northwest, Inc., P.O. Box 1050, MSIN B4-44, 1100 Jadwin Ave., Richland, WA 99352-1050
134. E. F. Trumble, Westinghouse Safety Management Solutions, P.O. Box 5388, 1993 South Centennial Dr., Aiken, SC 29803
135. J. J. Wagschal, Racah Institute of Physics, The Hebrew University of Jerusalem, 91904, Jerusalem, ISRAEL
136. M. Wangler, Office of Site Operations, EM-70/CLV-1059, U.S. Department of Energy, 19901 Germantown Road, Germantown, MD 20874-1290
137. L. Wetzel, BWX Technologies, Inc., Naval Nuclear Fuel, P.O. Box 785, Lynchburg, VA 24505
138. S. A. Whaley, U.S. Nuclear Regulatory Commission, MS O6-G22, Washington, DC 20555
139. B. H. White IV, U.S. Nuclear Regulatory Commission, MS O6-F18, Washington, DC 20555
140. D. W. Williams, Westinghouse Electric Corporation, 5801 Bluff Rd MS#15, Columbia, SC 29209
141. Mark Williams, Louisiana State University, Baton Rouge, LA 70803-5820

142. R. E. Wilson, Safe Sites of Colorado, P.O. Box 464, Golden, CO 80402-0464

143. C. J. Withee, U.S. Nuclear Regulatory Commission, MS O6-G22, Washington, DC 20555

NRC FORM 335
(2-89)
NRCM 1102
3201, 3202

U.S. NUCLEAR REGULATORY COMMISSION

BIBLIOGRAPHIC DATA SHEET

(See instructions on the reverse)

1. REPORT NUMBER (Assigned by NRC, Add Vol., Supp., Rev., and Addendum Numbers, if any.)

NUREG/CR-6655, Vol. 1
ORNL/TM-13692/V1

2. TITLE AND SUBTITLE

Sensitivity And Uncertainty Analyses Applied to Criticality Safety Validation

Methods Development

3. DATE REPORT PUBLISHED

MONTH	YEAR
November	1999

4. FIN OR GRANT NUMBER

W6479

5. AUTHOR(S)

B. L. Broadhead, C. M. Hopper, R. L. Childs, C. V. Parks

6. TYPE OF REPORT

Technical

7. PERIOD COVERED ***(Inclusive Dates)***

8. PERFORMING ORGANIZATION — NAME AND ADDRESS ***(If NRC, provide Division, Office or Region, U.S. Nuclear Regulatory Commission, and mailing address; if contractor, provide name and mailing address.)***

Oak Ridge National Laboratory
Managed by Lockheed Martin Energy Research Corporation
Oak Ridge, TN 37831-6370

9. SPONSORING ORGANIZATION — NAME AND ADDRESS ***(If NRC, type "Same as above"; if contractor, provide NRC Division, Office or Region, U.S. Regulatory Commission, and mailing address.)***

Division of Systems Analysis and Regulatory Effectiveness
Office of Nuclear Regulatory Research
U.S. Nuclear Regulatory Commission
Washington, DC 20555-0001

10. SUPPLEMENTARY NOTES

C. W. Nilsen, NRC Project Manager

11. ABSTRACT ***(200 words or less)***

This report develops the methodology for application of Sensitivity and Uncertainty (S/U) Analysis Techniques to the data validation tasks of a criticality safety computational study. The S/U methods which are presented in this volume are designed to provide a formal means of establishing the range or area of applicability for criticality safety data validation studies. The development of two parameters that are analogous to the standard trending parameters form the key to the technique. These parameters represent the differences by group of S/U-generated sensitivity profiles and traditional correlation coefficients, each of which give information relative to the similarity between pairs of selected systems.

A Generalized Linear Least Squares Methodology (GLLSM) tool is also described, which is used largely to provide an understanding of the magnitude and quantity (i.e., number of systems) of these new parameters that can be used in a formal definition of applicability and bias estimation.

These methods and guidelines will be applied to a sample validation for uranium systems with enrichments greater than 5 wt % in Volume 2 of this document.

12. KEY WORDS/DESCRIPTORS ***(List words or phrases that will assist researchers in locating the report.)***

criticality safety, data validation, sensitivity analysis, uncertainty analysis

13. AVAILABILITY STATEMENT

unlimited

14. SECURITY CLASSIFICATION

(This Page) unclassified

(This Report) unclassified

15. NUMBER OF PAGES

16. PRICE